UNIVERSITEIT VAN PRETORIA
UNIVERSITY OF PRETORIA
YUNIBESITHI YA PRETORIA

PAPR REDUCTION IN FBMC SYSTEMS USING AN FBMC OPTIMIZED ACE METHOD

by

Nuan van der Neut

Submitted in partial fulfilment of the requirements for the degree

Master of Engineering (Electronic Engineering)

in the

Department of Electrical, Electronic and Computer Engineering
Faculty of Engineering, Built Environment and Information Technology

UNIVERSITY OF PRETORIA

October 2015

SUMMARY

PAPR REDUCTION IN FBMC SYSTEMS USING AN FBMC OPTIMIZED ACE METHOD

by

Nuan van der Neut

Supervisor(s):	Professor B.T. Maharaj
Department:	Electrical, Electronic and Computer Engineering
University:	University of Pretoria
Degree:	Master of Engineering (Electronic Engineering)
Keywords:	Cognitive radio, OFDM, PAPR, ACE, FBMC, polyphase realization, prototype filter

The aim of this dissertation was to investigate peak-to-average power ratio (PAPR) reduction techniques for filter bank multicarrier (FBMC) modulated systems. Research into current PAPR reduction techniques in FBMC and orthogonal frequency division multiplexing (OFDM) found that the active constellation extension (ACE) method has not been exploited for use in FBMC systems. This is, in part, due to the complexities involved in signal processing inherent of FBMC systems, as well as FBMC being a relatively new subject matter in the telecommunications field.

The outcomes of the dissertation were four novel PAPR reduction techniques for FBMC systems. These techniques can be split up into two namely linear programming optimization ACE-based techniques and overlapping ACE techniques. The techniques compensate for the overlapping symbols in FBMC by utilizing a frame based approach. This characteristic makes them ideal candidates to be applied in burst transmission. Furthermore, because an ACE based technique is used, they do not require the transmission of side information. The PAPR performance of the techniques are shown to match, or in some cases improve, current PAPR techniques for FBMC. The analysis of the proposed approaches also address some complexity issues with current FBMC implementations.

The out-of-band (OOB) interference of the techniques under clipping scenarios is investigated. It is shown that the OOB interference can be minimized whilst still maintaining good PAPR performance. Additional results are also provided by means of a study of the PAPR reduction techniques proposed

as applied to a high power amplifier based model. The corresponding power amplifier efficiency as well as bit-error rate (BER) degradation are investigated and compared to other standard techniques for PAPR reduction in FBMC systems. It was found that the proposed techniques can achieve a higher amplifier efficiency than existing techniques at a marginal trade-off in BER degradation. This BER degradation is lower than existing techniques due to the marginal increase in average transmit power.

As illustrated by exhaustive simulations, the single scaling and overlapping smart gradient-project ACE-based techniques proposed, are ideal candidates for practical implementation in systems employing the low complexity polyphase implementation of FBMC modulators. The methods are shown to offer significant PAPR reduction and increase the feasibility of FBMC as a replacement modulation system for OFDM.

OPSOMMING

PAPR VERMINDERING IN FBMC STELSELS DEUR DIE GEBRUIK VAN 'N FBMC GEOPTIMISEERDE ACE TEGNIEK

deur

Nuan van der Neut

Studieleier(s):	Professor B.T. Maharaj
Departement:	Elektriese, Elektroniese en Rekenaar-Ingenieurswese
Universiteit:	Universiteit van Pretoria
Graad:	Magister in Ingenieurswese (Elektroniese Ingenieurswese)
Sleutelwoorde:	Kognitiewe radio, OFDM, PAPR, ACE, FBMC, veelfase realisasie, prototipe filter

Die doel van hierdie verhandeling is om top-tot-gemiddelde drywingsverhouding (PAPR) verminderingstegnieke vir filterbank veelvuldige draer (FBMC) -gemoduleerde stelsels te ondersoek. Huidige PAPR verminderingstegnieke in FBMC en ortogonale frekwensie verdeling multipleksering (OFDM) is ondersoek en daar is bevind dat die aktiewe konstellasie uitbreidingsmetode (ACE) nog nie vantevore ontgin is in FBMC stelsels nie. Dit is gedeeltelik as gevolg van die inherente kompleksiteit van seinverwerking in FBMC stelsels en ook omdat FBMC 'n relatief nuwe onderwerp in die veld van telekommunikasie is.

Die resultate van hierdie verhandeling is vier unieke PAPR verminderingstegnieke vir FBMC stelsels. Hierdie tegnieke kan opgedeel word in lineêre programeringsgeoptimiseerde tegnieke en oorvleuelende ACE tegnieke. Om vir die oorvleueling van simbole in FBMC te vergoed, word 'n raamgebaseerde benadering gebruik. Hierdie kenmerk maak hierdie tegnieke ideaal vir vlaaguitsending. Omdat 'n ACE-gebaseerde tegniek gebruik word, is transmissie van kant inligting onnodig. Die PAPR werkverrigting van dié tegnieke is op standaard met, en in sommige gevalle 'n verbetering op huidige PAPR tegnieke vir FBMC. Die ontleding van die voorgestelde benaderings spreek ook die kompleksiteitkwessies met die implementering van huidige tegnieke aan.

Die buite band (OOB) steuring van die tegnieke onder geknipte scenarios word ondersoek. Daar word

getoon dat die OOB steuring verminder kan word terwyl goeie PAPR verrigting gehandhaaf word. Addisionele studieresultate word ook voorsien deur ’n studie van die voorgestelde PAPR reduksietegnieke toegepas op ’n hoë drywing versterker (HPA) model. Die ooreenstemmende drywingsversterker doeltreffendheid asook die degradering van die bit fout waarde (BER) is ondersoek en vergelyk met ander tegnieke vir PAPR vermindering in FBMC stelsels. Daar is bevind dat die voorgestelde tegnieke ’n hoër drywing versterker doeltreffendheid kan bereik as bestaande tegnieke afgespeel ten koste van ’n marginale BER degradasie. Hierdie degradasie is laer as bestaande tegnieke as gevolg van die marginale toename in gemiddelde uitsendingskrag.

Uitvoerige simulasies toon dat die voorgestelde enkel skalering en oorvleuelende slim gradiënt projek ACE gebaseerde tegnieke die ideale kandidate is vir praktiese toepassing in stelsels wat gebruik maak van die lae kompleksiteit veelfase toepassing van FBMC modulators. Dié metodes bring ’n beduidende PAPR vermindering te weeg en maak FBMC meer haalbaar as ’n vervanging modulasie stelsel vir OFDM.

ACKNOWLEDGEMENTS

I would like to thank all the helping hands and minds that contributed in some way to this thesis. There are far too many to name, but I believe that I drew inspiration from all of you. The smallest of gestures from family, friends, colleagues and students often go unnoticed, but can make the largest of impacts. When all seems lost, its often the small things that provide enough motivation to get back on track.

To my mother, for her continued support. She believed in me, no matter the odds. Even though no words were written by her, most of the words in this thesis, I owe to her.

To my father, for his stern but unwavering backing. His methods are not always conventional, but often get the best results.

I am grateful and humbled by the opportunities that were given to me by my study leader, Prof Sunil Maharaj. His continued support and patience has taken me across the globe where I have met some of the most intelligent and influential people I am likely to ever meet.

I am grateful to my colleagues abroad, Gusatvo González, Prof. Fernando Gregorio and Prof. Juan Cousseau. Their assistance has been of paramount importance to the work presented in this thesis. They sacrificed their personal time assisting me through countless drafts of my conference paper and journal publication. Their patience was extraordinary and willingness to help was always astonishing.

To my office colleague, Phillip Botha with whom I shared an office for two years. He is an excellent teacher, colleague and friend. I am grateful for all the long discussions that kept us both out of work and countless arguments that I always seemed to lose. He kept me thinking out of the box and was instrumental in bouncing ideas off.

Last but not least, to my friends, who make it all worth it. Whether it be works discussions, life lessons, jokes, coffee breaks or walks around the campus, these activities shape the soul without which the mind would be an empty shell. Your company has made all the difference. In particular I would like to thank Johan Malan, Pieter Janse van Rensburg, Frikkie de Lange and Michael De

Villiers.

Credit and thanks goes to the University of Pretoria and in particular to the Sentech Chair in Broadband Wireless Communication (BWMC) for their financial support.

LIST OF ABBREVIATIONS

ACE	Active constellation extension
ACLR	Adjacent carrier leakage ratio
ACPR	Adjacent carrier power ratio
BER	Bit-error rate
CCDF	Cumulative complementary density function
CP	Cyclic prefix
CR	Cognitive radio
DP	Dynamic programming
EVM	Error vector magnitude
FBMC	Filter bank multicarrier
FFT	Fast Fourier transform
HPA	High power amplifier
IBO	Input back-off
ICI	Inter-carrier interference
IFFT	Inverse fast Fourier transform
ISI	Inter-symbol interference
LP	Linear programming
MIMO	Multiple-input, multiple output
OFDM	Orthogonal frequency division multiplexing
OOB	Out-of-band
OQAM	Orthogonal quadrature amplitude modulation
PA	Power amplifier
PAM	Pulse amplitude modulation
PAPR	Peak-to-average power ratio
POCS	Projection onto convex sets
PSD	Power spectral density
PTS	Partial transmit sequence
QAM	Quadrature amplitude modulation
QPSK	Quadrature phase shift keying
SGP	Smart gradient-project
SLM	Selective mapping
SW	Sliding window
TR	Tone reservation

TABLE OF CONTENTS

CHAPTER 1 INTRODUCTION

Frequency spectrum is a finite resource in wireless communications and therefore the search for an efficient modulation technique is an important area of research. Due to ever increasing demand for higher data rate wireless applications, cognitive radio (CR) applications are gaining popularity as a means for spectrum sharing. However, spectrum sharing between opportunistic users and licensed users require that both utilize a modulation method with well defined (non interfering) bands. As a result, both kinds of users can coexist and a higher level of total spectral efficiency can thus be attained.

Orthogonal frequency division multiplexing (OFDM) solutions, based on existing mobile access technologies (3GPP LTE and LTE Advanced), cannot solve the interference problem alone due to their high adjacent-channel power ratio (ACPR) [1, 2]. In fact, OFDM requires additional filtering to maintain a suitable ACPR, which leads to additional implementation complexity. Furthermore, efficient use of a fragmented spectrum requires a modulation scheme with fast decaying out-of-band (OOB) components, which may not be achievable using OFDM.

Recently, filter bank multicarrier (FBMC) modulation systems have drawn much attention as a viable alternative to OFDM, especially in cognitive radio (CR) applications [3, 4]. FBMC offers increased bandwidth efficiency as well as low out-of-band (OOB) interference, by employing a bank of well defined filters with tight spectral characteristics [5]. This efficient spectral containment and bandwidth efficiency are what makes FBMC an ideal candidate for fragmented spectral usage such as in CR applications [6]. However, FBMC suffers the same drawback that is present in all multicarrier modulation systems, namely a high peak-to-average power ratio (PAPR).

1.1 PROBLEM STATEMENT

FBMC systems suffer from high PAPR, inherent in multicarrier systems such as OFDM. A high PAPR greatly degrades the efficiency of high power amplifiers (HPA), as the HPA must be operated with a large input back-off (IBO), in order to operate in the linear region and avoid clipping [7].

HPAs that are driven into saturation, and start clipping, result in in-band distortion as well as OOB distortion. This OOB distortion leads to elevated side-lobes and therefore high ACPR. The main beneficial characteristics inherent of FBMC systems, namely the low sidelobes and ACPR, is negated when clipping occurs.

A reduction in the PAPR increases the efficiency of HPAs that is crucial for mobile transmitters, with limited energy resources. It also results in a lower probability of HPA clipping and therefore lower ACPR.

1.2 RESEARCH GAP

Several methods have been suggested for OFDM PAPR reduction. These include clipping, decision-aided reconstruction clipping, coding, partial transmission sequence (PTS), selective mapping (SLM), companding transform, tone reservation and active constellation extension (ACE), amongst others [8]. For FBMC PAPR reduction, a limited number of methods have been proposed. These include overlapping SLM, sliding window tone reservation and multi-block joint optimization methods [9, 10, 11]. Although these methods do not distort the magnitude of the original constellations, they do require additional side information to be sent. This effectively reduces the bandwidth efficiency prior to transmission.

The ACE method is of particular interest and uses an iterative clipping and filtering process of an up-sampled OFDM signal. In addition to the clipping and filtering, the ACE iteration includes an “extended constellation" selection that maintains the minimum Euclidian distance of the constellations points of the corresponding OFDM subcarrier symbol [12]. When the author commenced this work, no adaptation of an ACE based method existed for PAPR reduction in FBMC systems, and this dissertation aims to fill this gap.

1.3 RESEARCH OBJECTIVE AND QUESTIONS

This dissertation proposes four novel techniques for PAPR reduction in FBMC systems based on extended implementations of ACE methods as applied in OFDM systems [12]. The proposed methods can be divided into two classes, namely an optimization class and an overlapping ACE class. The optimization based approaches make use of linear programming (LP) in order to optimize an objective function based on a set of constraints. In addition, the second class of methods proposed, formed by two alternate methods, are based on simplifications of the previous optimization methods as well as an adaptation from smart gradient-project (SGP) ACE extended to FBMC systems. Since ACE is an iterative method and considering complexity constraints, it is of great importance to reduce the required number of iterations for an achievable PAPR. The proposed methods attempt to gain maximum PAPR reduction capabilities in a single iteration in order to lower overall system complexity.

The research questions that this dissertation aims to answer are as follows:

- Can ACE be used to achieve similar PAPR reduction performance in FBMC modulated systems, as in OFDM systems?
- Can the overlapping nature of FBMC symbols be exploited to achieve a greater degree of PAPR reduction capabilities?
- Do the proposed techniques offer superior PAPR reduction performance to other methods in the field for FBMC PAPR reduction?
- What are the negative effects of PAPR reduction, using the proposed techniques, in terms of BER degradation and increased complexity?
- What are the effects of the proposed PAPR reduction methods on the power spectrum and OOB interference of FBMC modulated systems?
- By how much can the proposed techniques increase power amplifier (PA) efficiency?

1.4 HYPOTHESIS AND APPROACH

ACE based PAPR reduction methods work exceptionally well in OFDM systems and are well documented [12, 13, 14]. Due to the effective use of ACE in OFDM and considering the research gap of ACE as applied to FBMC systems, the research approach was to test the feasibility of ACE for FBMC applications. The original hypothesis was that ACE should offer similar PAPR improvements in FBMC as it does in OFDM. The research approach of this dissertation therefore focuses on ACE as a plausible PAPR reduction method for FBMC systems. Throughout the dissertation, reference is made to OFDM as a basis of comparison to FBMC.

1.5 RESEARCH CONTRIBUTION

Four novel PAPR reduction methods, based on the ACE method, are proposed and presented in this dissertation. Their PAPR reducing capabilities are scrutinized using the cumulative complementary density function (CCDF) as a basis of performance comparison in Section 4.2. An effective means for measuring the PAPR in the overlapping symbols of FBMC modulated signals is proposed and supporting equations are presented in Section 2.5.2. The effects of PAPR reduction on the bit-error rate (BER) of FBMC systems is documented in Section 4.4. The power spectrum of PAPR reduced FBMC systems is investigated and the effect in terms of OOB interference is documented, using the ACPR as a basis of comparison, in Section 4.3. The key academic contributions of this dissertation can be summarized in the following bullet points:

1. A novel equation is developed in Section 2.5.2 which is used to accurately measure the PAPR in FBMC systems on the same metric as that of OFDM.

2. Two equations are formulated for the ACE optimization problem as applied in FBMC systems in Section 3.4.

3. Equation (2.10) was developed which allows for the mathematically description of the discrete sample points of an FBMC modulated signal in terms of it's constituent overlapping symbols.

4. Four techniques are proposed and then developed for reducing the PAPR in FBMC in Section 3.3.

1.6 PUBLICATIONS

This research work has lead to two international academic publications. The first being an international conference paper and the second an international journal article. The papers can be found below:

1. N. van der Neut, B. Maharaj, F. de Lange, G. González, F. Gregorio, and J. Cousseau, "PAPR reduction in FBMC systems using a smart gradient-project active constellation extension method," *in 2014 21st International Conference on Telecommunications (ICT)*, May 2014, pp. 134 – 139 [15].

2. N. van der Neut, B. Maharaj, F. de Lange, G. González, F. Gregorio, and J. Cousseau, "PAPR reduction in FBMC using an ACE-based linear programming optimization," *EURASIP Journal on Advances in Signal Processing*, vol. 2014, no. 1, 2014. [Online]. Available: http://dx.doi.org/10.1186/1687-6180-2014-172 [16]

1.7 OVERVIEW OF STUDY

Chapter 2 presents a literature study covering OFDM, FBMC modulation, PAPR reduction in OFDM and PAPR reduction in FBMC. Chapter 3 details the four methods proposed in this thesis, Chapter 4 focuses on the results obtained by these proposed methods and Chapter 5 presents a discussion and analysis of these results. The conclusion of the dissertation is presented in Chapter 6.

CHAPTER 2 LITERATURE STUDY

2.1 CHAPTER OBJECTIVES

In this chapter, the concepts of multicarrier systems and the evolution thereof are introduced. The notion of PAPR reduction as applied to multicarrier systems are also discussed and popular PAPR reduction techniques used in OFDM systems are introduced. The FBMC PAPR reduction techniques available in literature close off this chapter.

2.2 MULTICARRIER MODULATION

Multicarrier communication is fast replacing single-carrier as the modulation technique of choice for future generation wireless networks. By combining multiple subcarriers with long individual symbol periods, one can overcome the length of the channel impulse response, thereby greatly improving equalization capabilities. Its robustness to multipath effects, ease of equalization and handling of multiple users outweighs that of single-carrier.

Multicarrier modulation techniques combine multiple orthogonal subcarriers into a wideband signal with a large symbol period. Each subcarrier can be seen as a parallel bit-stream with a lower bit-rate than the total system and by combining them, one can still maintain the same bit-rate as in single-carrier communication. The main benefit of multicarrier modulation is the large symbol period which allows for improved equalization under adverse channel conditions such as frequency selective fading in multipath environments and narrowband interference [17, 18].

The multicarrier modulation equation can be expressed as:

$$s[n] = \sum_{m=0}^{M-1} \sum_{k=0}^{N-1} \left(\tilde{X}_m[k] p[n - mN] \right) e^{j2\pi k \frac{n}{N}}. \tag{2.1}$$

This can be seen as a generic equation from which the different modulation techniques such as OFDM and FBMC can be derived.

2.3 ORTHOGONAL FREQUENCY DIVISION MULTIPLEXING

The OFDM system model can be described as the sum of independent signals modulated onto subchannels with equal bandwidth as seen in Fig. 2.1 [19]. The complex baseband model can be represented mathematically by:

$$s[n] = \sum_{k=0}^{N-1} X_k e^{j2\pi nk/N}, \quad 0 \leq k \leq N-1. \tag{2.2}$$

Equation (2.2) can be seen as analogous to Eq. (2.1) with $p[n-mN]$ being a rectangular windowing function. An efficient implementation of OFDM can be done using the efficient fast Fourier transform (FFT) and inverse FFT (IFFT) algorithms. This replaces the need for each subcarrier to be modulated onto a carrier oscillator as the IFFT function effectively performs this task. The simplicity of this technique is the reason for it gaining favour in modern day communication as the multicarrier modulation technique of choice.

The rectangular window function results in a sinc-like frequency response of the subcarriers. If perfect orthogonality is maintained in an OFDM system, no inter-carrier interference exists between neighbouring subcarriers. However, the sinc-like frequency response results in the large sidelobes present in OFDM and is the main reason for applying a transmission filter to OFDM modulated systems, in order to prevent adjacent channel interference. These large sidelobes, which result in ICI, can be seen in Fig. 2.1.

2.3.1 Importance of cyclic prefix in OFDM

Due to the low bit-rate in a multicarrier system, the symbol period is longer than its single-carrier counterparts. It is therefore possible to insert a guard interval in-between the symbols. This guard interval prevents inter-symbol interference (ISI) which plagues single carrier systems [20]. OFDM systems utilize a cyclic prefix (CP) which acts as the guard interval. The CP in OFDM is simply a repeat of the last v samples added to the beginning of the symbol, prior to transmission, as shown in Fig. 2.2. The symbol length is therefore increased by v/N.

To avoid ISI, the CP length v should be longer than the impulse response of the time-invariant chan-

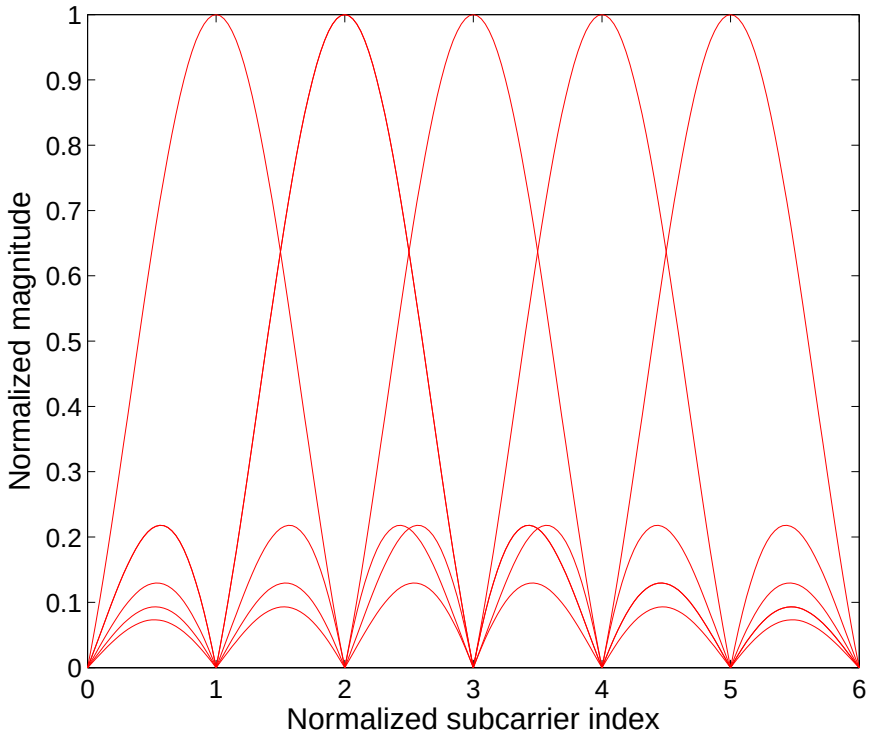

Figure 2.1: Subcarriers in OFDM modulated systems

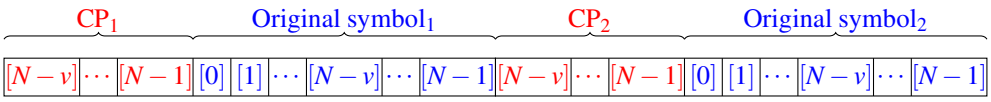

Figure 2.2: CP in OFDM systems

nel. By doing this, the effects of ISI in multipath channels can be negated. At the receiver, the CP portion of the OFDM symbol can be removed and the remaining portion is a function of the original OFDM symbol and its multipaths only. This allows for the channel model to easily be estimated and compensated for so long as the channel model does not vary significantly between transmission of adjacent symbols. The received signal at the receiver is a function of the transmit signal convoluted with the channel impulse response. The received signal with L distinctive multipaths can be written as [21]

$$y[n] = \sum_{l=0}^{L-1} h[l]s[n-l], \quad 0 \leq N-1+v \leq N-1. \tag{2.3}$$

Due to circular convolution, the frequency domain representation of Eq. (2.3), after the CP has been

removed, can be given by

$$Y[k] = H[k] \cdot S[k]. \tag{2.4}$$

The multipath propagation effects have therefore been reduced to simple multiplication of each frequency domain subcarrier by a scalar. This can now be removed by multiplying the received signal $Y[k]$ by the inverse of the channel frequency response. This simplified model for equalization is a key factor in OFDMs popularity.

2.4 FILTER BANK MULTICARRIER MODULATION

FBMC modulated systems consist of a bank of well defined filters with tight spectral characteristics. These filters are frequency and phase shifted versions of an original prototype filter which is designed to comply with Nyquist constraints and provide high frequency selectivity [22]. The FBMC modulation equation can be derived from Eq. (2.1) by effectively replacing $p[n-mN]$ with the prototype filter. The high frequency selectivity of FBMC is obtained by increasing the impulse response length of the prototype filter, thereby increasing resolution in the frequency domain. The prototype filter impulse response is designed to be K times longer than the number of subcarriers N. Thus the effective symbol length is increased to a length of $L = KN$. K is also referred to as the overlap factor and determines the number of overlapping complex FBMC symbols per sample. The overlap is required to maintain the same theoretical throughput as that of an OFDM system. Figure. 2.3 illustrates the impulse response for the PHYDYAS prototype filter with length $L = 256$. The sinc-like shape in the time domain equates to a highly selective filter in the frequency domain with sharp stop-band attenuation.

The higher frequency selectivity of FBMC makes it an ideal candidate for cognitive radio applications. This is because of the rapid decay of the sidelobes resulting in low inter-carrier interference (ICI). This is evident from Fig. 2.4 which illustrates the low ICI between adjacent subcarriers.

2.4.1 FBMC-OQAM

FBMC requires purely real input symbols. Orthogonal quadrature amplitude modulation (OQAM) is a staggering technique used to transform complex input data symbols into real symbols at twice

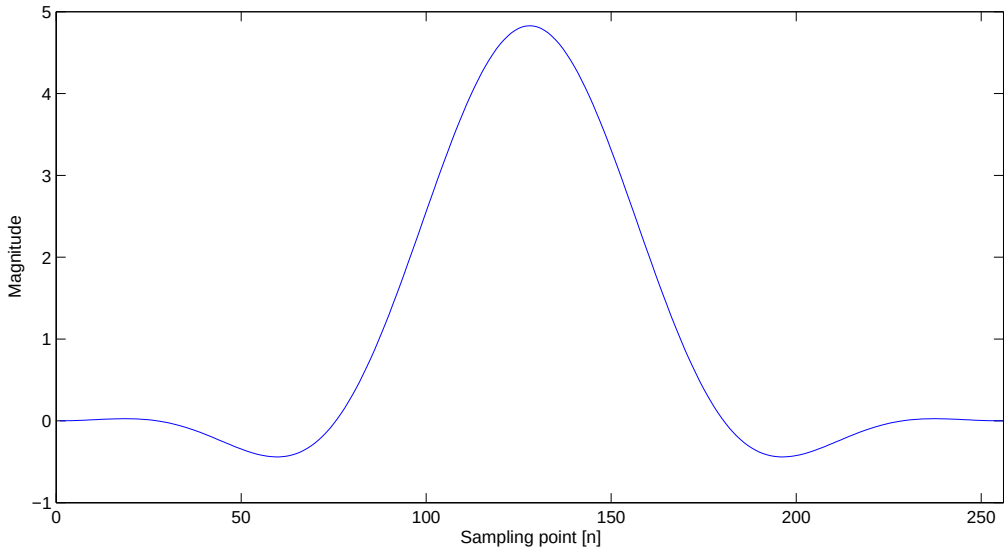

Figure 2.3: PHYDYAS prototype filter impulse response with K=4, L=256

the sampling rate [22]. OQAM is used in FBMC to ensure that only real symbols are fed into the filter bank. OQAM symbols are analogous to alternating real and imaginary pulse amplitude modulation (PAM) symbols staggered by $N/2$ samples. The OQAM symbols are then fed into the FBMC modulator, where they are filtered and modulated onto their respective subcarriers. The output of the FBMC modulator at sample n can be written as [23]:

$$s[n] = \sum_{q=-\infty}^{\infty} \sum_{k=0}^{N-1} \left(\theta_k \Re\{\tilde{X}_q[k]\} p[n-qN] + \theta_{k+1} \Im\{\tilde{X}_q[k]\} p\left[n-qN-\frac{N}{2}\right] \right) e^{jk(n-qN)\frac{2\pi}{N}}, \tag{2.5}$$

with

$$\theta_k = \begin{cases} 1, & \text{if } k \text{ is even} \\ j, & \text{if } k \text{ is odd,} \end{cases} \tag{2.6}$$

where $\tilde{X}_q[k]$ is the complex input symbol q at subcarrier k, $\Re$ and $\Im$ represent the real and imaginary components respectively and $p[n]$ is the prototype filter.

The OQAM pre-processing stage can also be considered as a source encoding technique. The OQAM encoder is fed with non-return-to-zero (NRZ) data and maps it to alternating real and imaginary symbols that are fed into the FBMC modulator. These symbols are fed at twice the sampling rate to maintain the same data rate as a corresponding OFDM system using a complex data source coding technique [22].

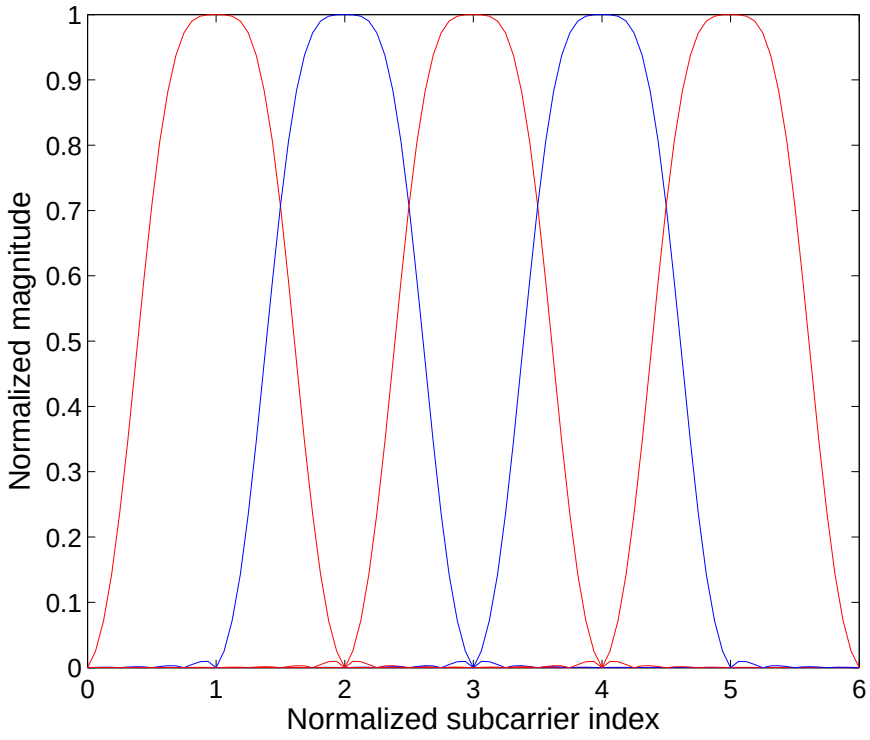

Figure 2.4: Subcarriers in FBMC modulated systems

By defining;

$$\begin{aligned} X_{2m}[k] &= \Re\{\tilde{X}_m[k]\}, \\ X_{2m+1}[k] &= \Im\{\tilde{X}_m[k]\} \end{aligned} \tag{2.7}$$

and considering a frame of M PAM symbols, (2.5) can then be reduced to

$$s[n] = \sum_{m=0}^{M-1} \sum_{k=0}^{N-1} \left(\theta_{k+m} X_m[k] p\left[n - m\frac{N}{2} \right] \right) e^{j2\pi k \frac{n}{N}}, \tag{2.8}$$

where $p[n]$ is the prototype filter. This is analogous to symbols of a PAM system that are transmitted with a time offset of half a symbol duration $T_0/2$, i.e. the effective symbol period is halved, thereby retaining the same data-rate capabilities as QAM modulated systems with symbol period T_0. The individual FBMC symbols of length L and fundamental period $T_0/2$ can then be written as:

$$x_m[n] = \sum_{k=0}^{N-1} \theta_{k+m} X_m[k] p[n - m\frac{N}{2}] e^{j2\pi k \frac{n}{N}}. \tag{2.9}$$

Eq. (2.9) allows the output signal of the FBMC modulator $s[n]$ in Eq. (2.8) to be written in terms of its constituent overlapping symbols, as

$$s[n] = \sum_{m=\left\lfloor \frac{n}{N/2} \right\rfloor -(2K-1)}^{\left\lfloor \frac{n}{N/2} \right\rfloor} x_m \left[|n|_{N/2} + \left(\left\lfloor \frac{n}{N/2} \right\rfloor - m \right) \frac{N}{2} \right], \tag{2.10}$$

with $m = [0,1,2,\cdots,M-1]$, $\lfloor x \rfloor$ representing the largest integer not greater than x and $|\cdot|_{N/2}$ is the module-$N/2$ operation.

By defining:

$$\boldsymbol{x}_m = [x_m[0],\cdots,x_m[L-1]]^T, \tag{2.11}$$

Eq. (2.10) can be used to compute the index points of the symbol set $\boldsymbol{x}_m,\ldots,\boldsymbol{x}_{m+2K-1}$, which overlap at each sample n in an FBMC modulated baseband signal $s[n]$. Equation (2.10) gives an indication of the overlapping nature of the FBMC symbols for a causal system starting at index $n = 0$. This representation is important to visualize how to perform PAPR reduction in FBMC by modifying individual symbols in a frame. Fig. 2.5 illustrates the overlapping nature of FBMC, as described by Eq. (2.10), in a frame of M symbols with an overlap factor $K = 4$ and $N = 4$ subcarriers. It should be clear that the fundamental symbol period in terms of discrete samples is $T_0/2 = N/2 = 2$.

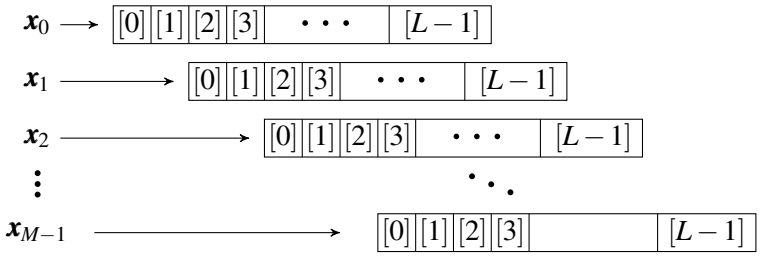

Figure 2.5: FBMC overlapping nature

FBMC can theoretically provide an increase in data throughput from OFDM. This is due to the absence of CP. The data rate can therefore be increased by a factor of v/N, where v is the length of CP required in OFDM. However, due to the absence of CP and the presence of overlapping symbols resulting in controlled ISI in FBMC, equalization becomes more complex than that of OFDM. Equalization can be performed using a simple one tap zero forcing equalizer which provides a low complexity solution. If the number of subcarriers is sufficiently large, the fading experienced per subcarrier can be estimated as flat fading and a single tap equalizer can provide reasonable performance. However,

in scenarios where a low number of subcarriers are used, the fading may not be accurately estimated to flat fading and poor performance is achieved [24]. In [24] a technique called "equalization with real interference prediction" (ERIP) is proposed which utilizes the real and imaginary interference present in FBMC to provide superior equalization performance. In [25] a minimum mean squared error based equalization method is obtained. This can be extended to an N-tap based equalizer depending on the number of subcarriers in order to retain the same performance and estimate flat fading per subcarrier. A concept known as "self-equalization", proposed in [26], has the potential to greatly decrease equalization complexity in massive multiple-input, multiple-output (MIMO) based systems. "Self-equalization" is based on the concept that combining the signal components, from different antennas, results in an averaged distortion. When applied to massive MIMO, the fading can therefore be reduced to flat fading across each subcarrier. Due to MIMO gaining popularity for use in next generation networks, the concept of "self-equalization" adds justification for the usage of FBMC as the standard for these future networks.

2.4.2 Polyphase implementation

A direct form implementation of Eq. (2.5) can be achieved using a transmultiplexer (TMUX) realisation. This is implemented using N up-samplers and a filter bank of N branches. However, filtering has to be applied to each up-sampled subcarrier branch at the higher sampling rate, greatly increasing system complexity [27]. A reduction in the complexity of the systems can be obtained with a polyphase realization employing the efficient FFT [28, 19, 29].

The output of the polyphase filtering process $Y(z)$ can be written in matrix notation as [29]:

$$Y(z) = \boldsymbol{G}^T(z)\tilde{\boldsymbol{X}}(z^{N/2}), \tag{2.12}$$

where

$$\tilde{\boldsymbol{X}}(z^{N/2}) = [\tilde{X}_0(z^{N/2})\ \tilde{X}_1(z^{N/2})\ \cdots\ \tilde{X}_{N-1}(z^{N/2})]^T \tag{2.13}$$

and

$$\boldsymbol{G} = [G_0(z)\ G_1(z)\ \cdots\ G_{N-1}(z)]^T, \tag{2.14}$$

with

$$G_k(z) = \sum_{n=0}^{L-1} p[n] e^{j\frac{2\pi k}{N}\left(m-\frac{L-1}{2}\right)} z^{-n}. \tag{2.15}$$

Making use of the low-rate polyphase filters [29]:

$$A_k(z^2) = \sum_{t=0}^{K-1} p[k+tN] z^{-2t}, \tag{2.16}$$

Eq. (2.12) can be implemented as illustrated in Fig. 2.6, where all up-sampling is moved through the filters and IFFT processes by using the multirate identity [28, 19]. This allows the filtering to be applied at a lower sampling rate, greatly reducing the number of computations required [29].

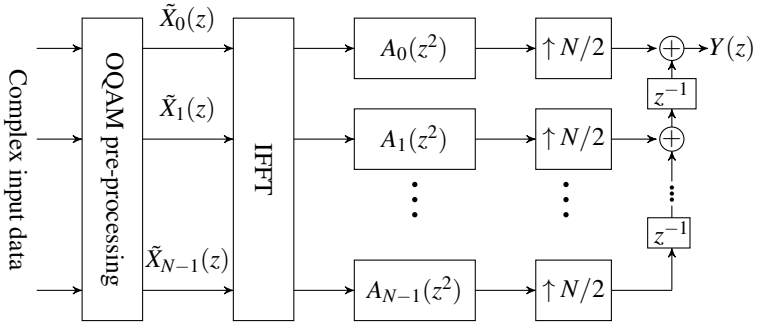

Figure 2.6: Polyphase implementation of FBMC modulator

The delay line in Fig. 2.6 is of length N whereas the up-sampling ratio is $N/2$ resulting in an effective delay line overlap. This can be seen as compensating for the rate loss due to the OQAM mapping by halving the effective symbol period $\tau_0 = T_0/2$. Ignoring the transient build up of the FBMC system, the efficiency of the system can be seen as one complex symbol per sample for a critically sampled implementation. The effective throughput is therefore equivalent to an OFDM system without cyclic prefix (CP).

2.5 PAPR IN MULTICARRIER SYSTEMS

PAPR is a logarithmic ratio of the peak transmit power to the average transmit power of a signal. For a rudimentary signal, it can be defined as

$$\text{PAPR} = 10\log\left(\frac{\text{Peak}^2}{\text{RMS}^2}\right) \tag{2.17}$$

with RMS defined as the root mean square. The PAPR of a single tone or sinusoidal signal is 3.01dB and is also referred to as constant envelope signal [30]. The application of Eq. 2.17 to a sinusoid is illustrated in Fig. 2.7.

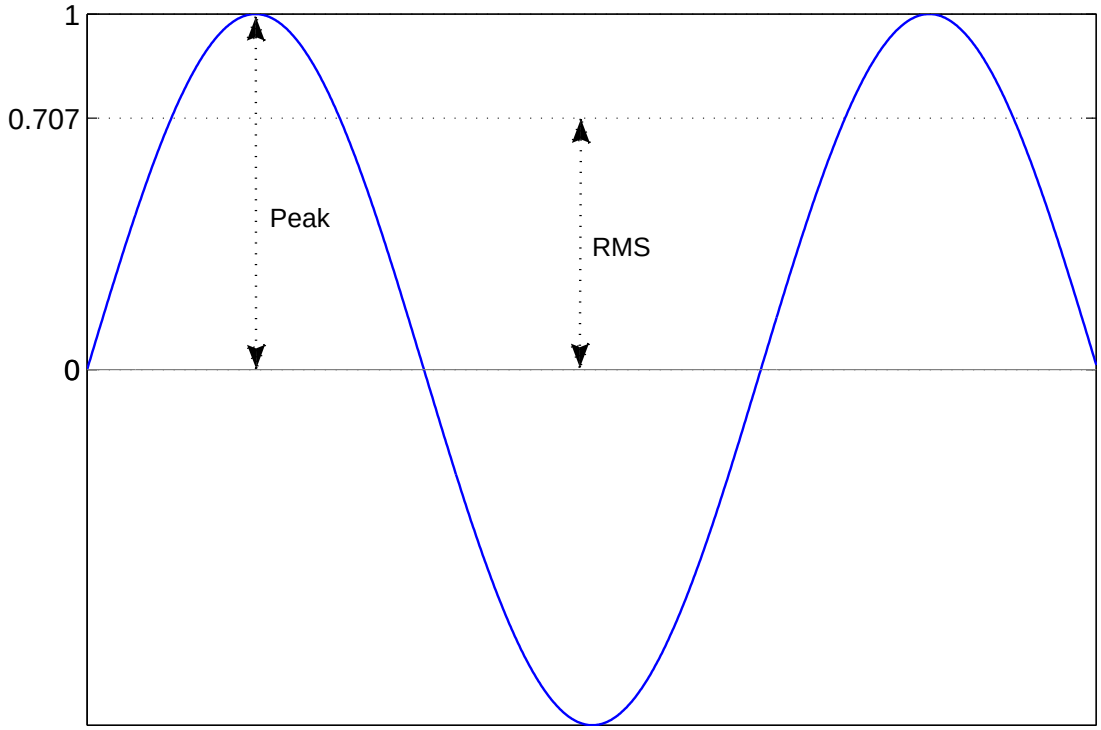

Figure 2.7: Peak and RMS of a sinusoidal signal (constant envelope)

Multicarrier transmission schemes such as OFDM and FBMC have non-constant envelopes. This is caused by the statistically random nature of the subcarrier data which after the IFFT process, can be approximated to a complex Gaussian process with statistically uncorrelated peaks [31]. The Gaussian like peaks are created as a result of the weighted sum of the independently distributed random data modulated onto the subcarriers [32]. These statistically uncorrelated peaks are impossible to predict and therefore HPAs must operate with a large input back-off so that the baseband signal always, with very high probability, remains in the linear region of the HPA.

PAPR is therefore an important metric in multicarrier transmission schemes as it is a measure of the peak to the average magnitude of samples of a signal. Systems with high PAPR require larger input back-offs on the HPAs to ensure clipping does not occur. This results in inefficient usage of the HPAs [33] which is effectively energy inefficiency translating into energy wastage and less "green" communication [34]. If clipping occurs, severe degradation of the spectral performance of the system occurs in the form of in-band and OOB distortion. In-band distortion affects your systems BER

whilst OOB distortion results in interference with neighbouring channels. An example of a high PAPR multicarrier signal is shown in Fig. 2.8. Figure. 2.8 is a section taken from an FBMC frame and the large difference between peak and RMS is clearly evident.

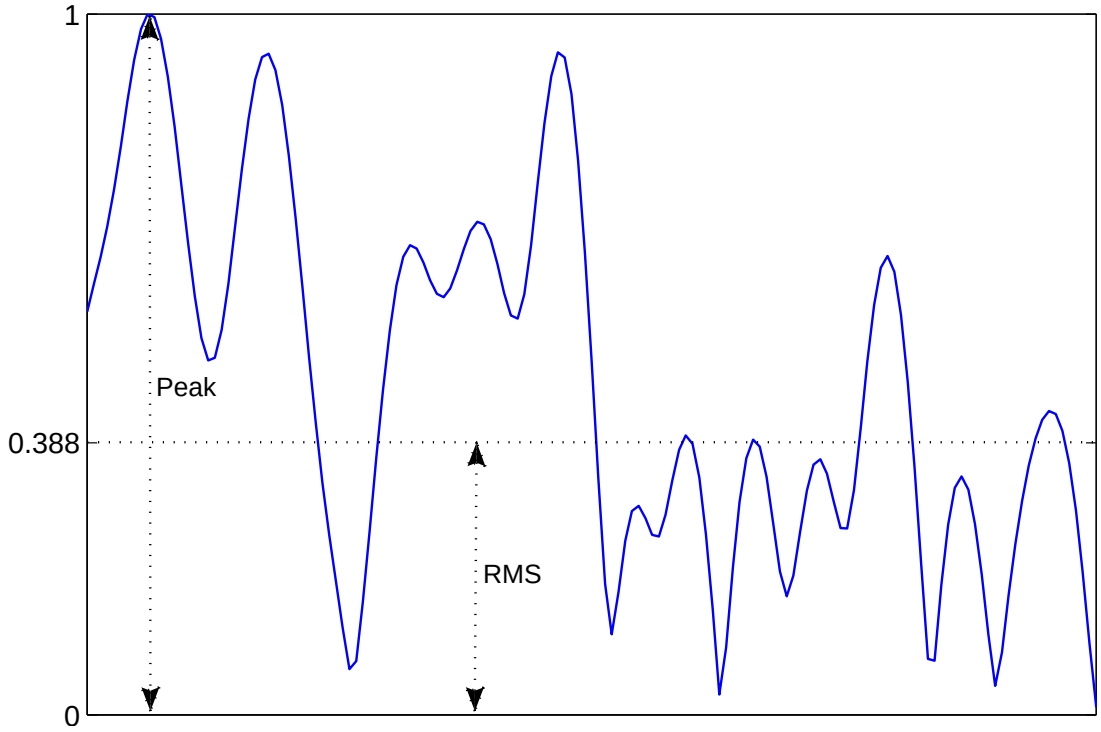

Figure 2.8: Peak and RMS of a multicarrier signal (non-constant envelope)

2.5.1 OFDM case

The PAPR for OFDM signals is defined as [31]:

$$\text{PAPR}(\mathbf{s}_m)_{dB} = 10\log\left(\frac{\max_{0\leq n\leq N-1}|\{\mathbf{s}_m\}_n|^2}{E|\mathbf{s}_m|^2}\right), \tag{2.18}$$

where $\mathbf{s}_m$ is the m-th symbol vector of length N and $E|\boldsymbol{s}_m|$ is the expected value of the m-th symbol vector.

The cumulative complementary density function (CCDF) is an established method of measure for PAPR in multicarrier systems [12]. The CCDF is defined as the probability that the PAPR of the m-th modulated symbol $\boldsymbol{s}_m$ exceeds a given threshold γ and is defined as [12]:

$$\text{CCDF}[\text{PAPR}(\boldsymbol{s}_m)] = \Pr(\text{PAPR}(\boldsymbol{s}_m) > \gamma). \tag{2.19}$$

However, it is well established in literature that in order to accurately estimate the true analogue signal, oversampling of some form needs to be performed [12, 35]. In a critically sampled system, Eq. (2.18) is therefore a very optimistic approach to the true PAPR of the symbol.

2.5.2 FBMC case

The PAPR for an FBMC symbol is slightly more complicated to analyse. Figure 2.9 illustrates the overlapping nature of FBMC symbols with $K = 4$ [9]. It is clear that after the filtering process is applied, the symbols are extended to a length of $L = KN$. To compensate for OQAM modulation, as well as the extended symbol length, the OQAM FBMC symbols are spaced $N/2$ samples apart, resulting in a symbol period of $T_0/2$ with $2K$ overlapping symbols at each sample during steady state.

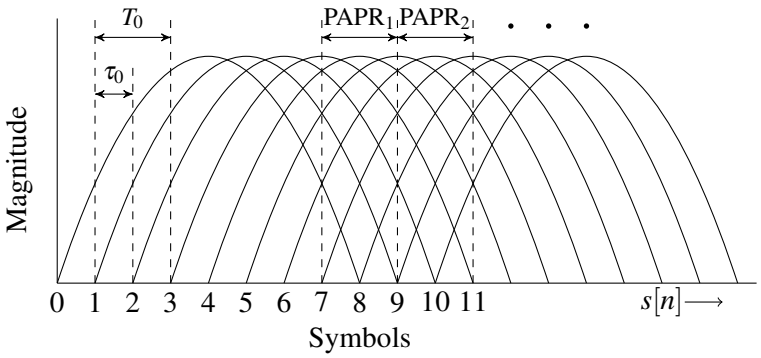

Figure 2.9: Overlapping nature of FBMC modulation

Due to the overlapping nature of FBMC, its symbols cannot be considered in isolation. Instead we define a frame containing M overlapping FBMC symbols over which the PAPR can be accurately measured. The output frame is of length $(M-1)N/2+L$. Two different measurements of PAPR can then be obtained for the FBMC system, namely the frame and symbol based PAPR. The PAPR of a frame containing M FBMC symbols, can therefore be defined, with $s[n]$ as the discrete samples, as:

$$\text{PAPR}(\mathbf{s}_l)_{dB} = 10\log\left(\frac{\max_{0\leq n\leq (M-1)N/2+L-1} |\{\mathbf{s}_l\}_n|^2}{E|\{\mathbf{s}_l\}|^2}\right) \tag{2.20}$$

where $\mathbf{s}_l = [s[0], \cdots, s[(M-1)N/2+L-1]]^T$.

For accurate PAPR comparisons to OFDM systems, the FBMC modulated signal $s[n]$ can be broken up into symbols of length T_0 over which the PAPR can be measured. However, due to the transient build up present in FBMC systems, the PAPR cannot be accurately measured at the start and end of an FBMC frame. Instead the PAPR should be measured during steady state operation of the system, ideally within a full filter length into the frame and concluding a full filter length before the end of the frame. For simulation purposes, it is necessary to consider a frame length of at least $M = 2K+1$ symbols. This allows for PAPR measurement over at least one symbol of length T_0 in the FBMC frame. Figure 2.9 illustrates the process of measuring the PAPR over two symbols of length T_0 each displayed by PAPR_1 and PAPR_2. Based on this idea, the PAPR of the v-th symbol of length T_0 in a frame, can be defined as as:

$$\text{PAPR}(\mathbf{s}_v)_{dB} = 10\log\left(\frac{\max_{0\leq n\leq N-1}|\{\mathbf{s}_v\}_n|^2}{E|\{\mathbf{s}_v\}|^2}\right) \tag{2.21}$$

where $\mathbf{s}_v = [s[L-N/2+vN],\cdots,s[L-N/2+(v+1)N-1]]^T$.

Equation (2.21) defines new symbols, S_v, over which the PAPR can be measured. If the steady state portion of the FBMC frame is split into isolated symbols, the PAPR equation reduces to the same as that of OFDM with symbol period T_0.

2.6 PAPR REDUCTION TECHNIQUES FOR OFDM

A number of methods exist for reducing the PAPR of an OFDM modulated system. These include ACE, selective mapping (SLM), partial transmit sequence (PTS), clipping and filtering, coding and tone reservation (TR) amongst others [36, 37].

All these methods work on the basic principle of reducing the PAPR of the transmit signal by distorting, clipping or adding additional side information to the signal. Unfortunately a drawback of PAPR reduction is always a decrease in the BER performance of the system. Changing the nature of a QAM modulated system, which is already at the highest efficiency achievable (in terms of Euclidean distance between bits), always results in a decrease in BER performance. Adding additional side-information also results in additional energy added to the signal which is not in the form of bit energy and therefore the efficiency of the system decreases.

The trade-off of PAPR reduction techniques is therefore an increase in the BER of the system and the

added complexity inherent in any additional signal processing required to perform the PAPR reduction techniques. Therefore the true benefits of PAPR reduction are found in systems that can minimize the PAPR, while at the same time minimize the BER degradation introduced by the PAPR reduction technique. Additional system complexity should also be avoided in order to maintain feasibility of the PAPR reduction technique.

2.6.1 The fallacy of improving BER performance through PAPR reduction

A number of papers have been published in literature which show that BER performance of systems improve after applying their proposed PAPR reduction techniques. These include "A fair comparison platform for OFDM systems with various PAPR reduction schemes" [38] which shows improved BER performance after ACE, SLM or scrambling is applied to the original OFDM envelope. The BER results however are presented as BER versus signal-to-noise ratio (SNR), instead of BER versus energy per bit (E_b/N_0). ACE increases the average transmit power of the signal and therefore the average energy per bit. Upon normalization however, the distorted constellations will lead to BER degradation. With SLM and scrambling, additional side information is required to be transmitted along with the bits. This also results in an increase in the energy required to send the same amount of bits and subsequently an increase in the BER of the signal.

In "Evaluation of Clipping Based Iterative PAPR Reduction Techniques for FBMC Systems" [39], a technique called TRACE is proposed. This combines ACE and TR methods to obtain a higher level of PAPR reduction. This paper however, also claims an improvement of almost 4dB in BER performance over the conventional signals. The simulation model appears not to have taken into account the large increase in average transmit power. Therefore no normalization was performed and as such, it would appear as though significant reduction in BER was achieved. Another factor in questions is the number of iterations being set to a mere 2000 symbols. This low number of iterations would also lead to poor confidence in the PAPR reduction or BER results.

In "Adaptive active constellation extension for PAPR reduction in OFDM systems" [40] and "Effects of clipping and filtering on the performance of OFDM" [41], it is clear that PAPR reduction methods do lead to BER degradation. These articles are amongst the few that investigate the effect that PAPR reduction has on BER performance.

2.6.2 Active constellation extension

The ACE algorithm for OFDM PAPR reduction is well documented in the literature [12, 36, 42, 43, 44]. It is an efficient method for reducing the PAPR in OFDM without requiring the transmission of side information. The idea behind projection-onto-convex-sets (POCS) of ACE involves clipping the time domain signal and correcting the distorted constellations to only allow extensions that do not decrease the minimum Euclidean distance.

Figure. 2.10 can be used to describe the fundamental principle behind the ACE technique for PAPR reduction. The grey regions represent areas into which constellations may be extended during the reconstruction phase after the planned clipping of the time domain signal. Extending the constellations into these regions results in PAPR reduction at the expense of a slight increase in average transmit power. This increase results in a degradation of the BER performance of the system. This degradation is however slightly offset by the fact that the grey regions result in an increase in the minimum Euclidean distance. The BER degradation is however a reasonable trade-off for the PAPR reduction capabilities obtained [12].

In [45] a technique called Adjustable Circle Constrain (ACC) is proposed. The ACC technique is designed to offer the benefits of the ACE technique whilst controlling the level of BER degradation. This is realized by applying a circular constraint around the original constellation positions which provides a maximum distance by which a bit can be moved away from its original position. This is in fact quite an effective way of controlling the BER degradation and based on this, the amount of BER degradation can theoretically be predicted.

The ACE POCS method for OFDM can be summarized as [12];

1. Clip the discrete OFDM modulated baseband signal $s[n]$ to an amplitude of δ, with $\phi[n]$ the phase angle of the complex signal $s[n]$ at sampling point n, such that:

$$s'[n] = \begin{cases} \delta e^{j\phi[n]}, & \text{if } |s[n]| > \delta \\ s[n], & \text{if } |s[n]| \leq \delta \end{cases}, \quad 0 \leq n \leq N-1\,. \tag{2.22}$$

2. Compute the negative of the clipped signal $c[n]$ such that

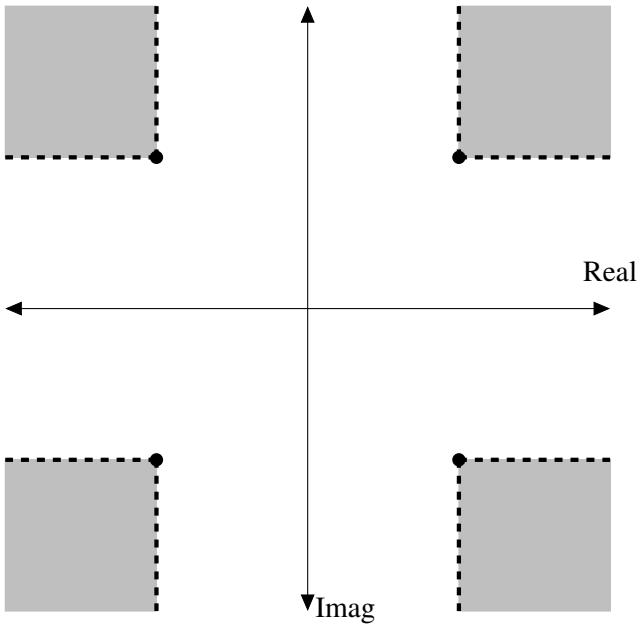

Figure 2.10: Constellation map illustrating the allowable extension regions for ACE for QPSK modulation in OFDM

$$c[n] = \begin{cases} \delta e^{j\phi[n]} - s[n], & \text{if } |s[n]| > \delta \\ 0, & \text{if } |s[n]| \leq \delta \end{cases}, \quad 0 \leq n \leq N-1\,. \tag{2.23}$$

3. Demodulate $c[n]$ to obtain the extension regions $C[k]$ with k the different subcarriers.

4. Maintain only those real or imaginary components of $C[k]$ which fall within in the allowable extension regions, i.e. those that do not decrease the minimum Euclidean distance and set the rest to zero.

5. For oversampling, set out-of-band (OOB) subcarriers to zero, i.e. null all points greater than N [46].

6. Modulate $C[k]$ to obtain the time domain portion of the corrected clipped signal $\hat{c}[n]$.

7. Scale $\hat{c}[n]$ by some constant μ and add it the original time domain signal $s[n]$ to obtain $\hat{s}[n]$ as

$$\hat{s}[n] = s[n] + \mu\hat{c}[n], \quad 0 \leq n \leq N-1. \tag{2.24}$$

8. Transmit $\hat{s}[n]$ if it meets the PAPR requirements, otherwise repeat from step (1) replacing $s[n]$ with $\hat{s}[n]$.

2.6.2.1 Smart gradient-project ACE

The POCS ACE method requires a large number of iterations to obtain a suitably low PAPR. The smart gradient-project (SGP) method was designed to greatly reduce the number of iterations required to obtain a low PAPR. SGP allows to find an optimal scaling factor μ to scale the clipped portions of the signal.

The POCS implementation of ACE involves a scaling factor μ of unity being applied to the clipped portion of the signal, which is added back to the original signal as in Eq. (2.24). The smart gradient-project algorithm was developed in [12] and scales the added portion of the signal $\hat{c}[n]$ by an optimal scaling factor. This greatly reduces the number of iterations required for the ACE algorithm to converge to a low PAPR. This is done by finding the maximum scaling value possible without causing peak regrowth of the signal. The algorithm can be summarized in the following steps [12];

1. Find the peak of the signal, P, as well as the peak position n_{peak}.

2. Calculate the projections $\bar{c}_{[}n]$ of the clipped signal $\hat{c}[n]$ by performing the dot product:

$$\bar{c}[n] = \frac{\Re\{\hat{c}[n] \cdot s[n]\}}{|s[n]|}, \tag{2.25}$$

for

$$0 \leq n \leq N-1.$$

3. Consider only the values of $\bar{c}[n]$ that are positive and therefore result in magnitude growth.

4. Compute the scaling factor for each of these projections:

$$\mu[n] = \frac{P - |s[n]|}{\bar{c}[n] - \bar{c}[n_{\text{peak}}]}, \quad n \neq n_{\text{peak}}. \tag{2.26}$$

5. Use the minimum value of $\mu[n]$ (so that no peak regrowth occurs), namely:

$$\mu = min(\mu[n]). \tag{2.27}$$

6. Scale the clipped signal $\hat{c}[n]$ by μ and add it to the original signal to obtain the new transmit signal:

$$\hat{s}[n] = s[n] + \mu\hat{c}[n], \quad n = [0, 1, \cdots, N-1]. \tag{2.28}$$

7. If μ is negative, stop the iterative ACE algorithm, as any further PAPR reduction attempts will result in peak regrowth.

2.6.3 Tone reservation

Tone reservation is a PAPR reduction technique that utilizes reserved subcarriers in order to reduce the PAPR of a multicarrier signal [32, 47, 48]. Much like the ACE algorithm, pre-transmission clipping and constellation reconstruction is utilized in order to limit the PAPR of the time domain baseband signal. However, the major difference is derived from the usage of reserved tones instead of distorted constellations. This is illustrated in Fig. 2.11 where subcarrier 3,6 and 9 are the reserved subcarriers for PAPR reduction. The exact positioning of the reserved tones does not play a significant role in the PAPR reduction performance of TR techniques and is often randomly pre-selected.

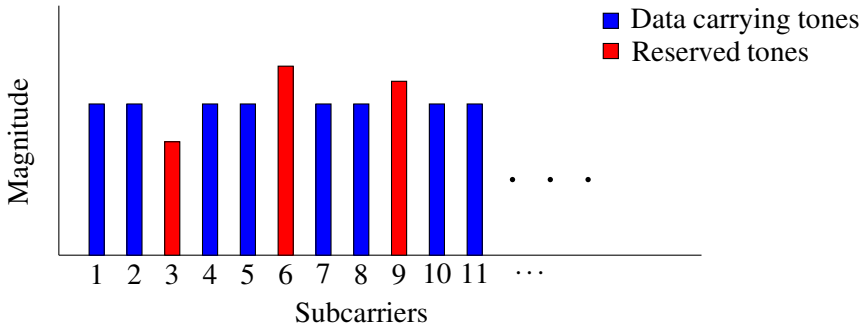

Figure 2.11: Reserved subcarriers in tone reservation for PAPR reduction

The TR technique can be summarized in the following steps;

1. Clip the baseband signal $s[n]$ to a threshold value δ as in step 1 for POCS ACE.

2. Demodulate the clipped signal to obtain the distorted subcarriers.

3. Return all data carrying subcarriers to their initial values to avoid distortion of these carriers, whilst holding the reserved tones at their distorted values. New frequency domain subcarriers are therefore obtained, which include the undistorted data carrying subcarriers as well as the distorted reserved subcarriers.

4. Remodulate the new frequency domain carriers to obtain $\hat{s}[n]$.

The main benefit claimed from this technique is that the data carrying subcarriers are not distorted and therefore the BER of the system is not degraded [47]. However this statement is incorrect. In TR, a percentage of the data carrying subcarriers are subcarriers. This leads to a drop in bandwidth efficiency and therefore the BER will in fact be degraded upon normalization. This is clear in the BER graphs presented in [47]. The reserved subcarriers can be seen as the transmission of additional side information, ergo a decrease in the data transmission rate resulting in an effective increase in the BER.

Standard TR has the same drawback as POCS ACE, namely a slow convergence time to a low PAPR for the baseband time domain signal [32]. In [32] it is proposed to use a gradient project method much in the same format as that of SGP ACE in order to speed up convergence time.

2.6.4 Selective mapping

Selective mapping is a technique whereby M different OFDM signals are generated, representing the same data, and the signal with the lowest PAPR is chosen and transmitted [49]. This is achieved by creating a set of M different phase rotated vectors by which the original subcarriers are multiplied as shown in Fig. 2.12. Thereafter each vector is modulated and the signal with the lowest PAPR is chosen as the transmit signal. This technique exploits the statistical independence of phase rotated subcarriers thus guaranteeing time domain signals with different PAPR values [49].

In order to reduce complexity, the phase rotation vectors are normally in multiples of $\pi/2$. The complexity of this technique stems from the need for M modulators, in order to acquire the M time domain signals. Another drawback is the need for side-information, as the receiver is required to know which sequence was transmitted in order to demodulate using the same phase rotation vectors. This side information is critical for accurate demodulation and therefore the side-information will require

additional levels of coding, in order to protect it against corruption. Techniques have been proposed, such as in [50], to reduce the dependency of the SLM technique on side-information. However this technique comes at the expense of additional complexity in the form of scramblers and interleavers which will need to be applied at the transmitter and the reverse operation at the receiver.

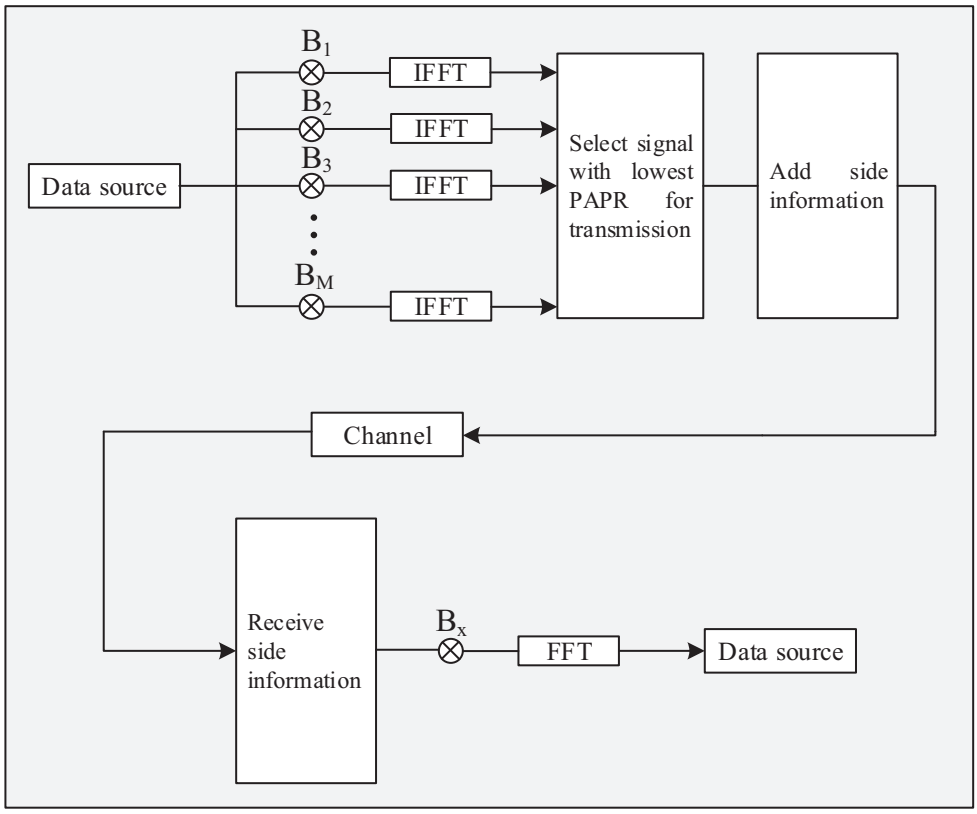

Figure 2.12: SLM technique for OFDM

When channel encoding the data, no side-information is required. At the receiver, M decoders are utilized and decode the received signal with each of the M possible phase rotated vectors [49]. However on the receiver side there are often space limitations on chips especially in mobile environments. This may lead to undesirable usage of limited processing power.

2.6.5 Partial transmit sequence

The partial transmit sequence technique involves partitioning the OFDM subcarriers into M disjointed frames. Each frame is then multiplied by an optimal rotational factor and then combined, in order to obtain a transmit signal with a lower PAPR [51]. The technique is detailed in Fig. 2.13 PTS is an optimization problem and the main complexity stems from searching for the optimal phase rotation

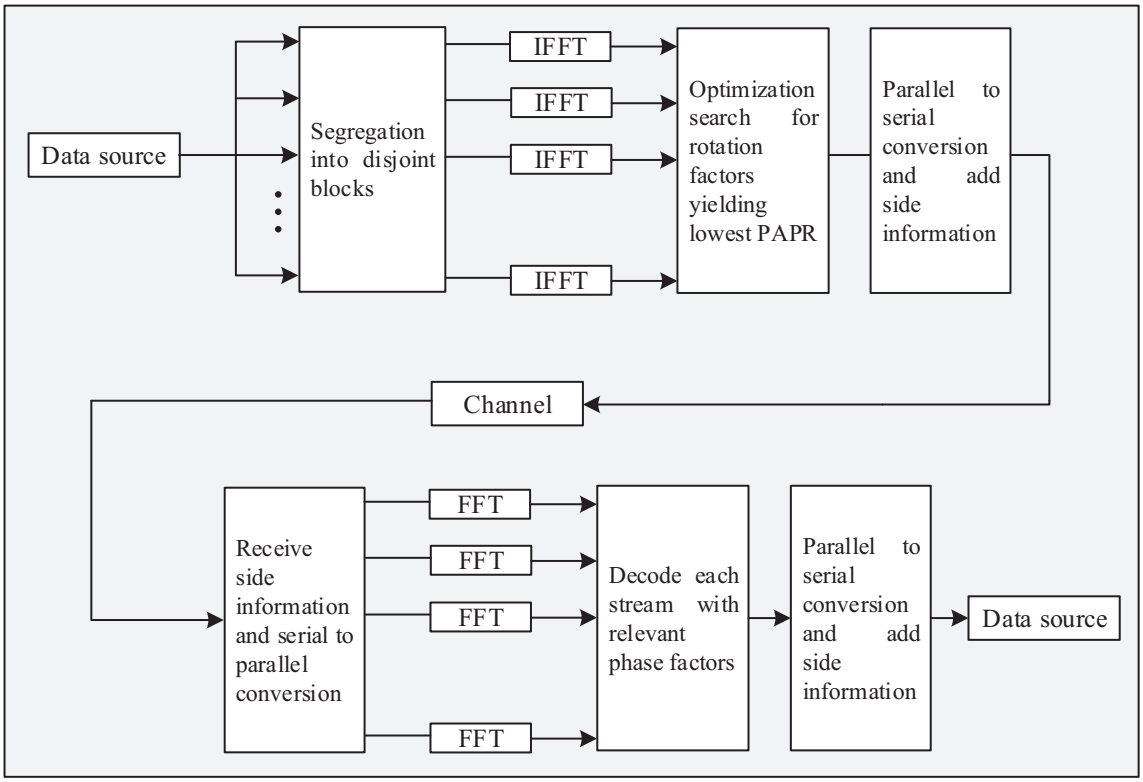

Figure 2.13: PTS technique for OFDM

vector which reduces the PAPR by the largest amount. By increasing the number of disjointed frames M and the number of possible phase rotation factors W, the PAPR reducing capability increases, however the complexity of the search algorithm increases exponentially with M [36]. That is to say the complexity is of the form $O(W^M)$. In order to reduce this, techniques normally utilize only two or four possible rotation factors and limit the number of disjoint frames, namely $W \leq 4$ and $M \leq 4$. A number of papers exist to reduce the computational complexity of the PTS technique. In [52] a threshold limit is set to avoid needless searching once the aimed PAPR performance is achieved. In [53] a smart search algorithm is used to reduce the complexity of searching for the optimal phase factors.

As with SLM, PTS requires the transmission of side information to accurately demodulate the data carrying subcarriers at the receiver and therefore suffers from same drawbacks, namely higher rate codes to guarantee reception of these bits.

2.7 PAPR REDUCTION TECHNIQUES FOR FBMC

A limited number of techniques to date have been proposed for FBMC techniques. This is due to the relatively underdeveloped FBMC modulation technique, in comparison with the well established OFDM technique. FBMC has only been adopted into a low number of standards with opportunistic communication in cognitive radio applications appearing to be the most promising. However, as the FBMC technique evolves and processing power increases, FBMC might still be incorporated into next generation telecommunication architectures, due to its attractive properties.

A major drawback of FBMC PAPR reduction techniques is the increase in complexity associated with the additional signal processing normally required in such techniques. The increased processing power required, on top of an already complex technique like FBMC, often leads to these techniques being infeasible for real life applications.

PAPR reduction in FBMC is also plagued with the added complexity of overlapping symbols. This makes single symbol processing difficult as symbols can not be considered in isolation. PAPR reduction techniques for FBMC therefore require a buffer of the length of multiple symbols in order to pre-process and perform PAPR reduction on them. This may possibly lead to an undesired increase in system latency.

The techniques listed in the following subsections, are the most noticeable techniques from literate for FBMC PAPR reduction. This is not a conclusive list, but the relatively low number of citations highlights the current gap in PAPR reduction research for FBMC. They include orthogonal selective mapping (OSLM), sliding window tone reservation (SW-TR), multi-block joint optimization (MBJO), TR and ACE.

2.7.1 Orthogonal selective mapping

In [9] it is proposed that the SLM technique can be adapted for use in FBMC systems. A technique called OSLM is proposed. This technique proposes searching over a longer overlapping interval in order to capture the overlapping properties of FBMC. Therefore contiguous symbols must be modulated in order to exploit the overlapping nature of FBMC. However [9] points out the main drawback with PAPR reduction in FBMC. In order to achieve an optimal solution, using SLM, a huge amount of memory and computational power must be utilized.

It is clear from the results in [9] that as the length of the prototype filter increase, the performance of the OSLM technique gets substantially worse. This is most likely caused by the need to increase the number of codes U utilized in order to achieve a suboptimal solution. Due to complexity increasing exponentially with the U, it is simulated to a maximum of $U = 4$ which provides poor performance when the overlapping factor K, is 4 or larger.

2.7.2 Sliding window tone reservation

The technique proposed in [11] is a SW-TR technique. This technique is a clipping based technique that, much like TR for OFDM, utilizes reserved subcarriers (or tones) to counteract the peaks in the original FBMC signal. A sliding window is utilized in order to clip the FBMC over an interval of the window length. In each interval, the FBMC signal is clipped and reserved tones are created before moving the filter onto the next segment. The window is shifted by a factor smaller than the length of the window. Therefore the window effectively overlaps on each shift with the previous window position.

The SW-TR technique does not have the added complexity of optimization and search algorithms. Due to the window stretching a larger length than an effective symbol period, in FBMC systems, the overlapping nature of FBMC is accounted for. This leads to a lower level of complexity and improved results over the OSLM and the multi-block joint optimization (MBJO) techniques.

This technique will suffer from the same drawbacks as TR for OFDM namely a decrease in BER performance of the system. Due to the addition of non-data carrying subcarriers, a lower throughput is to be expected which results in an effective increase in the BER of the system (energy is used for non-data carrying tones).

2.7.3 Multi-block joint optimization

The MBJO technique in [10] utilizes a dynamic programming (DP) optimization based PTS technique. The DP algorithm is employed to find the most optimal phase rotation factors that can be utilized in order to reduce the PAPR of the signal. This technique provides good results as the overlapping nature of FBMC is fully accounted for. However this performance, much like PTS for OFDM, is at the expense of an exponential increase in complexity with an increase in prototype filter length and number of phase factors used.

Optimization techniques are plagued with a fundamental increase in system complexity. This is clear from the trellis diagram depicted in [10] showing the possible states in the MBJO technique. As the number of sub-blocks V and the number of possible phase factors W increases, the trellis will become exponentially more complex. The complexity of the scheme is claimed to be $O(NW^V)$ which may be infeasible for practical implementations.

2.7.4 Tone reservation and ACE

In [39] a combined ACE and TR technique is presented called TRACE. The idea is to reduce the PAPR even further through the combined effects of TR and ACE, hence some subcarriers are reserved for PAPR reduction only and the rest have ACE applied to them. In [39] a significant PAPR reduction is claimed through the use of the TRACE technique.

The article however cites some misconceptions common to many PAPR reduction techniques. In [39] an improvement in BER performance is claimed along with very good PAPR reduction performance. This is counterintuitive as an increase in distortion as well as adding reserved tones, reduces the data carrying efficiency of the system and hence the BER is degraded. This claimed improvement could be attributed to improper normalization of the signal energy after the PAPR reduction is performed whilst the good PAPR reduction performance could possibly be attributed to a poor simulation platform employing a low number of iterations.

2.7.5 Partial transmit sequence

Partial transmit sequence has also been successfully simulated for FBMC systems. In [54] a technique called segmental PTS (S-PTS) is proposed. This technique follows the same principle as PTS for OFDM by searching for an optimal phase rotation vector for each symbol. However, due to FBMC containing overlapping symbols, the overlapping signal is first obtained and the segmented into multiple symbols. This allows for the effect of the overlap to be taken into consideration when performing a search for the phase rotation vectors. Unfortunately the same drawbacks inherent to PTS exist here, namely that the best searching method is an exhaustive search which can be massively complex.

2.7.6 Clipping and its iterative compensation

In [55] a clipping method is proposed which compensates for the clipping noise in order to increase the system performance. Channel coding is used at the transmitter and iterative Bussgang noise cancellation (BNC) is applied at the receiver. The BNC receiver is modified to accommodate FBMC based systems and the BER performance approaches that of unclipped FBMC signals. This demonstrates that through compensation methods, such as BNC, the BER performance lost due to clipping can be recovered at the receiver. The drawback is the increase in computational complexity of the receiver in order to perform an iterative decoding function.

2.8 CONCLUSION

It is clear from this chapter that PAPR reduction in OFDM systems is a well researched topic. However, PAPR reduction research as applied to FBMC systems is still in an infant stage. This is evident from the number of citations presented. Table. 2.1 summarizes the characteristics of the different PAPR reduction techniques. It is evident that all the techniques provide decent PAPR reduction performance and the trade-off comes into play with complexity, BER degradation or data rate loss (bandwidth efficiency).

The following chapter introduces the author's proposed techniques for PAPR reduction in FBMC systems. A thorough explanation, detailed mathematical models as well as examples are provided in this chapter.

Table 2.1: PAPR comparisons of the various techniques discussed

	OFDM			
Technique	PAPR performance	BER degradation	Data rate loss	Complexity
ACE	Good	Yes	No	Low
TR	Good	No	Yes	Low
SLM	Good	No	Yes	High
PTS	Good	No	Yes	High
	FBMC			
OSLM	Good	No	Yes	High
SW-TR	Good	No	Yes	Medium
MBJO	Good	No	Yes	High
TRACE	Poor	Yes	Yes	Medium
S-PTS	Good	No	Yes	High
BNC	Good	Yes	Yes	Medium

CHAPTER 3 PROPOSED METHODS FOR FBMC SYSTEMS

3.1 CHAPTER OVERVIEW

This section provides a background on how ACE can be utilized in FBMC systems. Thereafter the novel PAPR reduction methods proposed in this thesis, namely the two optimization based techniques and the two SGP based techniques, are introduced. The optimization techniques form a basis for mathematical evaluation with emphasis placed on the optimization problem and tight constraints from which the core of the SGP methods are deduced. The optimization problem is derived in the same fashion as that proposed in [12] however with a mathematical problem created for FBMC systems.

3.2 PAPR REDUCTION USING ACE FOR FBMC

The POCS ACE method can easily be adapted to be employed in FBMC systems. Due to the FBMC transmit signal being composed of multiple overlapping symbols, it is infeasible to apply clipping and rectification on a symbol-by-symbol basis. Therefore a frame based method is proposed, whereby the FBMC modulated signal is clipped in a continuous manner and no distinction is made between symbols until the demodulation step. The frame is comprised of multiple overlapping symbols and is required for simulation purposes in order to clearly distinguish between the start and end of transmission. This is achieved by following similar steps used in POCS ACE for OFDM where $s_l[n]$ is representative of an FBMC modulated baseband frame containing M symbols. POCS for FBMC can then be summarized as follows;

1. Clip the discrete FBMC modulated baseband frame $s_l[n]$ to an amplitude of δ such that

$$s_l'[n] = \begin{cases} \delta e^{j\phi[n]}, & \text{if } |s_l[n]| > \delta \\ s_l[n], & \text{if } |s_l[n]| \leq \delta \end{cases}, \quad 0 \leq n \leq (M-1)N/2+L-1\,. \tag{3.1}$$

2. Compute the negative of the clipped frame $c_l[n]$ such that:

$$c_l[n] = \begin{cases} \delta e^{j\phi[n]} - s_l[n], & \text{if } |s_l[n]| > \delta \\ 0, & \text{if } |s_l[n]| \leq \delta \end{cases}, \quad 0 \leq n \leq (M-1)N/2+L-1\,. \tag{3.2}$$

3. Demodulate $c_l[n]$ to obtain the extension regions $C_{l,m}[k]$ where m and k represent the frequency domain symbol and subcarrier, respectively, of the FBMC frame l.

4. Maintain only the real components of the PAM symbols $C_{l,m}[k]$ which fall within the allowable extension regions and set the rest to zero.

5. For oversampling or digital frequency domain filtering, set OOB components to zero, i.e. null all subcarriers greater than N [46].

6. Modulate $C_{l,m}[k]$ to obtain the time domain portion of the corrected clipped frame $\hat{c}_l[n]$.

7. Scale $\hat{c}_l[n]$ by some constant μ and add it to the original time domain signal $s_l[n]$ to obtain $\hat{s}_l[n]$

$$\hat{s}_l[n] = s_l[n] + \mu \hat{c}_l[n], \quad 0 \leq n \leq (M-1)N/2+L-1 \tag{3.3}$$

8. Transmit $\hat{s}_l[n]$ if it meets PAPR requirements, otherwise repeat from step (1) replacing $s_l[n]$ with $\hat{s}_l[n]$.

The adapted algorithm for FBMC has to maintain "real-only" PAM constellations as is required by FBMC-OQAM. This is achieved in step 4 above and the resultant extended constellations can be seen in Fig. 3.1. The red cross in Fig. 3.1 illustrate the original constellation points on the unity PAM circle and the blue circles illustrate the distorted constellations in the allowable direction i.e. no constellation points are distorted in a way that reduces the euclidean distance below unity. Figure 3.2 illustrates the ACE methods for 16-QAM equivalent FBMC systems. For this 16-QAM equivalent, there is no distortion on the inner constellations much like ACE as applied in 4-PAM OFDM systems.

This can be seen by noting that all the constellation points of the inner constellation exist on the unity circle (the red cross in Fig. 3.2.

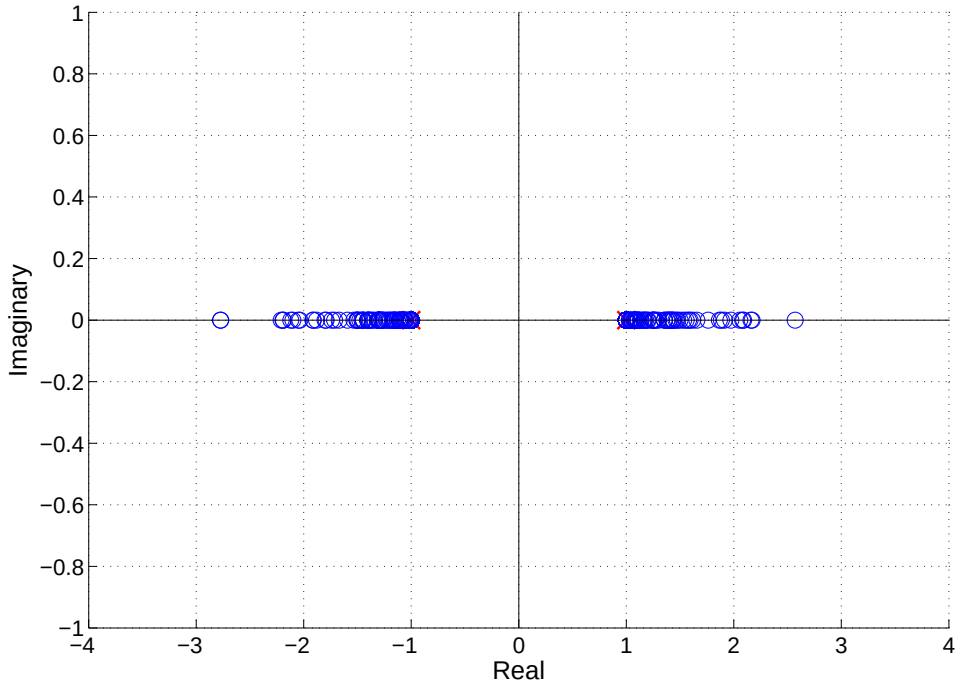

Figure 3.1: Extended real-only constellations for FBMC (QPSK equivalent)

The implementation of SGP ACE for OFDM systems is relatively straight forward due to discrete symbols being obtained without an overlap. However, the nature of FBMC systems results in multiple overlapping symbols and therefore an SGP implementation would require searching for multiple optimal scaling factors requiring additional signal processing. No method currently exists to expand an SGP type implementation of ACE to FBMC. A contribution of this paper is to propose a vectorial extension to the optimal scaling factor μ for the FBMC frame of M symbols. The main objective of this strategy is to speed up convergence as proposed in [12] for OFDM.

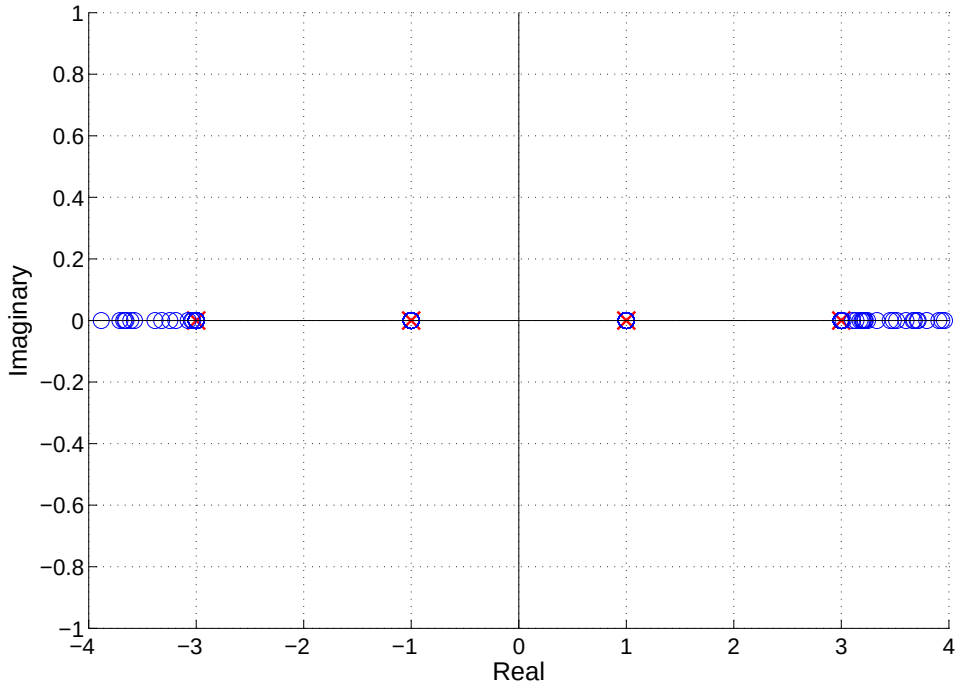

Figure 3.2: Extended real-only constellations for FBMC (16-QAM equivalent)

3.3 NOVEL PAPR REDUCTION TECHNIQUES FOR FBMC

The proposed PAPR reduction techniques are based on current ACE methods expanded to FBMC applications. Eq. (3.3) allows for scaling of the clipped portion $\hat{c}_l[n]$ by a single scaling value across the entire frame, i.e. all symbols in the frame will be scaled by the same value. This strategy does not lead to the best performance since the frame is made up of M overlapping symbols which may be scaled independently.

The main goal is to reduce the number of ACE iterations required to obtain a low PAPR, by finding an extended vectorial scaling factor. This scaling vector allows for independent scaling of each overlapping symbol effectively adding an additional handle, by which the PAPR can be mitigated, at the expense of additional signal processing.

We can rewrite Eq. (3.3) using a different scaling factor μ_m for each corresponding symbol of the frame as:

$$\hat{\mathbf{s}}_l = \mathbf{s}_l + \hat{\mathbf{C}}_l^T \boldsymbol{\mu} \tag{3.4}$$

$$\boldsymbol{s}_l = \begin{bmatrix} s[0], & \cdots & , s[(M-1)N/2+L-1] \end{bmatrix}^T, \tag{3.5}$$

$$\hat{\boldsymbol{C}}_l = \begin{bmatrix} \hat{c}_{l,0}[0] & \hat{c}_{l,0}[1] & \cdots & \hat{c}_{l,0}[N/2] & \cdots & \hat{c}_{l,0}[L-1] & 0 & \cdots \\ 0 & 0 & \cdots & \hat{c}_{l,1}[0] & \cdots & \hat{c}_{l,1}[L-N/2-1] & \cdots & \cdots \\ \vdots & & & & \ddots & & & \vdots \\ 0 & & \cdots & & \hat{c}_{l,M-1}[0] & \cdots & & \hat{c}_{l,M-1}[L-1] \end{bmatrix} \tag{3.6}$$

$$\hat{c}_{l,m}[n] = \sum_{k=0}^{N-1} \theta_{k+m} C_{l,m}[k] p[n - m\frac{N}{2}] e^{j2\pi k \frac{n}{N}} \tag{3.7}$$

and

$$\boldsymbol{\mu} = \begin{bmatrix} \mu_0 & \mu_1 & \cdots \mu_{M-1} \end{bmatrix}^T. \tag{3.8}$$

From Eq. (3.4), it is clear that the new baseband FBMC signal, after PAPR reduction, is a function of the individual overlapping clipped symbols, shown by the rows of matrix $\hat{\boldsymbol{C}}_l$ and scaled by their relevant scaling factor $\mu_0 \cdots \mu_{M-1}$. This is then added to back the original FBMC signal $\boldsymbol{s}_l$.

To obtain the discrete FBMC clipped symbol components of $\hat{\boldsymbol{C}}_l$, the individual FBMC symbols must be modulated in a non-contiguous manner. This is required to take into account the effect that each clipped signal has on the original signal looking for the optimal μ_m for $0 \leq m \leq M-1$. This process reduces much of the efficiency associated with the polyphase implementation.

Figure 3.3 illustrates the effective overlap of the clipped portions superimposed over the original baseband signal. Each sample of $\hat{\boldsymbol{s}}_l$ can then be seen as a function of the original baseband signal $\boldsymbol{s}_l$, as well as $2K$ samples of the overlapping clipped symbols $\hat{c}_{l,m}[n]$. Convergence time can therefore be decreased by optimizing μ_m to increase the effect that the clipped signals have on reducing the peaks in the original baseband signal. However, the μ_m must be scaled carefully in order to avoid peak regrowth.

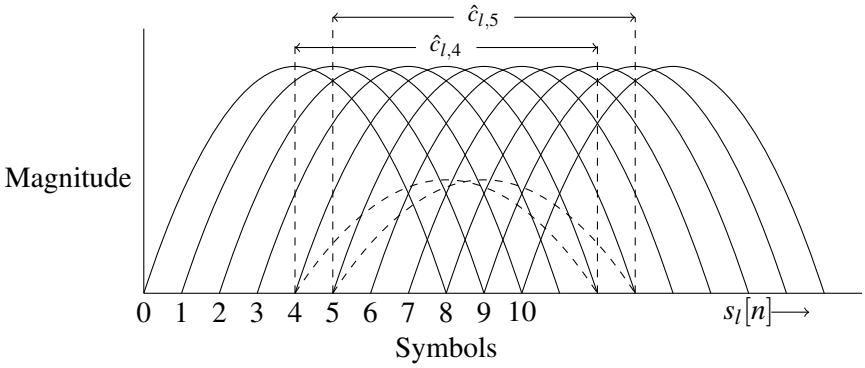

Figure 3.3: Clipped signals superimposed over original FBMC modulated signal

3.4 LP BASED OPTIMIZATION

Two methods are proposed, based on an LP optimization formulation, for finding the optimal scaling factors μ_m. In order to provide the largest amount of PAPR reduction, the optimization aims to maximize the μ_m scaling factors. The scaling factor is applied to the negative of the clipped portion of the signal and therefore is equivalent to minimizing the peaks of the signal. Constraints have to be placed on the μ_m values in order to prevent peak regrowth and provide tight bounds on the LP formulation which guarantees convergence to a lower or equal PAPR per iteration.

The second term of the right hand side of Eq. (3.4) can be written as:

$$\hat{\boldsymbol{C}}_l^T \boldsymbol{\mu} = \sum_{m=\left\lfloor \frac{n}{N/2} \right\rfloor -(2K-1)}^{\left\lfloor \frac{n}{N/2} \right\rfloor} \mu_m \hat{c}_{l,m} \left[|n|_{N/2} + \left(\left\lfloor \frac{n}{N/2} \right\rfloor - m \right) \frac{N}{2} \right], \tag{3.9}$$

with

$$n = [0, \cdots, (M-1)N/2 + L - 1], \quad m = [0, 1, 2, \cdots, M-1]. \tag{3.10}$$

It should be noted that in order to keep the symbol causal and to limit the frame length, the summation limits in Eq. (3.9) are limited by the constraints for m in Eq. (3.10). For example, a critically sampled

FBMC system with $N = 16$ subcarriers and a frame length of $M = 25$,

$$\begin{aligned}\{\hat{\boldsymbol{C}}_l^T \boldsymbol{\mu}\}_{150} &= \mu_{11}\hat{c}_{l,11}[62] + \mu_{12}\hat{c}_{l,12}[54] + \mu_{13}\hat{c}_{l,13}[46] + \mu_{14}\hat{c}_{l,14}[38] \\ &+ \mu_{15}\hat{c}_{l,15}[30] + \mu_{16}\hat{c}_{l,16}[22] + \mu_{17}\hat{c}_{l,17}[14] + \mu_{18}\hat{c}_{l,18}[6],\end{aligned} \tag{3.11}$$

with $\{\cdot\}_n$ representative of the n-th component of the vector. Equation (3.11) is an example which provides insight into the constituent components of the FBMC signal at the 150^{th} discrete sampling point. It is fundamentally important to understand the signal composition when applying a PAPR reduction scheme, to the FBMC system, as any alterations or distortion to the original symbols will have an effect on all of the sampling points which contain these constituent symbols. Once the compositional make up of the signals is understood, it is possible to manipulate the original symbols in order to meet certain constraints and improve on the PAPR of the signal. The following subsections go into the details of the proposed LP based PAPR reduction techniques.

3.4.1 LP formulation 1

The aim of LP 1 is to minimize the largest peak in an FBMC frame. Therefore only a single reference peak is chosen, namely the largest one in the frame. The optimization problem then prevents peak regrowth from scaling any of the other discrete sampling points larger than the magnitude by which the reference peak is reduced.

In order to prevent peak regrowth, the constraints for each sampling point are written in terms of the μ_m scaling factors. The constraints for sample n of frame l, with n_{peak} the position of the peak,can be written as;

$$\begin{gathered}\left|\left|s_l[n] + \{\hat{\boldsymbol{C}}_l^T \boldsymbol{\mu}\}_n\right|\right| \leq \left|\left|s_l[n_{\text{peak}}] + \{\hat{\boldsymbol{C}}_l^T \boldsymbol{\mu}\}_{n_{\text{peak}}}\right|\right|, \\ n = [0, 1, 2, \cdots, (M-1)N/2 + L - 1],\end{gathered} \tag{3.12}$$

with

$$\{\hat{\boldsymbol{C}}_l^T \boldsymbol{\mu}\}_{n_{\text{peak}}} = \sum_{m=\left\lfloor \frac{n_{\text{peak}}}{N/2} \right\rfloor - (2K-1)}^{\left\lfloor \frac{n_{\text{peak}}}{N/2} \right\rfloor} \mu_m \hat{c}_{l,m} \left[|n_{\text{peak}}|_{N/2} + \left(\left\lfloor \frac{n_{peak}}{N/2} \right\rfloor - m \right) \frac{N}{2} \right]. \tag{3.13}$$

Equation (3.12) implies that at each sample n, the magnitude of the baseband transmit signal $s_l[n]$, combined with the scaled $2K$ clipped symbols overlapping at n ($\{\hat{\boldsymbol{C}}_l^T \boldsymbol{\mu}\}_n$), cannot exceed the value of the peak of the frame, when combined with the scaled clipped symbols overlapping at the peaks position, as indicated on the right hand side of (3.12). Consequentially, the sample cannot be increased to a magnitude larger than that of the peak after it has been reduced. These constraints limit possible peak regrowth and place a tight upper bound on the problem formulation.

In order to reduce the complexity of an LP based method, it is desirable to have purely real samples. However, the output of the FBMC modulator is a complex baseband signal $s[n]$. For this reason, utilizing a similar approach to that of [12], the magnitude of the sample $||s[n]||$ and the projections of the clipped symbols onto the original signal $\bar{c}_m[n]$ are used, in order to obtain real values for the optimization problem. These projections provide good approximations of the magnitude of the clipped symbols in the same direction as the original signal and can be calculated as in [12];

$$\bar{c}_{l,m}[n] = \frac{\Re\{\hat{c}_{l,m}[n] \cdot s_l[n]\}}{||s_l[n]||}. \tag{3.14}$$

Equation (3.14) can be used to estimate Eq. (3.12) by replacing $\{\hat{\boldsymbol{C}}_l^T \boldsymbol{\mu}\}_n$ with $\{\bar{\boldsymbol{C}}_l^T \boldsymbol{\mu}\}_n$. The new equation is therefore purely real in nature as it is representative of magnitude only and can be written as

$$||s_l[n]|| + \{\bar{\boldsymbol{C}}_l^T \boldsymbol{\mu}\}_n \leq ||s_l[n_{\text{peak}}]|| + \{\bar{\boldsymbol{C}}_l^T \boldsymbol{\mu}\}_{n_{\text{peak}}}, \quad \text{for } n = 0, \cdots, (M-1)N/2 + L - 1, \tag{3.15}$$

with $\bar{\boldsymbol{C}}_l$ a matrix of the same form as Eq. (3.6) with $\hat{c}$ replaced by $\bar{c}$. After moving the constants to the right hand side and the variables to the left, Eq. (3.15) can be written as:

$$\{\bar{\boldsymbol{C}}_l^T \boldsymbol{\mu}\}_n - \{\bar{\boldsymbol{C}}_l^T \boldsymbol{\mu}\}_{n_{\text{peak}}} \leq ||s_l[n_{\text{peak}}]|| - ||s_l[n]||. \tag{3.16}$$

Equation (3.15) provides a tight upper bound for the LP problem. To guarantee convergence a lower bound is also required in the optimization formulation. A good lower bound can be formulated by ensuring that the negative of the absolute value of the scaled samples at each sampling point are

greater than the negative of the absolute value of the scaled peak. This can be formulated by adding an extra set of $(M-1)N/2+L$ constraints:

$$-||s_l[n]|| + \{\bar{\boldsymbol{C}}_l^T \boldsymbol{\mu}\}_n \geq -||s_l[n_{\text{peak}}]|| + \{\bar{\boldsymbol{C}}_l^T \boldsymbol{\mu}\}_{n_{\text{peak}}} \quad \text{for } n = 0, \cdots, (M-1)N/2+L-1. \tag{3.17}$$

As in Eq. (3.16), (3.17) can be written with all constants on the right and variables on the left resulting in the final optimization formulation being written as:

$$\max \text{ z} = \mu_0 + \mu_1 + \cdots + \mu_{M-1}, \tag{3.18}$$

s.t.

$$\{\bar{\boldsymbol{C}}_l^T \boldsymbol{\mu}\}_n - \{\bar{\boldsymbol{C}}_l^T \boldsymbol{\mu}\}_{n_{\text{peak}}} \leq ||s_l[n_{\text{peak}}]|| - ||s_l[n]||, \quad \text{for } n = 0, \cdots, (M-1)N/2+L-1, \tag{3.19}$$

$$\{\bar{\boldsymbol{C}}_l^T \boldsymbol{\mu}\}_n - \{\bar{\boldsymbol{C}}_l^T \boldsymbol{\mu}\}_{n_{\text{peak}}} \geq -||s_l[n_{\text{peak}}]|| + s_l[n]|| \quad \text{for } n = 0, \cdots, (M-1)N/2+L-1, \tag{3.20}$$

$$\mu_m \geq 0, \quad \text{for } m = 0, \cdots, M-1. \tag{3.21}$$

This algorithm is an approximation due to the samples being complex in nature and the projections being an approximation of the "growth" of the clipped signals in the direction of the original baseband signal. Equation (3.18) is therefore the maximizing objective function with Eq. (3.19) and Eq. (3.20) representing $(M-1)N+2L$ constraints. Equation (3.21) represents the positive requirement for the μ_m vector being optimized.

3.4.2 LP formulation 2

The aim of LP 2 is to minimize the PAPR of individual sections of the frame, instead of over the entire frame as in LP 1. This approach therefore handles smaller sections and can achieve superior PAPR performance with a lower average transmit power increase. This is done by changing the optimization

formulation. Instead of attempting to reduce a single peak in the frame, the goal is to reduce M peaks in overlapping sections of length L. The objective function is also scaled based on the magnitude of the peaks. This allows for higher priority on the larger peaks. In order to do this, we define a new peak position vector $\boldsymbol{n}_{\text{peak}}$ which can be defined as:

$$\boldsymbol{n}_{\text{peak}} = \begin{bmatrix} n_{\text{peak }0} & n_{\text{peak }1} & \cdots & n_{\text{peak }M-1} \end{bmatrix}^T, \tag{3.22}$$

with $n_{\text{peak }0}$ the position of the peak on the interval $0 \leq n \leq L-1$, $n_{\text{peak }1}$ the position of the peak on the interval $N/2 \leq n \leq L+N/2-1$, and so forth. These peaks set the limits for the intervals of length $N/2$.

The new optimization formulation can be set up as follows:

$$\max \text{ z} = \mu_0 + \mu_1 + \cdots + \mu_{M-1}, \tag{3.23}$$

subject to the following constraints;

$$\{\bar{\boldsymbol{C}}_l^T \boldsymbol{\mu}\}_n - \{\bar{\boldsymbol{C}}_l^T \boldsymbol{\mu}\}_{n_{\text{peak }0}} \leq ||s_l[n_{\text{peak }0}]|| - ||s_l[n]||, \quad \text{for } n = 0, 1, \cdots, L-1, \tag{3.24}$$

$$\{\bar{\boldsymbol{C}}_l^T \boldsymbol{\mu}\}_n - \{\bar{\boldsymbol{C}}_l^T \boldsymbol{\mu}\}_{n_{\text{peak }0}} \geq -||s_l[n_{\text{peak }0}]|| + ||s_l[n]||, \quad \text{for } n = 0, 1, \cdots, L-1, \tag{3.25}$$

$$\{\bar{\boldsymbol{C}}_l^T \boldsymbol{\mu}\}_n - \{\bar{\boldsymbol{C}}_l^T \boldsymbol{\mu}\}_{n_{\text{peak }1}} \leq ||s_l[n_{\text{peak }1}]|| - ||s_l[n]||, \quad \text{for } \frac{N}{2} \leq n \leq L + \frac{N}{2} - 1, \tag{3.26}$$

$$\{\bar{\boldsymbol{C}}_l^T \boldsymbol{\mu}\}_n - \{\bar{\boldsymbol{C}}_l^T \boldsymbol{\mu}\}_{n_{\text{peak }1}} \geq -||s_l[n_{\text{peak }1}]|| + ||s_l[n]||, \quad \text{for } \frac{N}{2} \leq n \leq L + \frac{N}{2} - 1, \tag{3.27}$$

$$\vdots$$

$$\{\bar{\boldsymbol{C}}_l^T \boldsymbol{\mu}\}_n - \{\bar{\boldsymbol{C}}_l^T \boldsymbol{\mu}\}_{n_{\text{peak M-1}}} \leq ||s_l[n_{\text{peak M-1}}]|| - ||s_l[n]||, \quad \text{for } \frac{N}{2}(M-1) \leq n \leq \frac{N}{2}(M-1) + L - 1, \tag{3.28}$$

$$\{\bar{\boldsymbol{C}}_l^T \boldsymbol{\mu}\}_n - \{\bar{\boldsymbol{C}}_l^T \boldsymbol{\mu}\}_{n_{\text{peak M-1}}} \geq -||s_l[n_{\text{peak M-1}}]|| + ||s_l[n]||, \quad \text{for } \frac{N}{2}(M-1) \leq n \leq \frac{N}{2}(M-1) + L - 1, \tag{3.29}$$

$$\mu_m \geq 0, \quad \text{for } m = 0, \cdots, M-1. \tag{3.30}$$

The objective function of Eq. (3.23) can also be scaled by the relevant peak magnitudes to which the symbols contribute. This adds priority to larger peaks. This can be done by noting the projections at the peak positions of the clipped symbols. The larger peaks will result in larger projections and therefore, these projections can be used as scaling factors in the objective function of Eq. (3.23) in order to speed up convergence time to a lower PAPR.

3.5 SGP EXTENSION

Two additional methods are proposed based on a more direct extension of the SGP ACE method to FBMC. These methods do not require the use of a linear programming methodology, which can have high computational complexity depending on the problem. Once again, both methods focus on finding an optimal scaling factor μ or scaling factor vector $\boldsymbol{\mu}$.

3.5.1 SGP Single scaling

This method follows closely to that of the SGP proposed in [12] for OFDM systems. The focus is on finding a single scaling factor μ by which we can scale the entire clipped frame $\hat{c}_l[n]$ given by Eq. (3.3). This approach can be seen as sub-optimal as the component clipped signals can be scaled independently for greater effect. However, due to the nature of the polyphase implementation of FBMC performing modulation in a contiguous manner on overlapping symbols, a single scaling method is well suited for polyphase implementation. The proposed single scaling method, does not require differentiation between the individual symbols in the FBMC frame, which can greatly reduce complexity.

The implementation of the single scaling SGP method is relatively straight forward and can be seen as a generalization of the OFDM method in [12] to an FBMC implementation. Once the clipped portion of the signal across the entire frame is obtained, it can be superimposed over the original signal to obtain the projections. This is illustrated in Fig. 3.4.

The projections are obtained in a manner similar to Eq. (3.14), but with a single vector spanning across the entire frame. In order to obtain the best suited scaling factor μ for the entire clipped frame $\hat{c}_l[n]$, only the projections in the steady-state part of the frame are observed, as illustrated by the solid line of the arc in Fig. 3.4. The samples in the transient state are often small in magnitude as they do not contain $2K$ overlapping symbols and as can be seen in Fig. 3.5, are scaled by a small magnitude

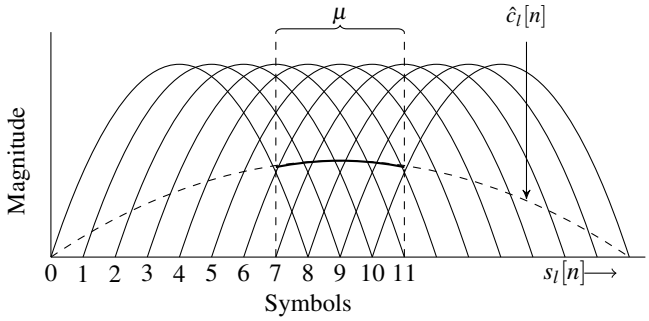

Figure 3.4: Clipped signals superimposed over original FBMC modulated signal for $M = 11$

of the corresponding filter response. The signal behaviour in the transient is therefore erratic and not accurate for use in calculating the μ value. The steady state section begins approximately a full filter length into the frame and ceases a full filter length from the end of the frame.

The single scaling SGP method for FBMC requires some alterations of the method in [12] and can be summarized as follows;

1. Find the peak of the frame, P_l, inside the steady state region (the peak should almost always exist in the steady state region of the transmit data block) as well as the peak position n_{peak}.

2. Calculate the projections $\bar{c}_l[n]$ of the clipped frame $\hat{c}_l[n]$ only along the viable interval by performing the dot product:

$$\bar{c}_l[n] = \frac{\Re\{\hat{c}_l[n] \cdot s_l[n]\}}{|s_l[n]|} \tag{3.31}$$

for

$$L - N/2 \leq n \leq (M-1)N/2. \tag{3.32}$$

3. Consider only the values of $\bar{c}_l[n]$ that are positive and therefore result in magnitude growth.

4. Compute the scaling factor for each of these projections:

$$\mu[n] = \frac{P_l - s_l[n]}{\bar{c}_l[n] - \bar{c}_l[n_{\text{peak}}]}, \quad n \neq n_{\text{peak}} \tag{3.33}$$

5. Use the minimum value of $\mu[n]$ (so that no peak regrowth occurs) as the scaling factor for the whole frame, namely

$$\mu = min(\mu[n]). \tag{3.34}$$

6. Scale the clipped signal $\hat{c}_l[n]$ by μ and add it to the original signal to obtain the new transmit signal,

$$\hat{s}_l[n] = s_l[n] + \mu\hat{c}_l[n], \quad n = [0,1,\cdots,(M-1)N/2+L-1]. \tag{3.35}$$

7. If μ is negative, stop the iterative ACE algorithm as any further PAPR reduction attempts will result in peak regrowth.

3.5.2 Overlapping SGP

As mentioned in section 3.5.1, the single scaling SGP method presented above scales the clipped signal, which spans the entire frame, by a single scaling factor. This method can be expanded to consider the impact of the individual symbols on the original baseband signal and obtain an optimal scaling vector $\boldsymbol{\mu}$ by which we can scale each individual symbol separately allowing for higher degrees of freedom.

Once again we obtain the discrete clipped FBMC symbols in isolation namely $\hat{c}_l[n]$. As in Fig. 3.6, each clipped symbol only has an effect on a portion of length L on the original transmit signal. However, when observing the impulse response of the filter as shown in Fig. 3.5, only the middle half of the impulse response actually has significant values. The rest of the impulse response values are almost negligible. This is also illustrated in Fig. 3.6 where the solid line of $\hat{c}_{l,4}[n]$ and $\hat{c}_{l,5}[n]$ represent the significant portion of the clipped signals. Therefore to calculate a more accurate estimate for μ we only consider the middle section of length N of the clipped symbols. The peak value of the original transmit signal $s_l[n]$ is then calculated between these intervals. This is used to calculate a ratio between the new positive projections and the peak on this interval. In order to calculate the projections $\bar{c}_{l,m}[n]$ of $\hat{c}_{l,m}[n]$ onto the phase angle of the original transmit signal, the dot product can be used. This calculates only the component of $\hat{c}_l[n]$ projected on the same phase angle as the original

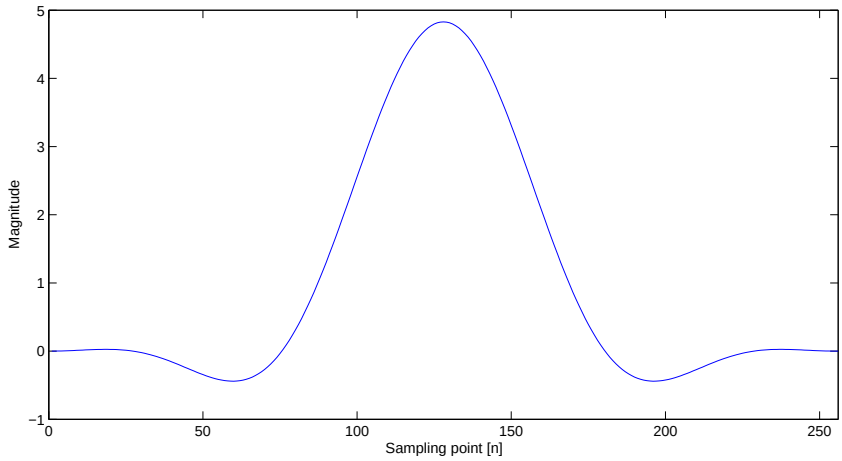

Figure 3.5: PHYDYAS filter impulse response with $K = 4$, $L = 256$

signal. In order to mitigate peak regrowth, the goal is to reduce the magnitude of the peak as much as possible, whilst simultaneously limiting new projections that occur on other samples that may result in peak regrowth. Once again only positive projections are considered as they indicate peak regrowth.

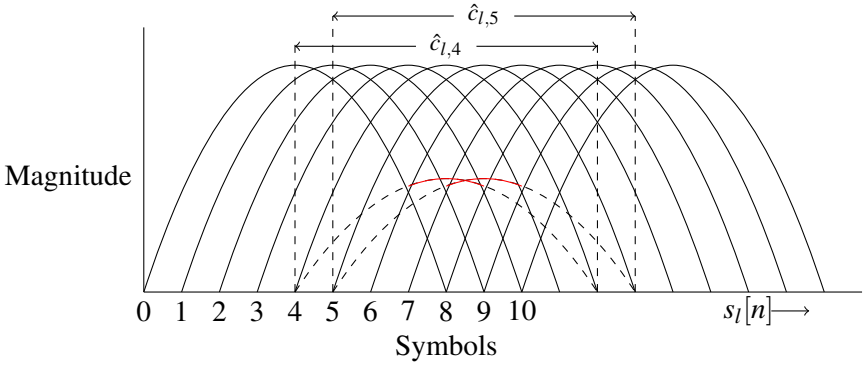

Figure 3.6: Clipped signals superimposed over original FBMC modulated signal

As can be seen by Fig. 3.6 the significant portion of the clipped signals only overlap on an interval of length N whereas the actual clipped signals overlap over the interval $L = KN$. The scaling of the clipped portions still have an effect on a length L of the original transmit signal.

The overlapping SGP technique can be summarized as follows:

1. Obtain the clipped symbols $\hat{c}_{l,0}[n], \cdots, \hat{c}_{l,M-1}[n]$.

2. Begin by setting $m = 0$.

3. Obtain the projections of $\hat{c}_{l,m}[n]$ on the meaningful intervals of length N as

$$\bar{c}_{l,m}[k] = \frac{\Re\{\hat{c}_{l,m}[k] \cdot s_l[n]\}}{|s_l[n]|} \tag{3.36}$$

with

$$n = mN/2 + k, \quad 3N/2 \leq k \leq 5N/2 - 1 \tag{3.37}$$

4. Find the peak P_m on the meaningful interval and its corresponding positions $n_{\text{peak}m}$ as

$$P_m = \max|s_l[n]| \tag{3.38}$$

with

$$\begin{aligned} mN/2 + 3N/2 \leq n \leq mN/2 + 5N/2, \\ m = [0, 1, \cdots, M-1]. \end{aligned} \tag{3.39}$$

5. Compute the scaling factors for all of the projections by only considering the positive projections, on the meaningful interval calculated in (3.36), as

$$\mu_m[n] = \frac{P_m - s_l[n]}{\bar{c}_{l,m}[n] - \bar{c}_{l,m}[n_{\text{peak}m}]} \tag{3.40}$$

6. Use the minimum value of $\mu_m[n]$ as the scaling factor for symbol m

$$\mu_m = \min(\mu_m[n]) \tag{3.41}$$

7. Scale the clipped symbol $\hat{c}_l[n]$ with its relevant scaling factor μ_m and add it to the original signal $s_l[n]$ to obtain the new transmit signal $\hat{s}_l[n]$ as

$$\hat{s}_l[n] = s_l[n] + \mu_m \hat{c}_q[n] \tag{3.42}$$

8. Return to step 3), set $m = m + 1$ and update $s_l[n]$ with $\hat{s}_l[n]$ obtained in step 7).

9. Once a scaling factor has been obtained for each clipped symbol, a full overlapping SGP iteration has been completed.

10. If the PAPR meets requirements, transmit the new updated $\hat{s}_l[n]$, otherwise repeat the clipping process.

It should be clear from the methodology described above for the overlapping SGP method, scaling values are obtained for each symbol starting at symbol 0 and the transmit signal is updated on a symbol by symbol basis. The updating therefore starts at symbol 0 and propagates through the entire frame until symbol $M-1$ has been updated. This can be considered as a forward progression through the frame. Each consecutive symbol therefore depends on the previous symbol to calculate its respective projections and scaling factor. If a scaling value smaller than zero is obtained for a specific symbol, the scaling factor for that symbol is set to zero as it indicates that scaling will result in peak regrowth. However, the process does not terminate. There may be other symbols that can reduce the PAPR and so the scaling factors for other symbols is continued.

The fact that the SGP type proposed methods depend only on previous symbols imply that the minimum system delay obtainable by the SGP type methods is the length of the filter, namely L. It can also be seen at step 6 that the minimum value of $\mu_m[n]$ is chosen whereas the proposed optimization methods aim to maximize the μ_m values. The justification for the difference is that the minimization criterion is built into the optimization problem in the form of constraints placed at each sample point, namely (3.19)-(3.20) and (3.24)-(3.29).

3.6 CONCLUSION

Four novel PAPR reduction methods are described in this section for FBMC PAPR reduction. They include the LP 1 and 2 based methods and the SGP single scaling and overlapping SGP methods. A

detailed mathematical model of the discrete sampling points in an FBMC frame is derived in Eq. (3.4)-(3.8) which will assist with future work in the PAPR reduction field for FBMC systems.

The following chapter contains the results of the proposed methods under a Monte Carlo based simulation environment.

CHAPTER 4 RESULTS

4.1 CHAPTER OVERVIEW

In this section, we illustrate the performance of the proposed ACE-based PAPR reduction techniques for FBMC modulation using different figures of merit namely: PAPR, out-of-band distortion, in-band distortion and effects of varied clipping levels. In addition, we present a study of the power amplifier efficiency improvement allowed with the implementation of the PAPR reduction methods introduced in this work.

In the illustrative simulations, the FBMC system is implemented by using a PHYDYAS [56] based prototype filter with overlap factor $K = 4$. The number of active subcarriers is set to $N = 64$ unless otherwise stated. It is shown in [56] that when considering near perfect reconstruction orthogonal prototype filters, the choice of prototype filter does not have a significant effect on the PAPR of the FBMC signal. On the other hand, the overlapping factor may in fact have an effect on the PAPR when considering the different techniques (i.e. slightly modified algorithms are required if a different overlap factor is chosen). The choice of $K = 4$ is done for accurate comparison to other current methods in the field which employ the same overlap factor. The clipping factor, δ, for all simulated methods, was chosen at 4dB unless otherwise stated.

4.2 PAPR REDUCTION PERFORMANCE

Clipping based PAPR reduction techniques work on the principle of reducing the peaks through clipping and reconstruction of the new constellations. By reducing the peaks in the time domain signal, the PAPR is effectively reduced. This effect is illustrated in Fig. 4.1 showing the original time domain frame and the transmitted, PAPR reduced, time domain frame. In Fig. 4.1b the SGP overlapping method was applied using QPSK modulation and the results are after the 2nd iteration of the PAPR re-

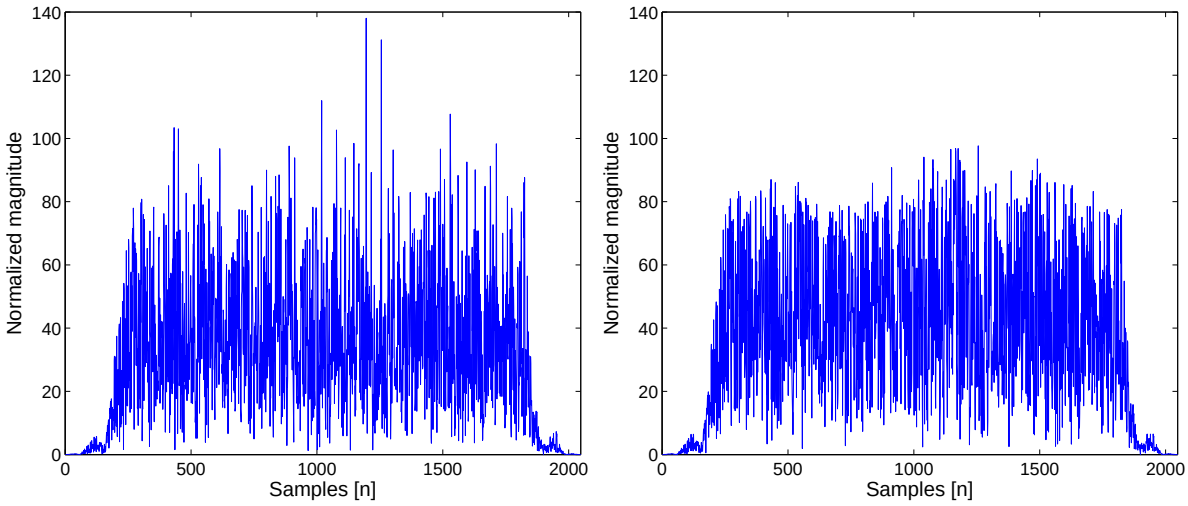

(a) Original frame **(b)** PAPR reduced frame

Figure 4.1: Discrete time domain FBMC frames illustrating the effects on reducing the peaks in the signal

duction technique. In Fig. 4.1b a much more condensed frame can be noted. This is important as large peaks such as those in 4.1a are reduced allowing for more efficient HPA operation. The large input back-off can now be reduced as the probability of obtaining a high PAPR has been reduced.

The CCDF, as defined in Eq. (2.19), of the PAPR can be used to evaluate the performance of different PAPR reduction techniques. The CCDF gives us the information to define an adequate power amplifier operation point, i.e. backoff, with minimum distortion at a predetermined probability. The amount of backoff to be applied is a function of the CCDF of the PAPR and the requirements of OOB and in-band distortion specified. The PAPR was measured using Eq. (2.21) so as to accurately compare to OFDM signals of the same symbol period length. Figure. 4.2 shows that in order to obtain a clipping probability of 10^{-3} an incredibly large input backoff would be required in the HPA. This reiterates the need for some kind of PAPR reduction technique prior to transmission in FBMC or any other multicarrier system.

Figure. 4.2 and Fig. 4.3 illustrate the CCDF of critically sampled FBMC systems employing 64 subcarriers, with QPSK modulation, for the SGP and LP based proposed methods respectively. From the results it is clear that significant reduction in PAPR performance is achievable with the proposed algorithms. In Fig. 4.2 a PAPR reduction of over 3.5 dB is achievable in a single iteration of the proposed SGP overlapping and SGP single scaling methods at a clipping probability of 10^{-3}. This offers

significant advantage over a standard POCS approach to FBMC, which only achieves PAPR reduction of approximately 2.5 dB after three iterations at the same clipping probability. The LP2 method in Fig. 4.3 provides similar PAPR reduction capabilities in a single iteration. The LP1 formulation does not achieve as high reduction upon the first iteration, but converges to similar performance upon the third iteration. All the proposed methods obtained PAPR reduction of over 4 dB upon the third iteration, with the SGP overlapping method achieving approximately 4.7 dB PAPR reduction from the original FBMC envelope at 10^{-3} clip probability.

It should be noted that in a critical sampled system, a clipping and filtering method can effectively be reduced to a hard clipping method as no spectral leakage can be emulated for this kind of system. Therefore the hard clipping results in significant PAPR reduction, however, at the expense of severe in-band distortion.

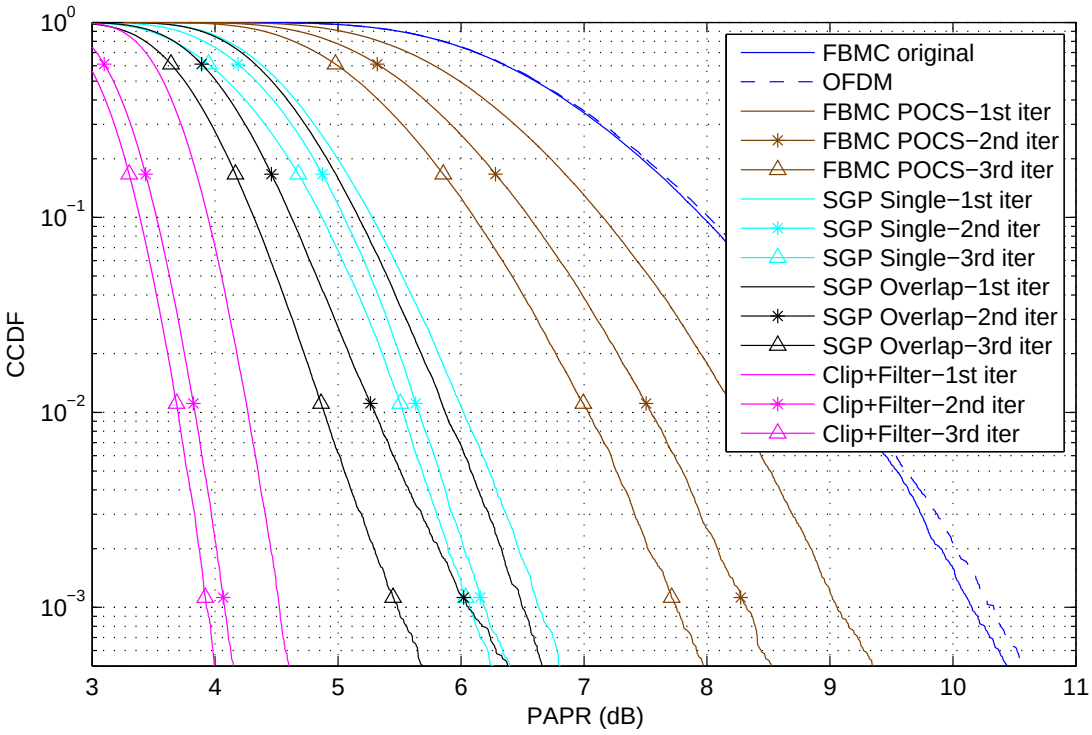

Figure 4.2: PAPR performance comparison for critically sampled QPSK FBMC modulation employing 64 subcarriers (SGP methods)

The algorithms were expanded to an equivalent 16 QAM modulation based FBMC to show the effects of higher order modulation on the PAPR reduction capabilities of the proposed methods. Due to

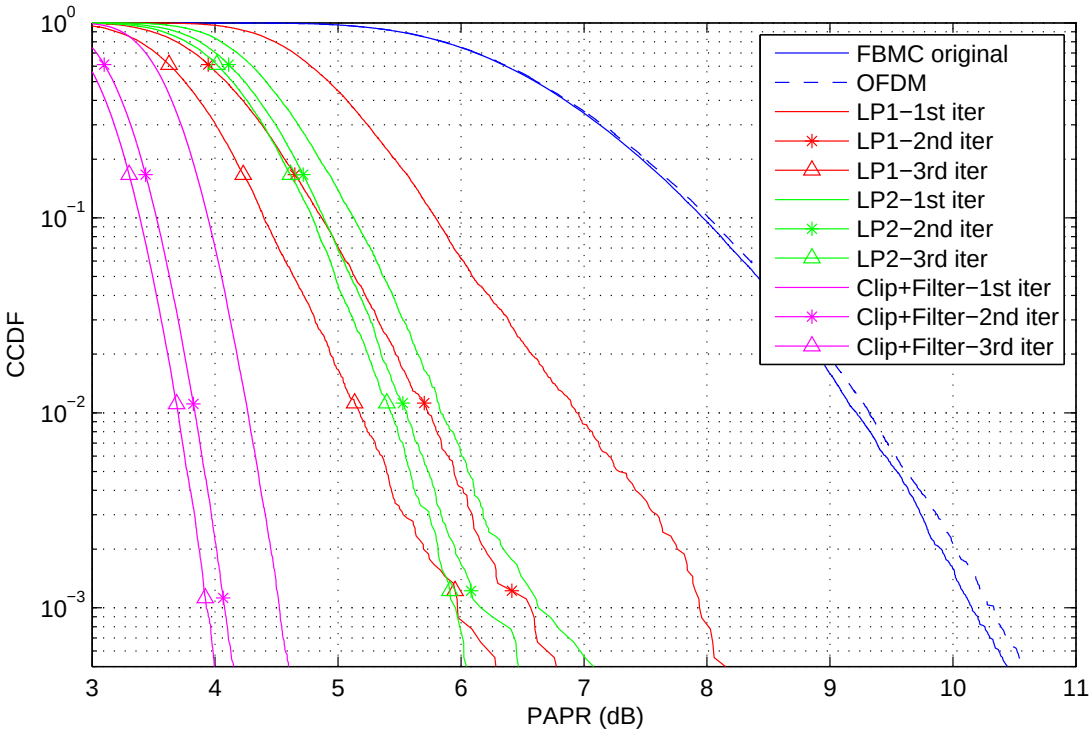

Figure 4.3: PAPR performance comparison for critically sampled QPSK FBMC modulation employing 64 subcarriers (LP methods)

the ACE based methods retention of the minimum euclidean distance in each constellation, PAPR reduction performance are less effective on higher order modulations. This is due to a reduction in the degrees of freedom in the algorithms as only the outer constellation points can be extended. Figure. 4.4 and Fig. 4.5 illustrate the PAPR performance of the proposed methods using 64 subcarriers in a critically sampled 16 QAM system.

The LP1 based technique suffers on the first iteration when scaled to 16 QAM based modulation technique as can be seen in 4.5. The technique however recovers and converges to under 7dB at a probability of 10^{-3}, along with the other proposed techniques barring the SGP single scaling technique, in three iterations. This still amounts to a reduction of around 3dB over the original FBMC envelope.

It should be noted that critically sampled systems offer very ideal PAPR performances and excellent PAPR reduction across almost all methods. However, a critically sampled system poorly simulates the

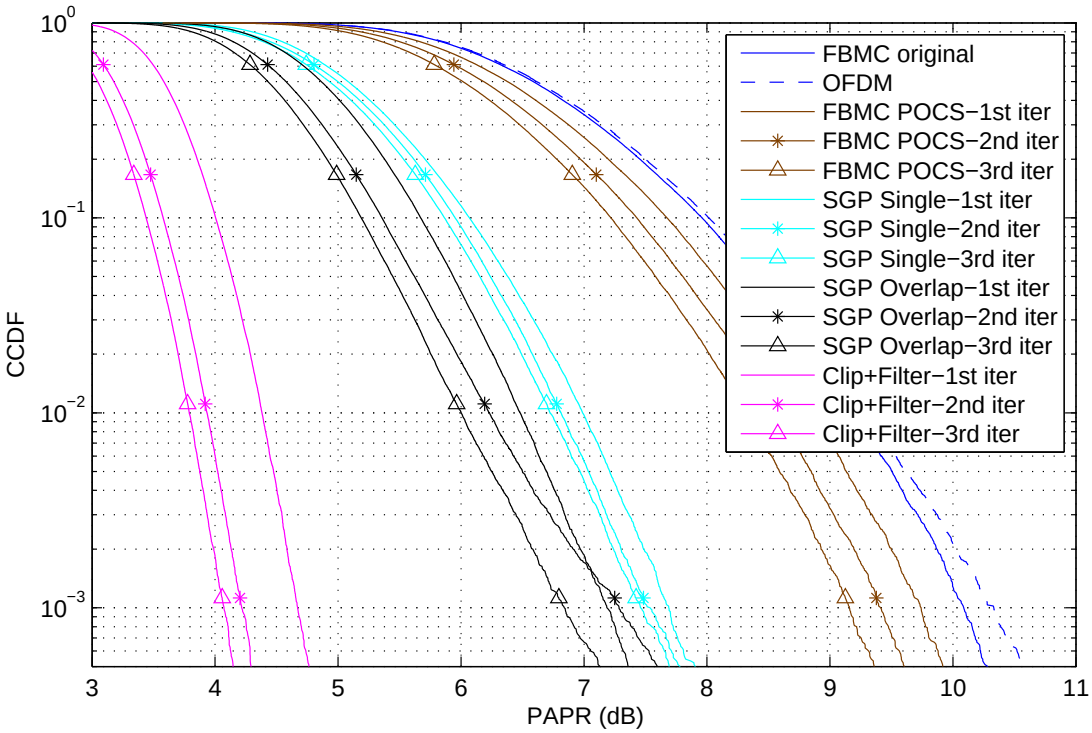

Figure 4.4: PAPR performance comparison for critically sampled 16 QAM FBMC modulation employing 64 subcarriers (SGP methods)

true analogue nature of the signal [12]. The PAPRs achieved in Fig. 4.2, 4.3, 4.4 and 4.5 are therefore highly optimistic at best. These however remain important as most literature published is based on critically sampled systems. A more accurate representation of the PAPR of a signal can be achieved through up-sampling. This allows for closer approximation to analogue signals and is achievable in an OFDM or FBMC system by applying a highly up-sampled IFFT block [12]. This can be done by adding trailing zeros to all subcarriers greater than N thereby creating an upsampled IFFT.

In order to retain the performance of any PAPR reduction technique, it is imperative to perform processing on an already upsampled signal. It is therefore necessary to perform the proposed PAPR reduction techniques on an oversampled system and then up-sample again after the technique has concluded [12]. This allows for better estimation of the peak regrowths in the true analogue domain, as the samples in the time domain have a higher resolution and possible peaks in between samples are not missed. As the upsampling factor of the processed signal is increased, so to does the PAPR performance after the signal is converted to the true analogue domain. Due to processing constraints, there is a limitation on the amount of upsampling which can be performed. A good trade-off of computing power versus PAPR performance was found by upsampling by only a factor of two for

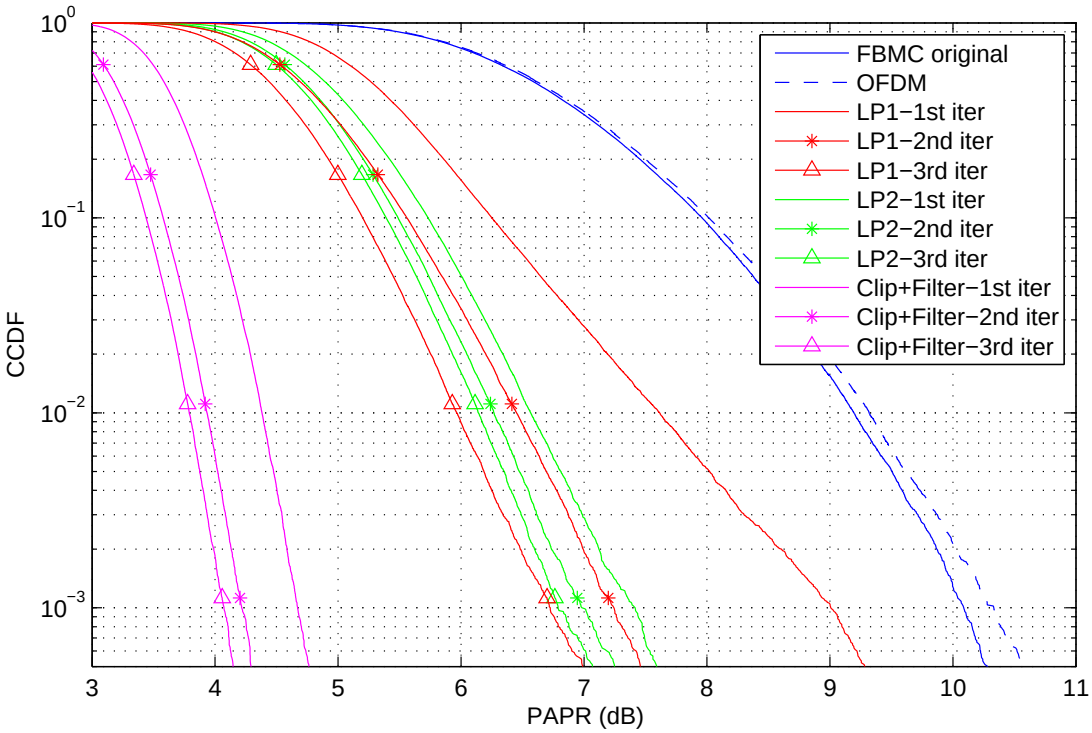

Figure 4.5: PAPR performance comparison for critically sampled 16 QAM FBMC modulation employing 64 subcarriers (LP methods)

the PAPR processing. Due to the law of diminishing returns, significantly less PAPR performance is gained by upsampling further as shown in [12].

Figure. 4.6 and 4.7 illustrate results after twice oversampling the PAPR reduction techniques and then applying an oversampling of 8 times to estimate the true analogue nature of a 64 subcarrier, QPSK system. The results in Fig. 4.6 and 4.7 allow for a clear distinction between the proposed methods and more accurately provide expectations for real world performance. It is clear that all proposals far exceed the performance of a POCS type implementation, with only clipping and filtering offering superior performance. Once again, the LP1 proposal provides the weakest performance on the first iteration, but tends to converge to the best performance upon the third iteration. The LP2, SGP single scaling and SGP overlapping proposals offer PAPR reduction of 2.9, 3 and 3.3dB respectively upon the first iteration at a clip probability of 10^{-3}.

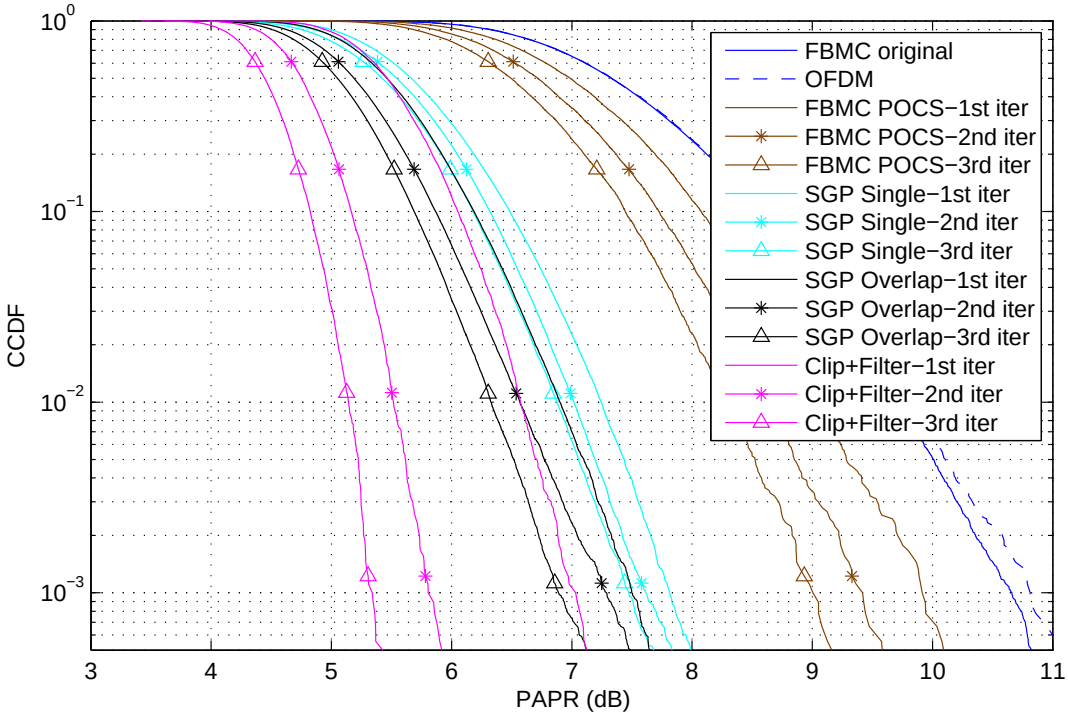

Figure 4.6: PAPR performance comparison for estimation to analogue, upsampled QPSK FBMC modulation employing 64 active subcarriers (SGP methods)

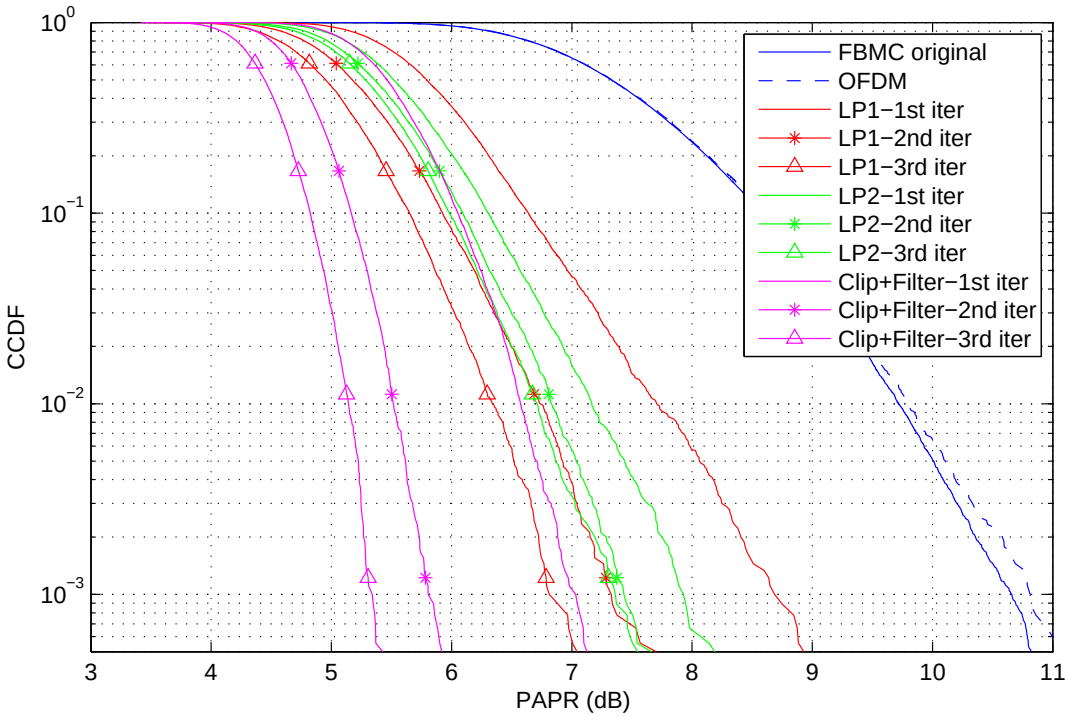

Figure 4.7: PAPR performance comparison for estimation to analogue, upsampled QPSK FBMC modulation employing 64 active subcarriers (LP methods)

The LP based proposals provide a benchmark for theoretical upper limit on PAPR reduction capabilities per iteration. It can be seen from Fig. 4.6 and Fig. 4.7 that the performance of the SGP overlap method is negligibly close to that of the upper limit per iteration with a much lower level of computation complexity. Therefore, for the rest of the simulations in this section, the LP formulations will be excluded. The remaining simulations were all performed on upsampled systems so that a true indication of analogue performance can be illustrated.

Figure. 4.8 illustrates the performance of 16 QAM modulated FBMC employing the SGP based techniques. It is clear that once upsampling techniques are employed on a 16 QAM modulated system, the PAPR reduction capabilities are reduced. This is an inherent flaw in ACE based methods for higher order modulation systems and the PAPR reducing capability reduces significantly as the modulation order is increased higher than 16 QAM.

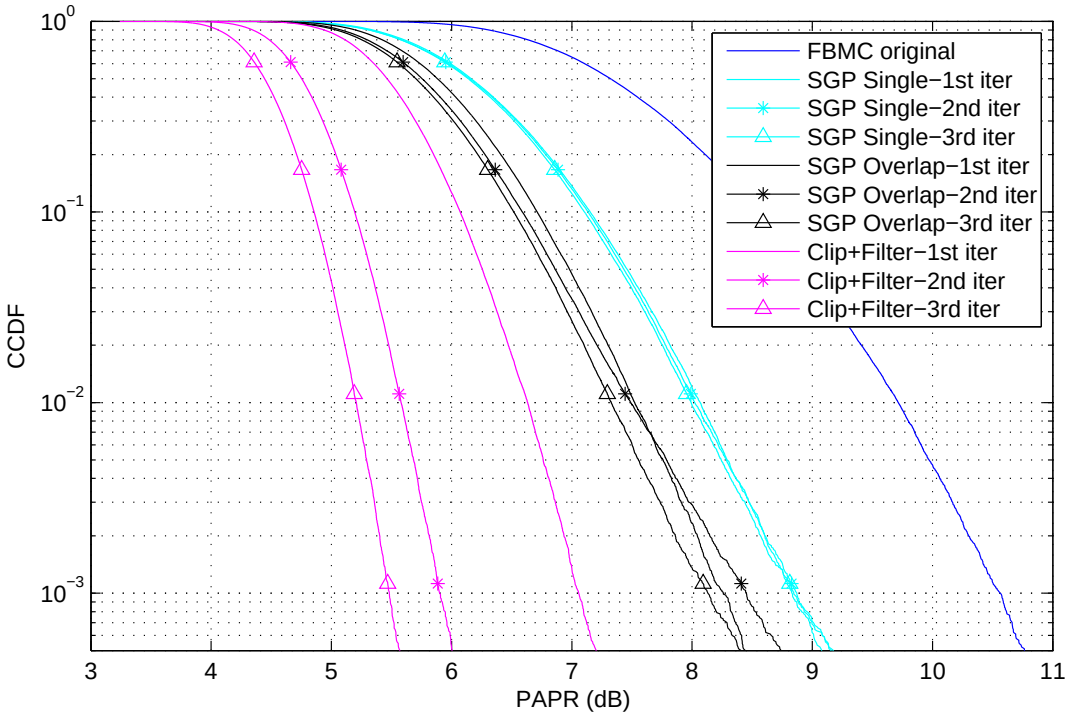

Figure 4.8: PAPR performance comparison of FBMC, 16 QAM modulation employing 64 subcarriers

One of the benefits of ACE type PAPR reduction techniques is the scalability as the subcarrier count increases. As the subcarriers count is increased, the PAPR reduction capabilities of ACE is also increased. This is because more subcarriers exist to which the ACE method can be applied, effectively providing more handles for controlling the PAPR. This is a major benefit over alternative methods of

reducing PAPR which often require the addition of additional tones or more complex optimization problems in order to retain PAPR reduction performance as subcarrier count increases.

Figure. 4.9 and 4.10 presents the results of 128 subcarrier, oversampled FBMC systems. It can be seen in Fig. 4.9 and 4.10 that the PAPR of the original FBMC envelope, when employing N=128 subcarriers, has increased by 0.5dB. The PAPR of the signals after the techniques have been employed, remain almost unchanged from the 64 subcarrier simulations presented in Fig. 4.6 and 4.8. This is indicative of an increase in PAPR reduction capabilities as the subcarrier count is increased. This result reinforces that the techniques scale very well with an increase in subcarrier count.

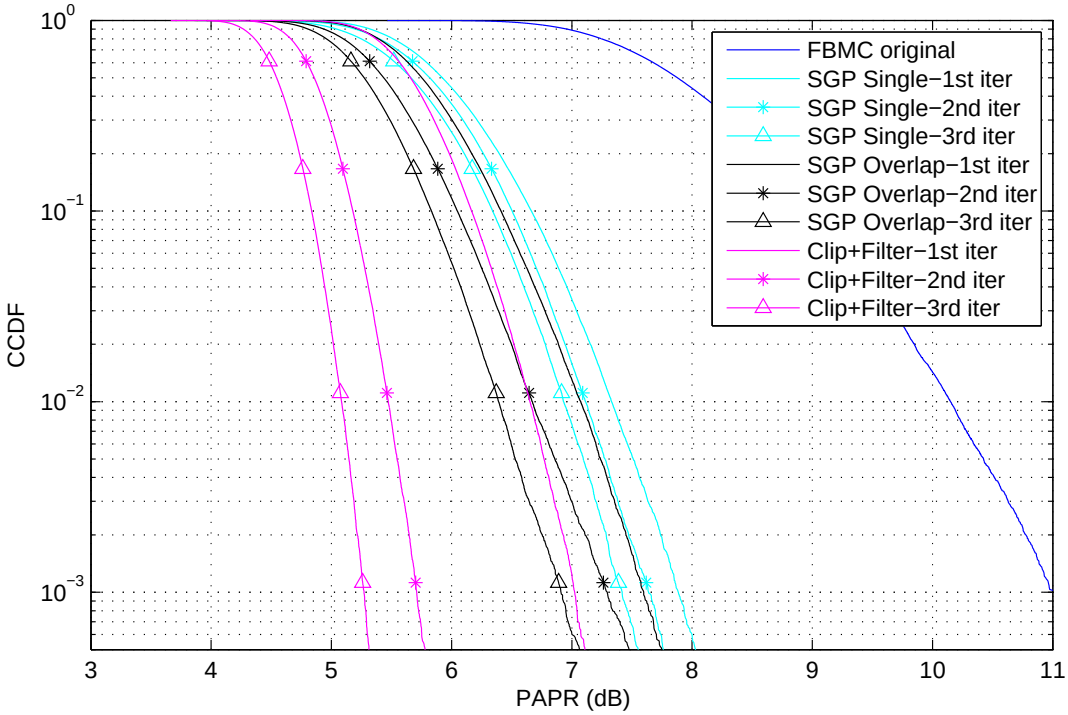

Figure 4.9: PAPR performance comparison of FBMC employing QPSK modulation with 128 subcarriers

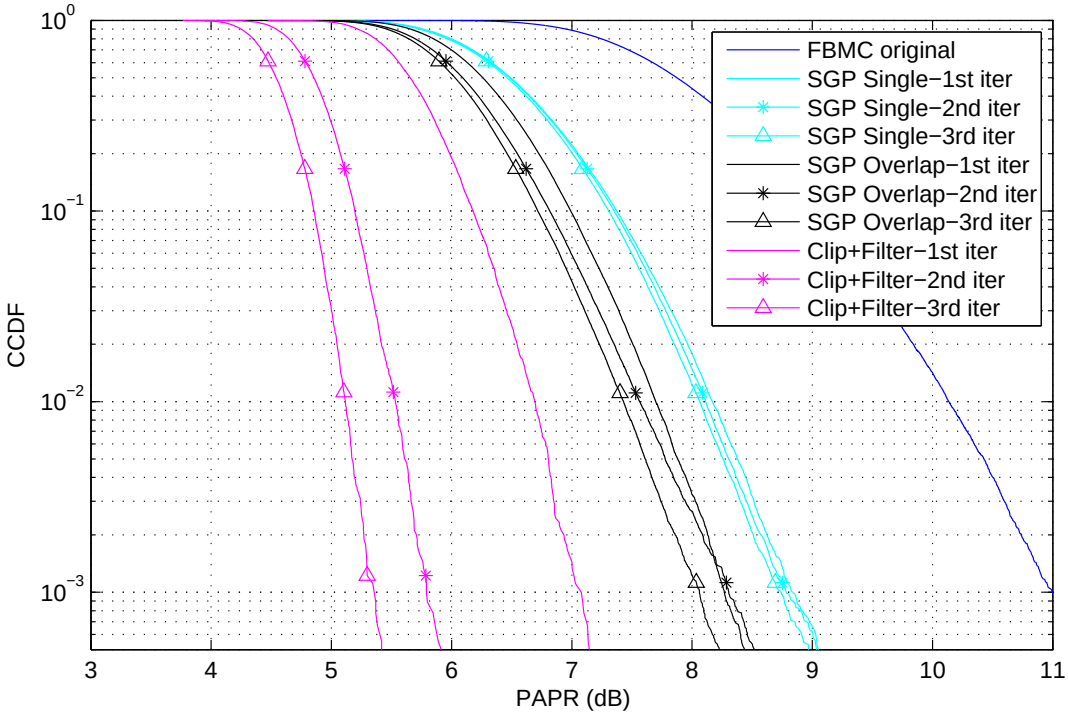

Figure 4.10: PAPR performance comparison of FBMC, employing 16 QAM modulation employing 128 subcarriers

4.2.1 Effects of varying clipping levels on PAPR reduction performance

The chosen level of clipping can have an effect on the final PAPR reduction performance. The extent of the performance reduction however is not always apparent and varies between PAPR reduction methods. In order to evaluate these effects, the simulations in this section show the PAPR reduction performance of the proposed techniques at 3,4 and 5dB clipping levels. For simplicity, a critically sampled system was chosen with 64 active subcarriers in this section.

From Fig. 4.11 to Fig. 4.14 it is interesting to note that the changes in the clipping level do not have a significant effect on the proposed PAPR reduction algorithms. This can be attributed to the tight constraints surrounding the SGP algorithm limiting peak regrowth and allowing maximum constellation extension per iteration. The clipping and filtering algorithm can achieve significant reduction in PAPR if an aggressive clipping level is chosen. This however comes at the expensive of severe in-band distortion as can be seen in Section. 4.4.1.

The POCS algorithm is shown to provide more varied results based on the clipping level and increas-

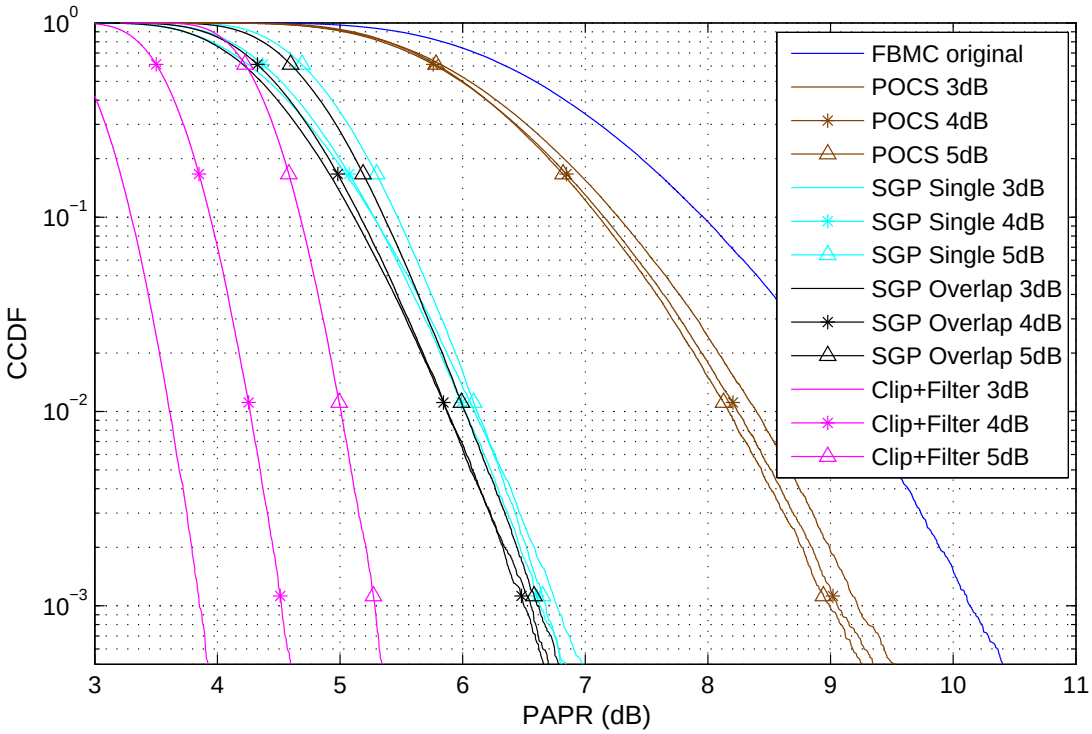

Figure 4.11: PAPR performance comparison on 1st iteration with varying clipping levels

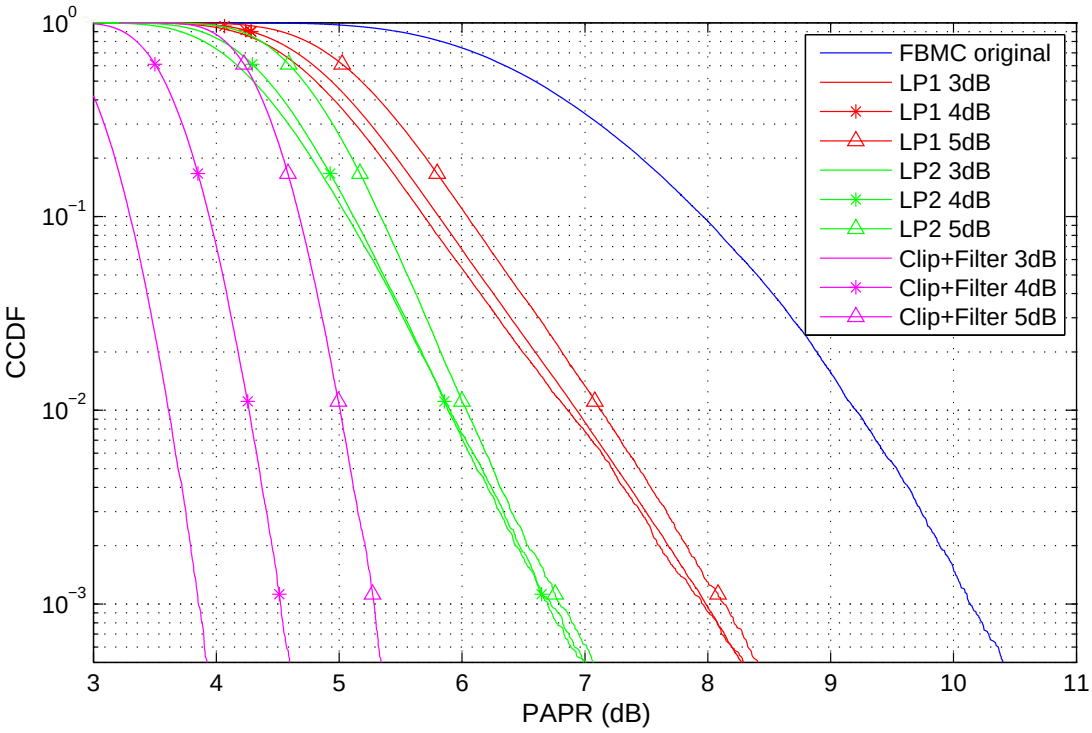

Figure 4.12: PAPR performance comparison on 1st iteration with varying clipping levels

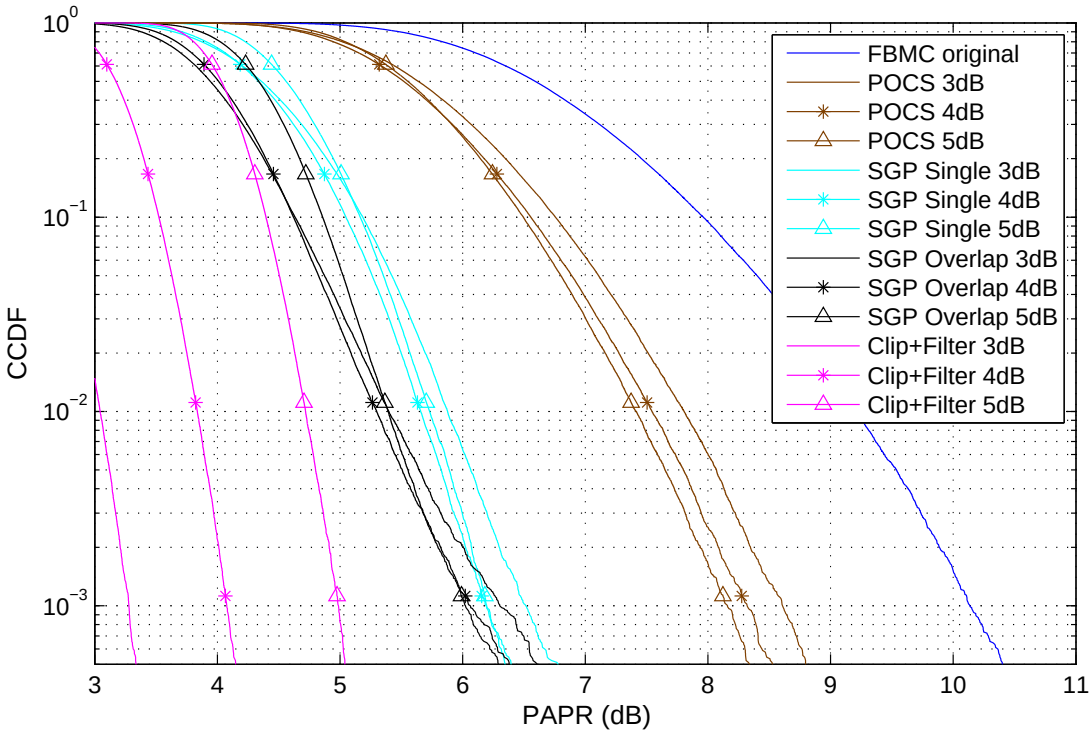

Figure 4.13: PAPR performance comparison on 2nd iteration with varying clipping levels

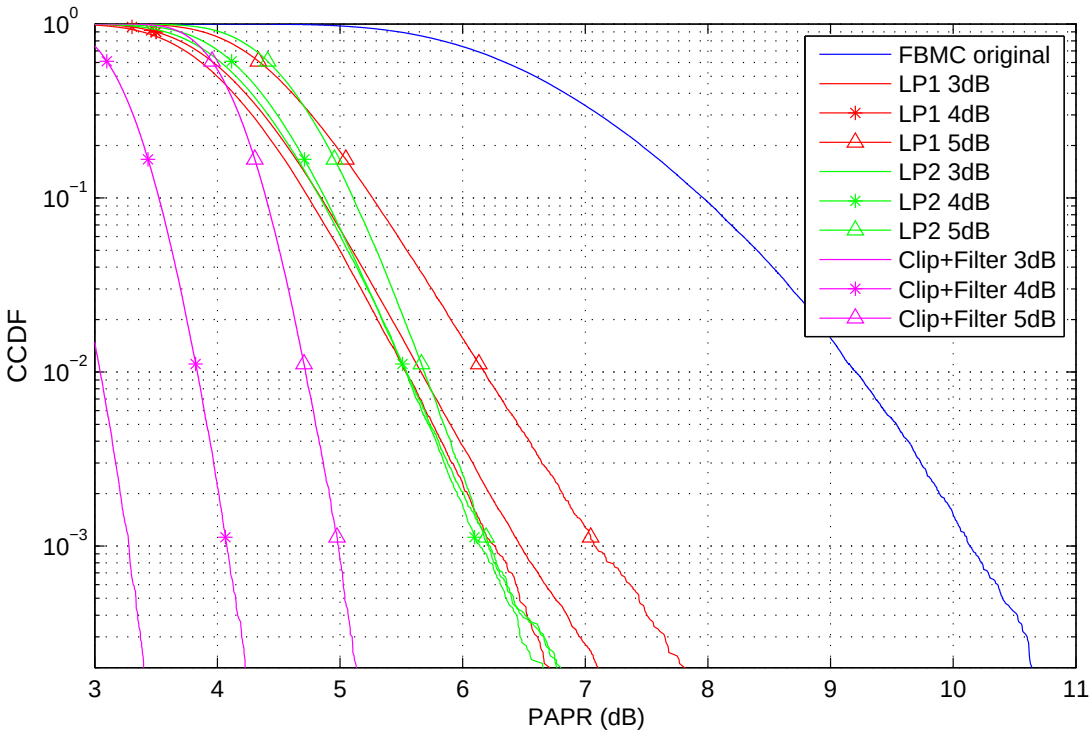

Figure 4.14: PAPR performance comparison on 2nd iteration with varying clipping levels

ing the amount of clipping does not necessarily decrease the PAPR of the signal as can be seen in Fig. 4.11 and 4.13. In fact in the range 3-5dB, increasing the amount of clipping actually decreased the PAPR performance. This is the opposite effect to all of the other simulated techniques. A possible explanation for this is that the POCS algorithm does not have any smart scaling capabilities and by increasing the amount of clipping, additional constellation correction is required which ends up reducing the PAPR performance.

4.3 OUT-OF-BAND DISTORTION EVALUATION

A matter of critical importance is the spectral leakage of the proposed methods. FBMC has gained much favour due to the very low spectral leakage. However, when a high power amplifier clips, severe spectral leakage can occur. That is one of the fundamentally important features of PAPR reduction techniques, i.e. they prevent high power amplifier (HPA) clipping and therefore reduce unwanted out-of-band interference. In order to accurately simulate and observe the results of the proposed PAPR reduction techniques in terms of power spectral density (PSD), a system was simulated using 64 active subcarriers with twice oversampling prior to 8 times oversampling for estimation to analogue. An ideal class A HPA was simulated with a hard clipping level of 5 dB. This allows regular clipping and hence the effects of the out-of-band distortion created by the HPA clipping, after PAPR reduction processing, can be observed. It should be noted that the PSD only gives an indication of the out-of-band leakage and no indication of the in-band distortion caused by HPA clipping. This will be evaluated in terms of BER performance.

The tight spectral shaping achievable by an unclipped FBMC systems versus unclipped OFDM systems is illustrated in Fig. 4.15. However, this fundamentally important characteristic, inherent to FBMC, can be severely degraded should clipping occur at the HPA. This can be seen by the FBMC clipped signal in Fig. 4.15 and 4.16. As in the OFDM scenario, the sidelobe amplitudes are greatly increased, when clipping occurs. This is illustrated when comparing the OFDM ideal/unclipped and FBMC ideal/unclipped plots to the OFDM clipped and FBMC clipped plots. The performance of the proposed techniques is evaluated and it is clear that significant reduction in out-of-band leakage can be achieved, after clipping, when any of the proposed techniques are implemented. The SGP Overlapping technique after a single iteration provides superior performance to that of an unclipped OFDM signal highlighting the effectiveness of the PAPR reduction technique. However, it is still clear that the rather rudimentary technique of clipping and frequency domain filtering provides the

best performance. This is to be expected as the PAPR reduction of the clipping and filtering technique is superior to all other techniques due to no in-band distortion correction.

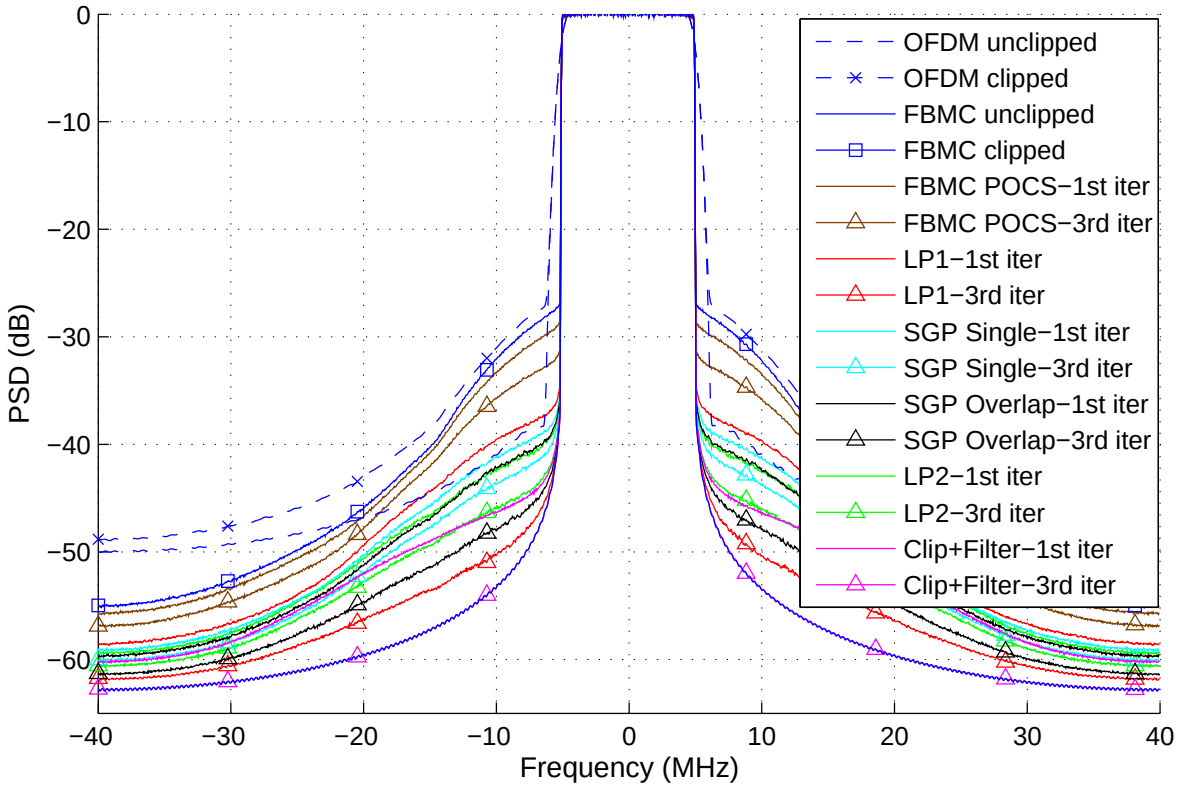

Figure 4.15: PSD of the proposed PAPR reduction techniques employing 64 active subcarriers and oversampling estimation to analogue

Figure. 4.15 utilizes the PWELCH averaging function to display the power spectral density of the signals. The true extent of the sidelobes can be lost when applying a windowing filter function as is present in the PWELCH function as samples are averaged. This allows the zeros to greatly reduce the average. Figure. 4.16 illustrates the frequency spectrum utilizing a direct application of the FFT function. This allows for clear distinction of the sidelobes. Here, the clear distortion of the OOB components can be seen when clipping occurs. Figure. 4.17 shows a zoomed in section of the sidelobes so that a clearer distinction between the methods can seen. To avoid clutter, only the SGP single and overlapping techniques are illustrated.

From Fig. 4.17 the SGP Single and SGP Overlap methods have on par performance. This would imply similar PAPR reduction performance. However, 4.1 highlights the small differences in terms of performance. Figure. 4.17 also highlights the significant improvement of FBMC PAPR reduced signals over that of OFDM in terms of the OOB spectral leakage.

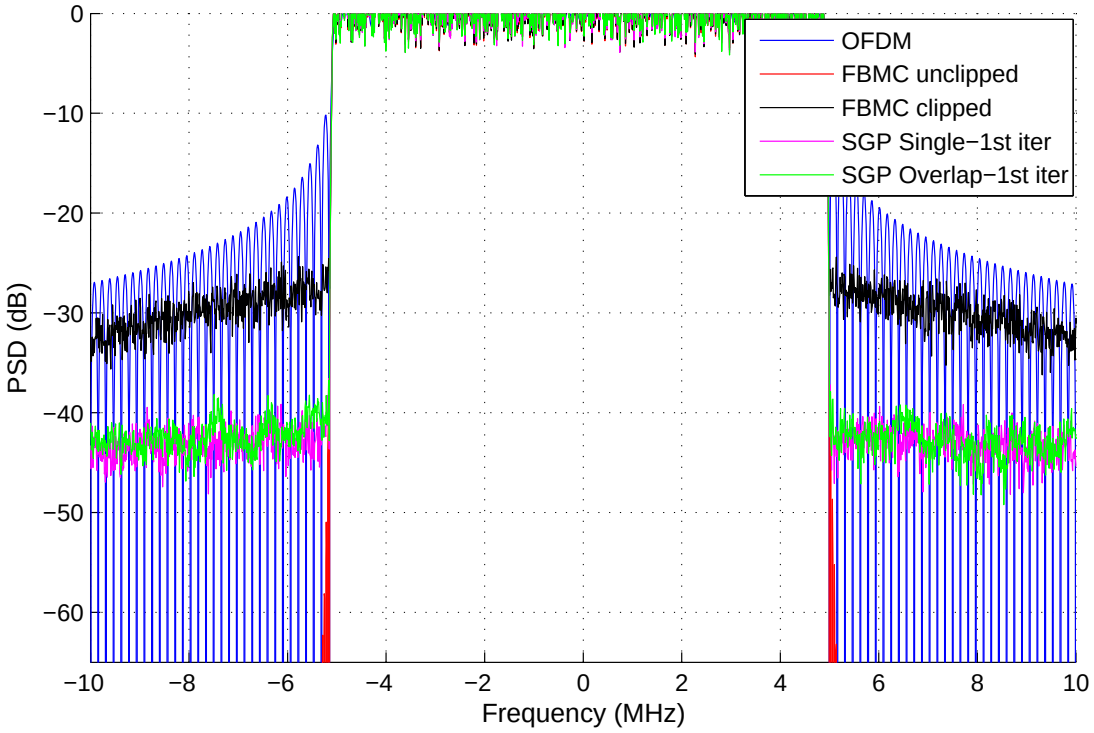

Figure 4.16: PSD of the proposed PAPR reduction techniques using an FFT illustrating the sidelobes

The adjacent channel power ratio (ACPR) is a figure of merit that can be calculated from Fig. 4.15 and provides an indication on the spectral leakage into adjacent bands. It effectively measures the ratio of in-band power to OOB power and is defined as [57]

$$\text{ACPR} = 10\log_{10}\left(\frac{\int_f Y(f)df}{\int_{f\text{main}} Y(f)df}\right), \tag{4.1}$$

with $Y(f)$ the power spectral distribution at the output of the HPA and f and $f$main the frequency range of the adjacent channel into which leakage occurs and the main in-band channel respectively. For the ACPR calculations, the main channel was considered between 0 and 2 MHz and adjacent channel was considered between 7 and 9 MHz. The results can be found in table 4.1. These results illustrate the benefits of the proposed techniques in cognitive radio environments where ACPR must be minimized in order to mitigate interference between neighbouring bands. This can greatly benefit opportunistic communications where secondary users can now utilize a smaller spectral gap without interfering with the primary users around them.

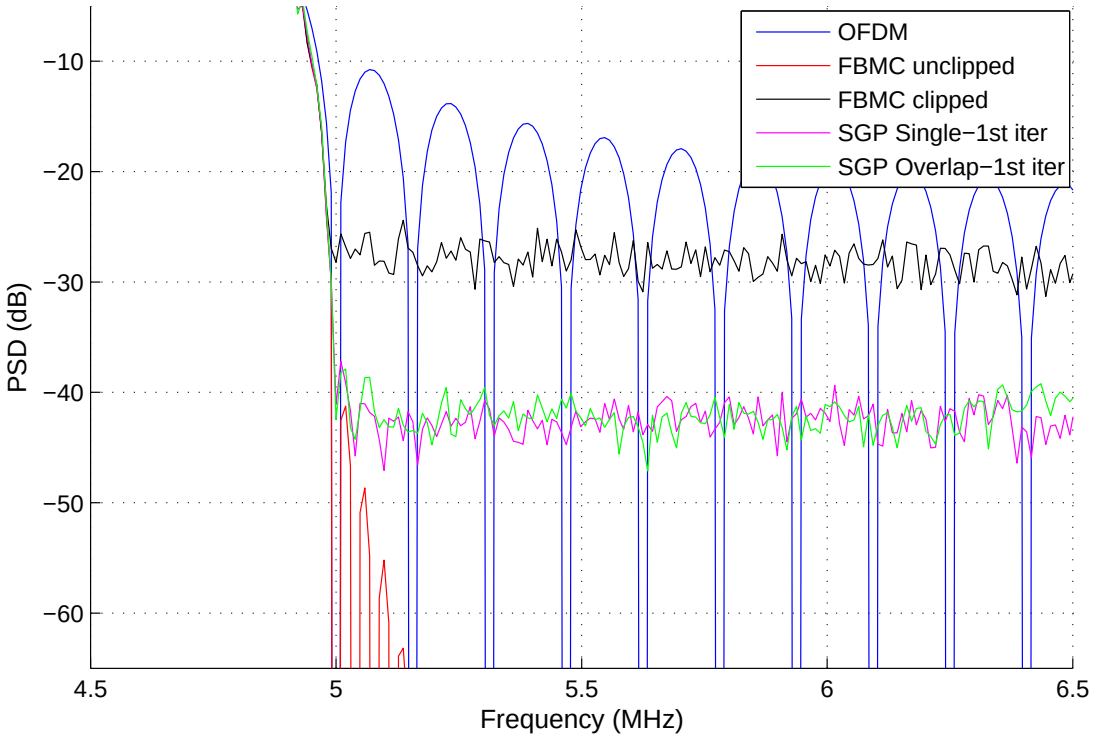

Figure 4.17: PSD of the proposed PAPR reduction techniques using an FFT illustrating zoomed sections of the sidelobes

Table 4.1: ACPR comparison of PAPR reduction techniques with 8 times oversampling

	Original envelope				FBMC PAPR reduction method					
ACPR	Ideal FBMC	Clipped FBMC	Ideal OFDM	Clipped OFDM	SGP1	SGP2	LP1	LP2	POCS	Clip+filter
1st iter(dB)	−50.6	−29.84	−39.49	−29.18	−40.13	−41.19	−38.84	−41.44	−31.38	−45.19
3rd iter(dB)	−50.6	−29.84	−39.49	−29.18	−42.56	−46,61	−48.73	−44.97	−34.13	−50.6

4.4 IN-BAND DISTORTION EVALUATION

The matter of BER degradation is often left unattended to due to poor performance when PAPR reduction techniques are applied. The trade-off for all PAPR reduction techniques is a fundamentally important sacrifice in BER performance. This is due to the inherent nature of increase average transmit power, applying constellation distortion or lowering the data-rate (which can be modelled as an increase in average bit energy required to transmit the same information). This is explained in more depth in Section. 2.6.1.

A figure of merit and often a factor for consideration, when in-band distortion arises, is the error

vector magnitude (EVM). This is a measure of the root mean square (RMS) of the absolute distance introduced between the original unmodified constellations and the new distorted constellations. The EVM process can accurately predict BER degradation in distortion techniques as the distortion can be modelled as a random statistical process. However, when considering a constellation extension method such as the ACE technique, the EVM does not provide the same linear relationship between BER degradation and EVM. This is due to the non-random nature in which the constellations are distorted, as ACE only allows distortion which increase the minimum Euclidean distance. ACE methods do however result in an increase in average transmit power. This factor must be taken into consideration for BER analysis, as the new modified constellation points have larger transmit power than in the unmodified case.

Fig. 4.18 presents the BER results of the proposed techniques, by evaluating the in-band distortion produced by the relevant techniques. These results are produced using a critically sampled, 64 subcarrier QPSK system. It should be noted that Fig. 4.18, does not consider the effects of amplifier clipping distortion and only considers the effects of the distortion inherent in the PAPR reduction techniques prior to amplification. As is to be expected, there is BER degradation across all techniques. However, it should be noted that, even though the clipping and filtering technique offers superior PAPR reduction capabilities, this comes at the expense of severe in-band distortion. The ACE based methods mitigate some of that distortion by only allowing extensions into allowable regions and therefore offer superior BER performance. It is clear that the single scaling proposal offers the least amount of BER degradation of the proposed methods. This is due to the lower scaling factors inherent of this technique. LP1 seems to offer rather poor BER performance in relation to the other proposals, whilst LP2 provides an acceptable amount of BER degradation even at higher iterations. The first iteration of the overlapping SGP algorithm offers very good BER performance, however this performance tends to worsen significantly after the first iteration. This can be attributed to the less strict constraints applied to the overlapping SGP proposed method. The tight constraints on LP2 provide excellent BER performance combined with significant PAPR reduction.

The BER performance of all the proposed techniques can be increased by limiting the maximum allowable scaling factor, or limiting the maximum allowable constellation extension regions. This allows a hard-limit to be placed on the maximum possible increase in average transmit power. This trade off comes at the expense of slight degradation in PAPR reduction capabilities. However, if the maximum scaling value is chosen smartly, almost negligible sacrifice can be made to PAPR reduction capabilities with significant boosts to BER performance. This is because the large increase in average

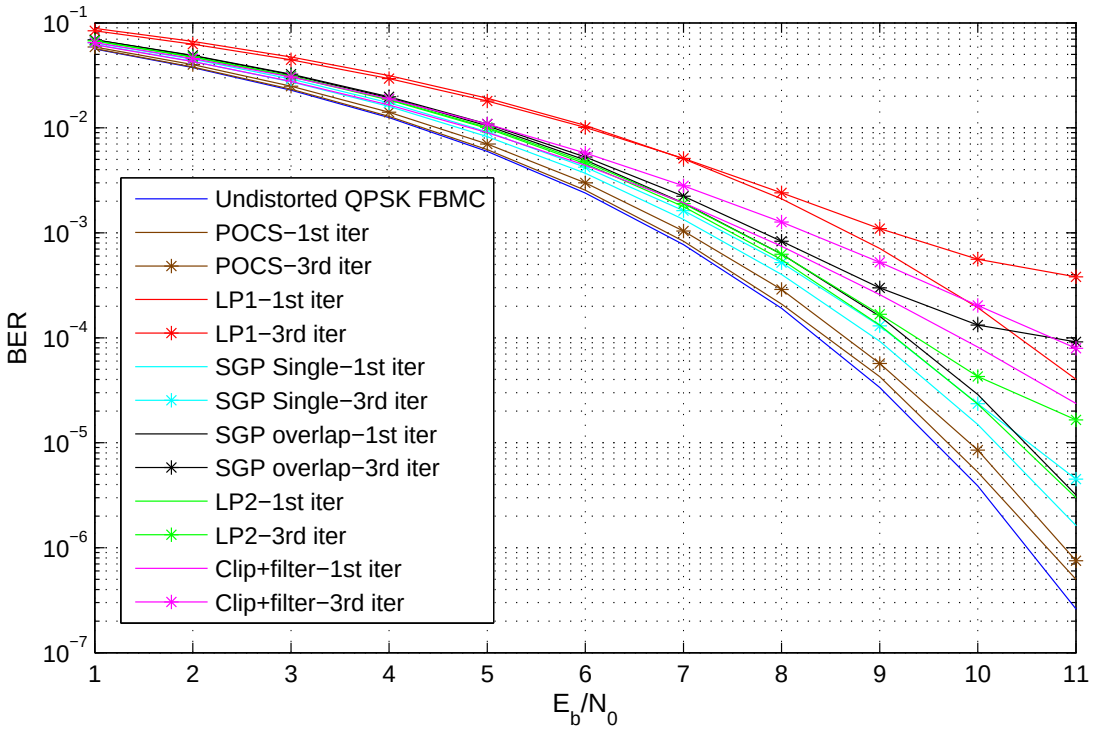

Figure 4.18: BER results of the proposed FBMC PAPR reduction methods of a critically sampled system

transmit power comes predominantly from clipped values that are very small, and so the algorithms tend to favour large scaling values when these situations occur. Due to the very small size in the clipped signals, their peak reducing capabilities are not significant and require large scaling to make a contribution. By limiting the maximum scaling factor, we essentially limit predominantly these points and therefore almost negligible performance is lost in terms of PAPR reduction capabilities. In fact, a new optimization formulation can be proposed that can set a limit on maximum constellation extension in order to obtain a tight trade-off between PAPR reduction and BER performance degradation caused by constellation distortion.

The BER performance degradation for ACE based methods are closely related to the average transmit power increase and do not reach an error floor as fast as a hard clipping method. Table 4.2 illustrates the average power increase across 10 000 frames. The average transmit power increase caused by LP1 is significant at 1dB on the first iteration. This closely resembles the BER performance degradation. The rest of the methods follow similar trends with lower BER degradation corresponding to the lowest power increase of the POCS based methods.

Table 4.2: Average transmit power increase comparison of proposed methods

Average power increase (dB)	POCS	Clip+filter	SGP Single	SGP overlapping	LP1	LP2
1st iter	0.084	-0.312	0.333	0.499	1.009	0.446
2nd iter	0.151	-0.420	0.373	0.522	1.047	0.467

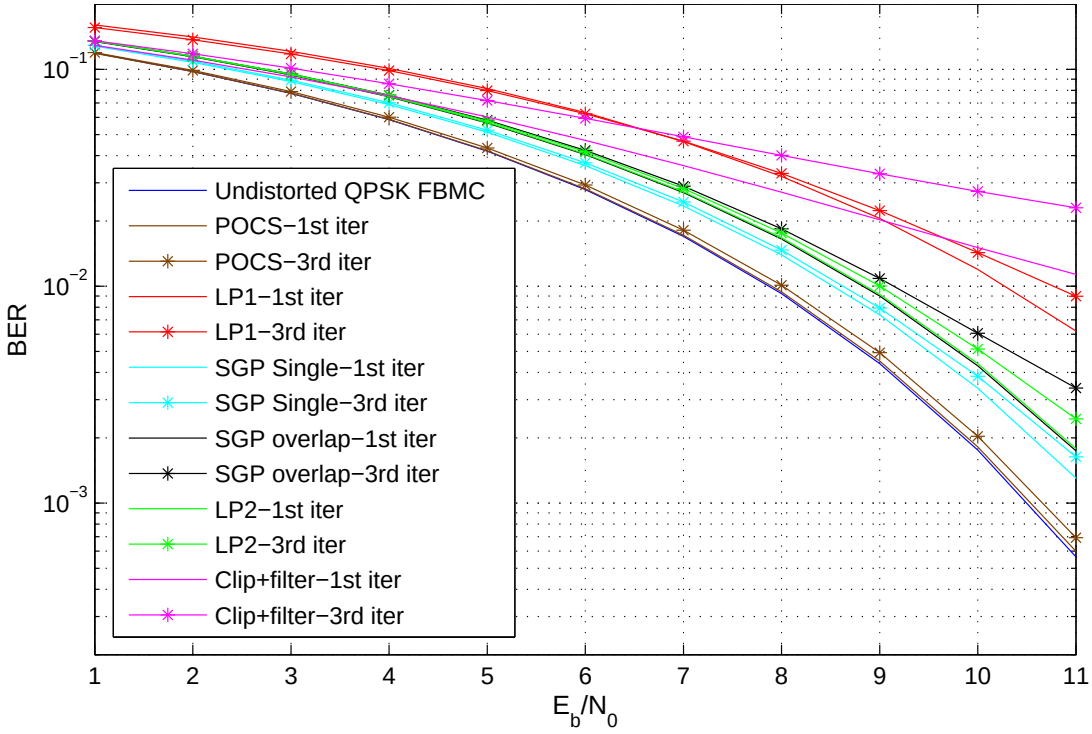

Figure 4.19: BER results of the proposed FBMC PAPR reduction methods of a critically sampled 16 QAM system

In Fig. 4.8 and Fig. 4.10 it was shown that by increasing the modulation order we reduce the PAPR reducing capabilities of the system. The effects on the BER degradation, when using a 16 QAM modulation scheme, are shown in Fig. 4.19. The BER degradation of the proposed techniques is not as severe as a clipping and filtering based technique. This can be attributed to the limitations placed on the extension regions of the ACE algorithm. The reduction in the degrees of freedom of the ACE algorithm, when applied to 16 QAM modulated systems, tend to prevent most constellation points from being distorted (the inner constellations remain unchanged). This limits the BER degradation when compared to a clipping and filtering based approach with no constellation correction.

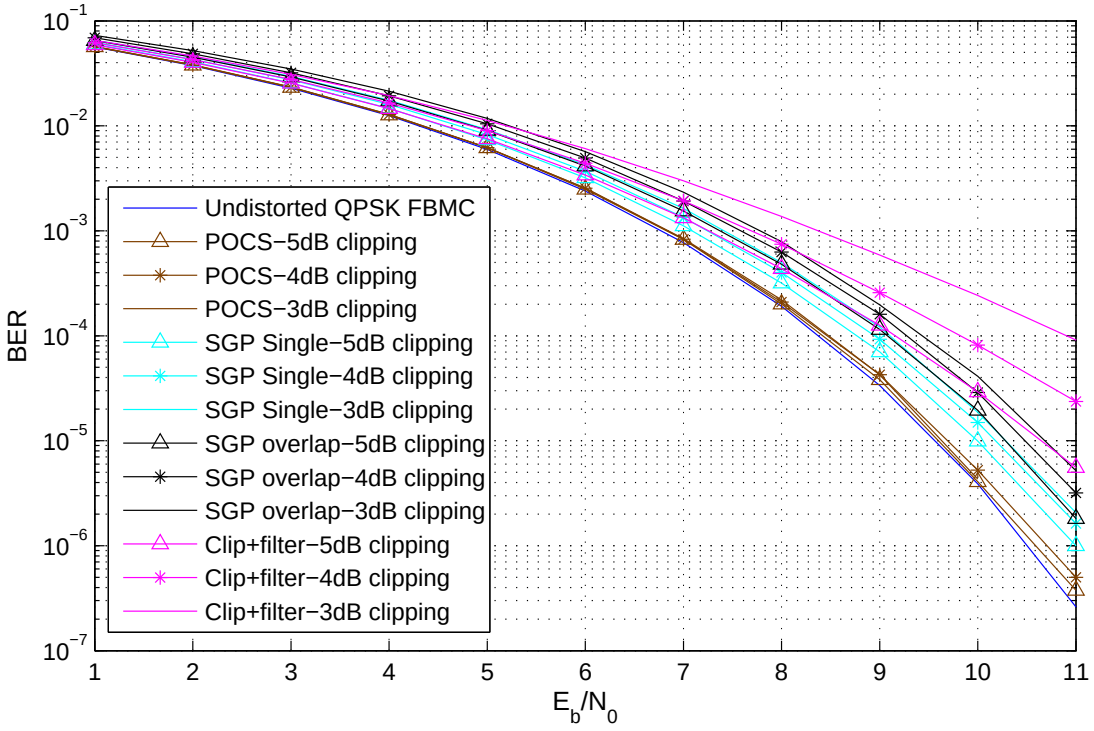

Figure 4.20: BER comparisons with varying clipping levels

4.4.1 Effects of varying clipping level of BER performance

In Section. 4.2.1, the effects on PAPR reduction were compared when the clipping levels are varied. The simulations in this section compare the BER degradation with the same varied clipping levels.

It is clear from Fig. 4.20 and Fig. 4.21 that varying the clipping levels also has an effect on the BER performance of the system. This highlights the trade off present when applying PAPR reduction techniques to multicarrier modulation schemes. Increasing the PAPR reduction performance comes at the expense of a decrease in BER performance. It is clear that the clipping and filtering technique degrades significantly in BER performance as the clipping level is increased to 3dB as can be seen with the error floor being reached fairly quickly.

From the simulations, a clipping level of 4dB was found to provide a good compromise between PAPR reduction performance and BER degradation.

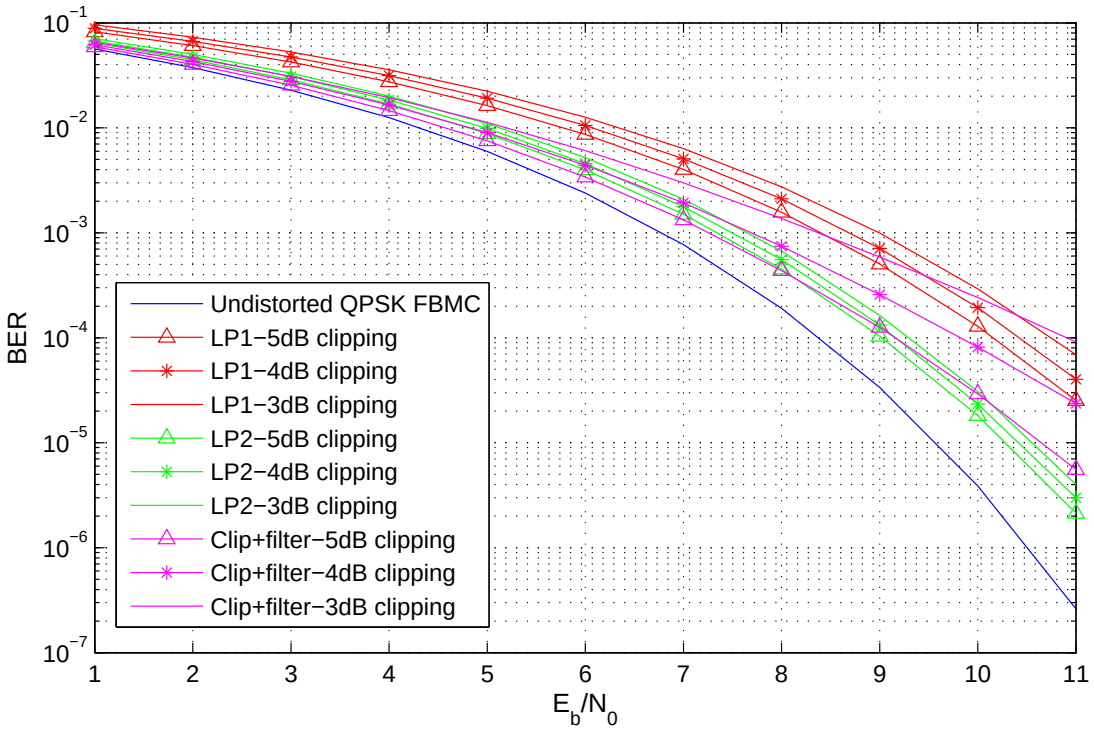

Figure 4.21: BER comparisons with varying clipping levels

4.5 POWER AMPLIFIER EFFICIENCY EVALUATION

The required amount of PA backoff is closely related to the PAPR of the multicarrier signal. Large PAPR levels lead to increased backoff and reduced power efficiency. The power saving achieved with each PAPR reduction methods can be drawn in the field using the theoretical upper limit for efficiency η of class A amplifiers. This is given by [58]

$$\eta = 58.7 \times \exp\left(-0.1247 \times \text{PAPR}_{dB}\right). \tag{4.2}$$

In order to compare the efficiency of the proposed methods to that found in [9, 10, 11], the best case scenarios presented in the literature were compared to the proposed methods. Due to most current methods in literature only simulating up to a clip probability of 10^{-3} for critical sampled FBMC employing 64 subcarriers, this was decided as the base metric for comparison. Using the PAPR reduction capabilities at a probability 10^{-3} it is easy to calculate an estimate for the efficiency of the different methods. The efficiency comparison between the proposed methods and current methods available in literature is calculated using (4.2) on the third iteration of the proposed methods at a

clipping probability of 10^{-3} and is given in Table. 4.3. As can be seen in the table, the overlapping SGP proposed method offers the highest amplifier efficiency.

Table 4.3: Class A power amplifier efficiency (η) comparison of critically sampled PAPR reduction performance for FBMC systems

		Proposed PAPR reduction method				Current literature		
	Original FBMC	SGP1	SGP2	LP1	LP2	OSLM	SW-TR	Optimized PTS
PAPR at 10^{-3} (dB)	10.15	6.07	5.49	5.97	5.96	8.4	6.15	5.9
$\eta(\%)$	16.56	27.56	29.60	27.88	27.92	20.59	27.09	27.43

4.6 IMPLEMENTATION COMPLEXITY

Implementation complexity costs are a serious factor for consideration for any newly proposed technique. Considering the results obtained for the cognitive radio scenario for filtered OFDM and FBMC in [2], both implementation complexities are comparable but high. Adding to this, the iterative characteristic of PAPR reduction techniques may lead to system complexity that is completely infeasible in practice.

For the LP based problems, each ACE iteration requires the use of the simplex algorithm to solve on optimization problem involving M decision variables and $2((M-1)\times N/2+L)$ constraints. This can be considered a significantly “hard" problem to solve, especially when introducing a higher number of subcarriers. The simplex algorithm has in the worst case an exponential time complexity whilst the complexity of a randomized simplex implementation is not known [59]. The per iteration based complexity of the LP formulated problems therefore far exceed the proposed SGP methods and most likely render their practical implementation infeasible. The LP formulations are included as a benchmark for a theoretical upper bound on PAPR performance of the proposed SGP techniques.

The overlapping SGP and single scaling SGP methods involve a dot product computation to calculate the clipped projections for each sample combined with additional signal processing to find the optimal scaling factor per symbol and per frame respectively. The complexity can be implicitly evaluated by comparing the number of real multiplications present in the proposed techniques. The number of real multiplications of the modulating C_{SFB} and demodulating C_{AFB} filter banks can be calculated using [56]

$$C_{SFB} = C_{AFB} = 2 \times (2N + N(log_2(N) - 3) + 4 + 2KN). \tag{4.3}$$

The proposed SGP techniques require an additional demodulation and modulation phase prior to transmission, as well as additional signal processing in order to calculate the projections as well as the scaling factors. The projection calculations of Eq. (3.36) can be seen to contribute $4N$ real multiplications, N real integer divisions and N real square root functions per FBMC symbol. Equation (3.40) can be calculated at a worst case scenario of N real divisions per FBMC symbol. The net real multiplications required in order to implement the SGP techniques, per SGP iteration, is therefore

$$C_{SGP} = 6 \times (2N + N(log_2(N) - 3) + 4 + 2KN) + 4N. \tag{4.4}$$

Considering $N = 64$, $K = 4$,

$$C_{SFB} = 1672 \text{ real multiplications}, \tag{4.5}$$

$$C_{SGP} = 5272 \text{ real multiplications} \tag{4.6}$$

and

$$\Omega = \frac{C_{SGP}}{C_{SFB}} = 3.15. \tag{4.7}$$

Considering $N = 128$,

$$\Omega = \frac{C_{SGP}}{C_{SFB}} = 3.14. \tag{4.8}$$

From Eq. (4.7) and Eq. (4.8) we can see that the complexity ratio remains constant when the subcarrier count, N, increases. This implies that the complexity increase scales linearly with the N or equivalently in big O notation, the additional complexity of the proposed FBMC SGP algorithms can be inferred to be $O(N)$.

4.7 CONCLUSION

This chapter presents the Monte Carlo simulation results as performed on a MATLAB platform. The simulations are performed with a high number of symbols in order to provide more accurate results. Oversampling methods are also applied for more accurate real world performance estimates.

The following chapter provides a brief discussion on the simulation results obtained.

CHAPTER 5 DISCUSSION

5.1 CHAPTER OVERVIEW

In this section, the results of the proposed algorithms are summarized and a detailed evaluation is given. The evaluation is split up into three sections focusing on PAPR reducing performance and BER evaluation, power spectrum and amplifier efficiency and implementation complexity.

5.2 PAPR REDUCING PERFORMANCE AND BER EVALUATION

The four proposed algorithms can provide significant PAPR reducing performance for FBMC systems. Theoretical performance of over 4dB in PAPR reduction can be achieved as shown in Fig. 4.2 and 4.3. Practical performance, when estimating to analogue, of 3dB can still be achieved by the proposed algorithms as shown in Fig. 4.6 and 4.7.

PAPR reduction and BER degradation for clipping based techniques are closely linked. As is highlighted in Section. 4, there is always a trade-off when improving the PAPR of a system and this often comes in the form of BER degradation. The PAPR results obtained in Fig. 4.2 to Fig. 4.10 clearly favour a clipping and filtering technique. However, as is evident from the BER analysis of Fig. 4.18, the clipping and filtering technique suffers severe BER degradation, introduced by the non-linear in-band distortion inherent of a clipping system. The effects of the distortion tend to diverge the BER curve away from the theoretical QPSK curve due to the error floor being reached faster the more aggressive the clipping. The proposed LP1 technique suffers similar BER degradation after the first iteration and therefore the PAPR reduction obtained may not be worth the trade-off. However of particular interest is the achievable BER in the single scaling and LP2 proposals. Even after the first iteration, the BER is not as significantly degraded as other comparative methods. The overlapping SGP proposal may also offer significant PAPR reduction on the first iteration with minimal BER degradation. However,

after the first iteration, any gains associated with PAPR reduction are mitigated by extensive increase in BER degradation. This may be attributed to the less stringent constraints placed on this method, when compared to the LP2 proposal, leading to some divergence after the first iteration. This however can be mitigated by limiting the maximum scaling value, thereby ensuring convergence.

The scalability of the algorithms, to 16 QAM, is important due to the need for higher order modulations, as data usage demands are increasing constantly. The results obtained in Fig. 4.8 and Fig. 4.10 for extensions to 16 QAM are less favourable than their QPSK counterparts. This is however to be expected from an ACE based method as only the outer constellations can be extended effectively reducing the degrees of freedom allowed for PAPR reduction. However, because of this, ACE in 16-QAM modulated systems suffers less BER degradation than other techniques. The clipping and filtering technique, as an example, suffers severe BER degradation on a 16 QAM platform, as is evident in Fig. 4.8 and Fig. 4.10. PAPR reduction, using the proposed techniques, of over 2dB is still achievable under 16 QAM scenarios as shown in Fig. 4.8. A downwards trend will be seen in higher order modulation systems, namely 64 QAM and 256 QAM, whereby the PAPR reducing ability degrades as the number of constellation points increase. Therefore ACE based techniques cannot be recommended for modulations higher than 16 QAM.

As previously mentioned, the trade-off of PAPR reduction comes at the expense of an increase in BER degradation across any PAPR reduction technique [13, 14]. In an FBMC scenario, constellation distortion results in BER degradation to the same degree as in OFDM. However, increasing the average transmit power in FBMC also results in an increase in the controlled interference inherent to FBMC systems. This will also contribute to BER degradation. Techniques exist which limit the maximum allowable in-band distortion [60], which if extended to the proposed techniques, may result in significant BER performance gains at negligible PAPR reduction capability loss. In conclusion, an optimal solution still needs to be found between BER performance degradation and PAPR reduction capabilities for FBMC systems such as a decision metric presented in [8].

The proposed techniques scale well with increased subcarrier count and the PAPR reducing performance is increased as the subcarrier count increases, as shown in Fig. 4.9 and 4.10. This is due to the higher number of subcarriers available upon which the ACE algorithm can be applied. This simple scalability, with no performance, loss is one of the main benefits of using an ACE based technique.

The chosen clipping factor, δ, of 4dB was found to provide a good trade-off between PAPR reducing ability and BER performance. The clipping factor however does not prove to have a significant effect on the PAPR performance as is shown from Section. 4.2.1. This is due to the nature of the SGP and optimization based algorithms, in which a maximum scaling factor is searched for and the peak reducing portion is scaled to achieve this maximum. However, the clipping factor should still be selected within reason and choosing a factor between 3-5dB provides the best results. Choosing a clipping factor lower than 3dB will result in an unnecessary loss in BER performance with minimal, if any, PAPR performance increase. Choosing a clipping factor larger than 5dB leads to minimal clipping prior to transmission and with this, insufficient signal points available to perform the actual PAPR reduction.

5.3 POWER SPECTRUM AND AMPLIFIER EFFICIENCY

The main benefit of FBMC lies within its tight power spectrum and this should always be a factor for consideration when employing any distortion technique to FBMC systems. Figure. 4.15, Fig. 4.16 and Fig. 4.17 illustrate the significant advantage of FBMC over OFDM in terms of the power spectral density of the modulation techniques. It is important to note the severe degradation of this important aspect of FBMC when clipping occurs. Clipping effectively destroys the tight spectral characteristics of FBMC and reinforces the need for PAPR reduction techniques prior to transmission. Without PAPR reduction techniques, the trade-off between the additional complexity of FBMC and its performance disqualify it as a contender to OFDM. However, as is evident from Fig. 4.15 to Fig. 4.17, the positive characteristics of FBMC can still be maintained, even after clipping, if a suitable PAPR reducing technique is applied.

The ACPR achievable by the proposed techniques are all within 12dB of ideal FBMC, as shown in Table. 4.1, upon the first iteration. By the third iteration, the overlapping SGP proposed technique improves on clipped FBMC's ACPR by 26dB. This is a significant reduction in interference of neighbouring frequency bands. This can reduce the requirement of filtering prior to transmission which normally adds an additional level of complexity to systems.

The amplifier efficiency is closely linked to the PAPR of any modulation technique. Unfortunately, the high PAPR is a notable characteristic inherent to any multicarrier modulation technique. In order to combat this, amplifiers are required to operate with high back-off regions which leads to low efficiency systems. However, with the successful reduction in PAPR, the probability of high PAPR sym-

bols is significantly reduced thereby allowing a smaller back-off and therefore increases the amplifier efficiency. This leads further emphasis on the need for PAPR reduction prior to transmission.

5.4 IMPLEMENTATION COMPLEXITY

FBMC systems are inherently more complex than their OFDM counterparts. Therefore, increasing the complexity by adding additional layers to the modulation portion, utilizing search algorithms, adding additional iterations or solving complex optimization problems, should be avoided.

The optimization techniques presented in this thesis, namely the two linear programming formulations, are used to create a theoretical upper limit benchmark, for PAPR reducing capabilities, to compare the other techniques to. However, because real and imaginary domain optimization problems can be infinitely complex, the optimization techniques proposed are based on approximations to the real domain. This can be seen in Eq. (3.36) where the maximum possible magnitude of the scaling factors is limited by the projections in the direction of the original signal and is a real scaling factor as opposed to a complex one.

The SGP type proposals provide feasible solutions that do not sacrifice PAPR reduction capabilities. They also maintain a lower level of complexity when compared to their optimization counterparts. With the SGP overlapping technique, PAPR reduction can be performed on a symbol by symbol basis, with an initial buffer, which provides a feasible solution for PAPR reduction in FBMC systems. The complexity of the SGP type solutions is summarized in Section. 4.6. This shows an approximate three times higher level of complexity than standard FBMC at the transmitter. This level of complexity is believed to be a reasonable trade-off for the PAPR reduction capabilities enabled by the techniques. The fact that the complexity scales linearly with an increase in subcarrier count, with the SGP based proposals, is a promising characteristic and therefore a practical implementation is feasible.

5.5 HARDWARE IMPLEMENTATION FOR PRACTICAL INDUSTRIALIZED SOLUTIONS

Due to the overlapping nature of FBMC, frame based processing cannot be achieved in a trivial manner. The overlap must always be accounted for and therefore, the best approach is to make provision for a buffer with feedback. This can allow for the last portion of the modified transmit signal to be passed back for processing. Transmission will then be possible with a small delay created

by the buffer. For transmission of packets, an entire frame can be processed and then transmitted in the form of a packet without much added delay (if processing can be performed at a sufficiently high speed). The FBMC frame size can also be modified in order to fit the requirements of each packet.

5.6 CONCLUSION

This chapter provides an in depth discussion of the simulation results of the proposed techniques. The discussion highlights the pros of the techniques and justifies the cons.

The following chapter concludes this thesis and provides recommendations for future work in this research field.

CHAPTER 6 CONCLUSION

The proposed peak-to-average power ratio (PAPR) reduction techniques presented in this paper provide a fast converging active constellation extension (ACE) alternative to PAPR reduction for filter bank multicarrier (FBMC) systems. Much like the smart gradient-project (SGP) ACE method for orthogonal frequency division multiplexing (OFDM), an SGP type implementation can be extended to FBMC systems, if the overlapping nature of FBMC is exploited. In this thesis two SGP type ACE methods were proposed and successfully extended to FBMC modulated systems. Two linear programming based optimization methods were also proposed. Significant gains in PAPR reduction capabilities are attained by the proposed methods and compare very favourably with current FBMC PAPR reduction techniques in literature. The adjacent channel power ratio (ACPR) of unclipped FBMC is maintained after being passed through a high power amplifier even with input back-off levels as low as 5dB. Bit error rate (BER) degradation varies across the proposed methods and a viable trade-off can be found between PAPR reduction capabilities and BER degradation by limiting the number of iterations. The SGP overlap technique proposed, from inspection, provides the most suitable trade-off between PAPR reduction and BER degradation.

The proposed optimization techniques require frame based processing in order to fully exploit the overlapping nature of FBMC symbols. This would ultimately lead to an increase in system latency in order to account for future symbols and maintain a causal system. This can be partially mitigated by decreasing the frame size over which the optimization occurs. These proposed techniques are therefore ideal candidates for burst transmission. The proposed SGP methods can however still retain causality by performing PAPR reduction on a symbol by symbol basis without much additional delay.

Due to the high level of complexity of FBMC modulated systems, significant increases in complexity should be avoided. The SGP proposed techniques increase linearly in complexity with increases in subcarrier count. These techniques provide good PAPR reducing performance, retain the tight spec-

tral characteristics of FBMC, maintain good BER performance and do not significantly add to the complexity of FBMC systems. The techniques are therefore a good candidate for practical implementation on FBMC systems and provide further justification to the implementation of FBMC, as a viable successor to OFDM, for future generation networks.

6.1 FUTURE RECOMMENDATIONS

The work presented in this thesis can easily be expanded on. The author has made every attempt to describe the model in the most rudimentary manner possible in the hope that students, following a similar line of research, are not plagued by fundamental challenges in the understanding of FBMC systems.

The following topics are recommended for future research:

1. An FBMC symbol scrambling based technique in order to reduce the PAPR of the FBMC system. This would involve re-ordering the initial FBMC symbols in a frame so that an optimally low PAPR is found across the frame. This could follow an optimization approach or a trial an error based method. Side-information would most likely be required unless a maximum likelihood decoding method is applied at the receiver when re-ordering the symbols.

2. Concatenating the research presented in this thesis with additional PAPR reduction such as TR or coding on top of the PAPR reduction technique.

3. Applying an OM-OFDM type adaptation such as in [8] on top of the proposed techniques.

4. A hardware based implementation on a digital signal processing or a field-programmable gate array development board. This will provide practical results to reinforce the simulation results presented in this thesis.

5. Maximum likelihood coding using the ICI inherent of FBMC systems. This will combat the BER degradation due to the deliberate distortion imposed by FBMC modulation on neighbouring carriers.

REFERENCES

[1] V. Berg and D. Noguet, "IEEE 1900.7 White Space Radio, ACLR issues with OFDM for TVWS operation," Dec. 2011.

[2] V. Berg, D. Noguet, A. Gameiro, M. Ariyoshi, Y. Futatsugi, M. Schühler, Z. Kollár, P. Horváth, and R. Datta, "D4.3 Flexible PHY concepts for white spaces - Final Report," *QoSMOS*, 2012.

[3] S. Srinivasan, S. Dikmese, and M. Renfors, "Spectrum sensing and spectrum utilization model for ofdm and fbmc based cognitive radios," in *2012 IEEE 13th International Workshop on Signal Processing Advances in Wireless Communications (SPAWC)*, 2012, pp. 139–143.

[4] S. Premnath, D. Wasden, S. Kasera, B. Farhang-Boroujeny, and N. Patwari, "Beyond OFDM: Best-effort dynamic spectrum access using filterbank multicarrier," in *2012 Fourth International Conference on Communication Systems and Networks (COMSNETS)*, Jan. 2012, pp. 1–10.

[5] M. Bellanger, "Physical layer for future broadband radio systems," in *2010 IEEE Radio and Wireless Symposium (RWS)*, Jan. 2010, pp. 436–439.

[6] M. Renfors, F. Bader, L. Baltar, D. Le Ruyet, D. Roviras, P. Mege, M. Haardt, and T. Hidalgo Stitz, "On the Use of Filter Bank Based Multicarrier Modulation for Professional Mobile Radio," in *2013 IEEE 77th Vehicular Technology Conference (VTC Spring)*, June 2013, pp. 1–5.

[7] T. Jiang, C. Li, and C. Ni, "Effect of PAPR reduction on spectrum and energy efficiencies in OFDM systems with class-A HPA over AWGN channel," *IEEE Trans. Broadcast.*, vol. 59, no. 3, pp. 513–519, 2013.

[8] K. Dhuness and B. Maharaj, "Analysis of an offset modulation transmission," *EURASIP*

Journal on Wireless Communications and Networking, vol. 2013, no. 1, p. 19, 2013. [Online]. Available: http://jwcn.eurasipjournals.com/content/2013/1/19

[9] A. Skrzypczak, J.-P. Javaudin, and P. Siohan, "Reduction of the peak-to-average power ratio for the OFDM/OQAM modulation," in *2006. VTC 2006-Spring. IEEE 63rd Vehicular Technology Conference*, vol. 4, May 2006, pp. 2018–2022.

[10] D. Qu, S. Lu, and T. Jiang, "Multi-block joint optimization for the peak-to-average power ratio reduction of FBMC-OQAM signals," *IEEE Trans. Signal Process.*, vol. 61, no. 7, pp. 1605–1613, Apr. 2013.

[11] S. Lu, D. Qu, and Y. He, "Sliding window tone reservation technique for the peak-to-average power ratio reduction of FBMC-OQAM signals," *IEEE Wireless Commun. Lett.*, vol. 1, no. 4, pp. 268–271, Aug. 2012.

[12] B. Krongold and D. Jones, "PAR reduction in OFDM via active constellation extension," *IEEE Trans. Broadcast.*, vol. 49, no. 3, pp. 258–268, Sep. 2003.

[13] T. Jiang and Y. Wu, "An Overview: Peak-to-Average Power Ratio Reduction Techniques for OFDM Signals," *IEEE Trans. Broadcast.*, vol. 54, no. 2, pp. 257–268, June 2008.

[14] M. Niranjan and S. Srikanth, "Adaptive active constellation extension for PAPR reduction in OFDM systems," in *2011 International Conference on Recent Trends in Information Technology (ICRTIT)*, June 2011, pp. 1186–1189.

[15] N. van der Neut, B. Maharaj, F. de Lange, G. Gonzalez, F. Gregorio, and J. Cousseau, "PAPR reduction in FBMC systems using a smart gradient-project active constellation extension method," in *2014 21st International Conference on Telecommunications (ICT)*, May 2014, pp. 134–139.

[16] N. van der Neut, B. Maharaj, F. de Lange, G. GonzÃąlez, F. Gregorio, and J. Cousseau, "PAPR reduction in FBMC using an ACE-based linear programming optimization," *EURASIP Journal on Advances in Signal Processing*, vol. 2014, no. 1, 2014. [Online]. Available: http://dx.doi.org/10.1186/1687-6180-2014-172

[17] M. Morelli and U. Mengali, "A comparison of pilot-aided channel estimation methods for OFDM systems," *IEEE Transactions on Signal Processing*, vol. 49, no. 12, pp. 3065–3073,

Dec. 2001.

[18] P. H. Moose, "A technique for orthogonal frequency division multiplexing frequency offset correction," *IEEE Transactions on Communications*, vol. 42, no. 10, pp. 2908–2914, Oct. 1994.

[19] P. Vaidyanathan, *Multirate systems and filter banks*. Englewood Cliffs, NJ, USA: Prentice Hall, 1993.

[20] D. Tse and P. Viswanath, *Fundamentals of Wireless Communication*. Cambridge University Press, 2005.

[21] W. G. Jeon, K. H. Chang, and Y. S. Cho, "An equalization technique for orthogonal frequency-division multiplexing systems in time-variant multipath channels," *IEEE Transactions on Communications*, vol. 47, no. 1, pp. 27–32, Jan 1999.

[22] B. Farhang-Boroujeny, "OFDM Versus Filter Bank Multicarrier," *IEEE Signal Process. Magaz.*, vol. 28, no. 3, pp. 92–112, May 2011.

[23] Z. Kollar, L. Varga, and K. Czimer, "Clipping-based iterative papr-reduction techniques for FBMC," in *Proceedings of 17th International OFDM Workshop 2012 (InOWo'12); OFDM 2012*, Aug. 2012, pp. 1–7.

[24] G. Ndo, H. Lin, and P. Siohan, "FBMC/OQAM equalization: Exploiting the imaginary interference," in *2012 IEEE 23rd International Symposium on Personal Indoor and Mobile Radio Communications (PIMRC)*, Sept 2012, pp. 2359–2364.

[25] D. Waldhauser, L. Baltar, and J. Nossek, "MMSE subcarrier equalization for filter bank based multicarrier systems," in *2008. SPAWC 2008. IEEE 9th Workshop on Signal Processing Advances in Wireless Communications*, July 2008, pp. 525–529.

[26] A. Farhang, N. Marchetti, L. Doyle, and B. Farhang-Boroujeny, "Filter Bank Multicarrier for Massive MIMO," in *2014 IEEE 80th Vehicular Technology Conference (VTC Fall)*, Sep. 2014, pp. 1–7.

[27] P. Siohan, C. Siclet, and N. Lacaille, "Analysis and design of OFDM/OQAM systems based on filterbank theory," *IEEE Trans. Signal Process.*, vol. 50, no. 5, pp. 1170–1183, May 2002.

[28] M. Bellanger, G. Bonnerot, and M. Coudreuse, "Digital filtering by polyphase network: Application to sample-rate alteration and filter banks," *IEEE Trans. Acoust., Speech, Signal Process.*, vol. 24, no. 2, pp. 109–114, Apr. 1976.

[29] F. Schaich, "Filterbank based multi carrier transmission (FBMC); evolving OFDM: FBMC in the context of WiMAX," in *2010 European Wireless Conference (EW)*, Apr. 2010, pp. 1051–1058.

[30] C. Langton. (2002) All about modulation - Part I. [Online]. Available: www.complextoreal.com

[31] H. Ochiai and H. Imai, "On the distribution of the peak-to-average power ratio in OFDM signals," *IEEE Trans. Commun.*, vol. 49, no. 2, pp. 282–289, Feb. 2001.

[32] B. S. Krongold and D. Jones, "An active-set approach for ofdm par reduction via tone reservation," *Signal Processing, IEEE Transactions on*, vol. 52, no. 2, pp. 495–509, Feb 2004.

[33] S. Thompson, A. Ahmed, J. Proakis, J. Zeidler, and M. Geile, "Constant Envelope OFDM," *IEEE Transactions on Communications*, vol. 56, no. 8, pp. 1300–1312, August 2008.

[34] M. Masonta, Y. Haddad, L. De Nardis, A. Kliks, and O. Holland, "Energy efficiency in future wireless networks: Cognitive radio standardization requirements," in *2012 IEEE 17th International Workshop on Computer Aided Modeling and Design of Communication Links and Networks (CAMAD)*, Sep. 2012, pp. 31–35.

[35] D. Waldhauser, L. Baltar, and J. Nossek, "Comparison of filter bank based multicarrier systems with OFDM," in *IEEE Asia Pacific Conference on Circuits and Systems, 2006. APCCAS 2006.*, Dec. 2006, pp. 976–979.

[36] S. H. Han and J. H. Lee, "An overview of peak-to-average power ratio reduction techniques for multicarrier transmission," *IEEE Trans. Wireless Commun.*, vol. 12, no. 2, pp. 56–65, Apr. 2005.

[37] L. Wang and C. Tellambura, "An overview of peak-to-average power ratio reduction techniques for OFDM systems," in *2006 IEEE International Symposium on Signal Processing and Information Technology*, Aug. 2006, pp. 840–845.

[38] X. Zhao, S. Jones, and R. Abdul-Alhameed, "A fair comparison platform for OFDM systems

with various PAPR reduction schemes," in *2012 Mosharaka International Conference on Communications, Computers and Applications (MIC-CCA)*, Oct 2012, pp. 136–141.

[39] Z. KollÃąr, L. Varga, B. HorvÃąth, P. Bakki, and J. BitÃş, "Evaluation of clipping based iterative papr reduction techniques for fbmc systems," *The Scientific World Journal, vol. 2014*, vol. 2014, Feb 2014.

[40] M. Niranjan and S. Srikanth, "Adaptive active constellation extension for PAPR reduction in OFDM systems," in *2011 International Conference on Recent Trends in Information Technology (ICRTIT)*, June 2011, pp. 1186–1189.

[41] X. Li and L. Cimini, "Effects of clipping and filtering on the performance of ofdm," in *Vehicular Technology Conference, 1997, IEEE 47th*, vol. 3, May 1997, pp. 1634–1638 vol.3.

[42] Z. Yang, H. Fang, and C. Pan, "ACE with frame interleaving scheme to reduce peak-to-average power ratio in OFDM systems," *IEEE Transactions on Broadcasting*, vol. 51, no. 4, pp. 571–575, Dec. 2005.

[43] Y. Zhou and T. Jiang, "A novel clipping integrated into ACE for PAPR reduction in OFDM systems," in *WCSP 2009. International Conference on Wireless Communications Signal Processing*, Nov 2009, pp. 1–4.

[44] R. S. Prabhu and E. Grayver, "Active constellation modification techniques for OFDM PAR reduction," in *2009 IEEE Aerospace conference*, March 2009, pp. 1–8.

[45] M.-J. Hao and C.-H. Lai, "PAPR reduction with Adjustable Circle Constrain for OFDM systems," in *International Symposium on Intelligent Signal Processing and Communication Systems, 2009. ISPACS 2009.*, Jan 2009, pp. 323–326.

[46] J. Armstrong, "New OFDM peak-to-average power reduction scheme," in *IEEE VTS 53rd Vehicular Technology Conference, 2001. VTC 2001 Spring.*, vol. 1, May 2001, pp. 756–760 vol.1.

[47] L. Wang and C. Tellambura, "Analysis of clipping noise and tone-reservation algorithms for peak reduction in ofdm systems," *Vehicular Technology, IEEE Transactions on*, vol. 57, no. 3, pp. 1675–1694, May 2008.

[48] B. S. Krongold and D. Jones, "An active-set approach for OFDM PAR reduction via tone reservation," *IEEE Transactions on Signal Processing*, vol. 52, no. 2, pp. 495–509, Feb. 2004.

[49] R. Bauml, R. Fischer, and J. Huber, "Reducing the peak-to-average power ratio of multicarrier modulation by selected mapping," *Electronics Letters*, vol. 32, no. 22, pp. 2056–2057, Oct 1996.

[50] M. Breiling, S. Muller-Weinfurtner, and J. Huber, "Slm peak-power reduction without explicit side information," *Communications Letters, IEEE*, vol. 5, no. 6, pp. 239–241, June 2001.

[51] S. Muller and J. Huber, "Ofdm with reduced peak-to-average power ratio by optimum combination of partial transmit sequences," *Electronics Letters*, vol. 33, no. 5, pp. 368–369, Feb 1997.

[52] L. Yang, R. Chen, Y. Siu, and K. Soo, "PAPR reduction of an OFDM signal by use of PTS with low computational complexity," *IEEE Transactions on Broadcasting*, vol. 52, no. 1, pp. 83–86, March 2006.

[53] S. H. Han and J. H. Lee, "PAPR reduction of OFDM signals using a reduced complexity PTS technique," *IEEE Signal Processing Letters*, vol. 11, no. 11, pp. 887–890, Nov 2004.

[54] C. Ye, Z. Li, T. Jiang, C. Ni, and Q. Qi, "PAPR Reduction of OQAM-OFDM Signals Using Segmental PTS Scheme With Low Complexity," *IEEE Transactions on Broadcasting*, vol. 60, no. 1, pp. 141–147, Mar. 2014.

[55] Z. Kollar and P. Horvath, "PAPR Reduction of FBMC by Clipping and Its Iterative Compensation," *Journal of Computer Networks and Communications*, vol. 2012, 2012.

[56] Phydyas5.1, *PHYDYAS deliverable D5.1: Prototype filter and structure optimization*. PHYsical layer for DYnamic AccesS and cognitive radio, 2008.

[57] F. Gregorio, J. Cousseau, S. Werner, T. Riihonen, and R. Wichman, "Power amplifier linearization technique with IQ imbalance and crosstalk compensation for broadband MIMO-OFDM transmitters," *EURASIP Journal on Advances in Signal Processing*, vol. 2011, no. 1, p. 19, 2011. [Online]. Available: http://asp.eurasipjournals.com/content/2011/1/19

[58] D. Wulich, "Definition of efficient PAPR in OFDM," *IEEE Commun. Lett.*, vol. 9, no. 9, pp.

832–834, 2005.

[59] N. Megiddo, “On the complexity of linear programming,” in *Advances in Economic Theory*, Jul. 1989, pp. 225–227.

[60] S.-K. Deng and M.-C. Lin, “Recursive Clipping and Filtering With Bounded Distortion for PAPR Reduction,” *IEEE Trans. Commun.*, vol. 55, no. 1, pp. 227–230, 2007.